UNIVERSITY OF TRENTO

Doctoral School in Civil, Environmental and Mechanical Engineering

Curriculum 1. Civil and Environmental Engineering

Silvia D'Agostino

Particle segregation and mixing in a dry free surface granular flow

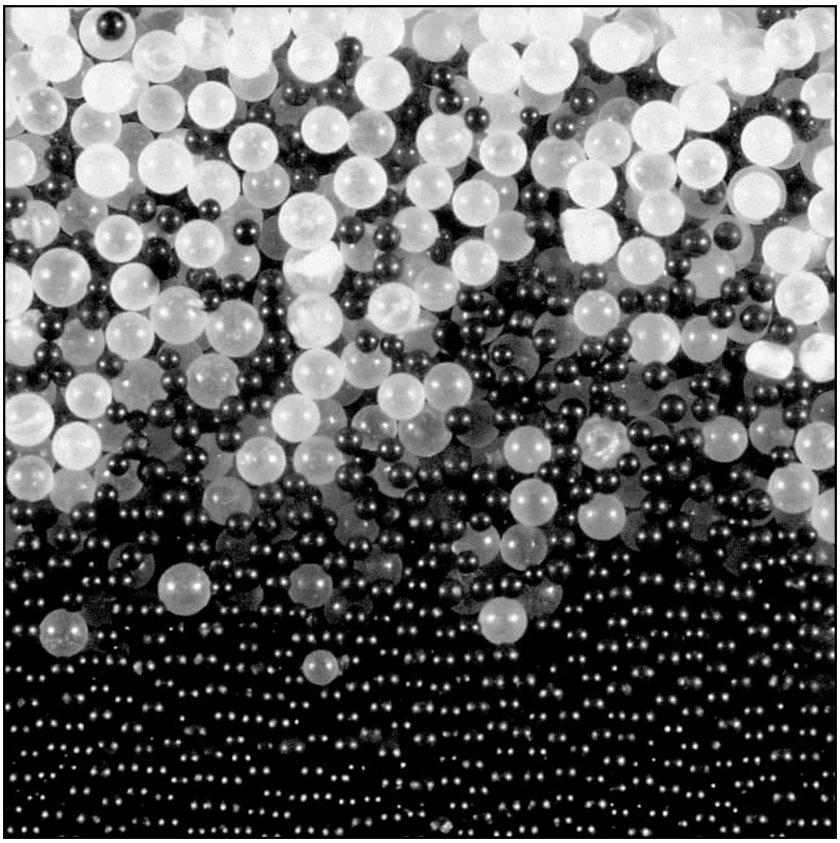

2021 - Doctoral thesis

Geophysical massive flows as snow avalanches and debris flows are characterized by a wide grain size distribution. The interactions between particles among the granulometric classes are a consequent of a such large distribution. However, most of the studies on the geophysical massive flows assume the simplifying hypothesis of a constant granulometry. The aim of this work is studying the coexistence of two granulometric classes in statistically stationary and homogeneous conditions and investigating the physical processes responsible for the particles transfer.
Experimental investigations using two different grain size classes were conducted to reproduce the two-phases mixture. The granular material was recirculated in a close system and the experiments were carried out in a laboratory flume having a loose two-size granular bed. A proper optical technique was innovatively improved to obtain the average and instantaneous values of the velocity and concentration from the side-walls.
Through these values, the average particle profiles of velocity, concentration and granular temperature of the two solid fractions were computed. Moreover, the instantaneous values provide the average profiles of the second order correlation of the variables, such as the component of the granular temperature and the fluctuating components of the velocity and the concentration.
The average distribution profiles in time of velocity and concentration prove the statistically stationary and homogeneous condition in a stretch sufficiently long of the running flow. Moreover, two types of regimes were identified: in case of low and intermediate discharges, the frictional regime nearly prevails at the free surface; for high discharges there is a coexistence across the flow depth of two regimes, the frictional regime in the intermediate flow-depth region and the collisional regime in the free surface. The existence of a vertical velocity component of both phases brings to hypothesize the presence of secondary circulations in the flow.

Silvia D'Agostino studied at the University of Padova, Italy, where she had the MSc in CivilEngineering in 2017 with a thesis on flow resistence in urban flooding. She moved to Trento whereshe enrolled as a PhD student in Environmental Engineering.
During the PhD experience she focused on studying environmental granular flows under the goal toempower the knowledge and the modelling of massive flows in mounatin environment. Her researchdealt with the analysis of the mechanims involved in segregation of particles that she developedthrough experimental investigations. She also had the opportunity to work on projects on advanceddesigning criteria of protection structures in mountain catchments.

UNIVERSITY OF TRENTO - Italy
Department of Civil, Environmental and Mechanical Engineering

Doctoral School in Civil, Environmental and Mechanical Engineering
Topic 1. Civil and Environmental Engineering - XXXIII cycle 2017/2020

Doctoral Thesis - September 2021

Silvia D'Agostino

Particle segregation and mixing in a dry free surface granular flow

Supervisor
Aronne Armanini, University of Trento

Credits of the cover image: Silvia D'Agostino

University of Trento
Doctoral School in Civil, Environmental and Mechanical Engineering
http://web.unitn.it/en/dricam
Via Mesiano 77, I-38123 Trento
Tel. +39 0461 282670 / 2611 - *dicamphd@unitn.it*

Abstract

Geophysical massive flows are characterized by a wide grain size distribution. This peculiarity is present both in dry gravitational phenomena, such as snow and rock avalanches, and in submerged gravitational phenomena, as debris flows, where huge blocks and tiny gravels are transported together.

The interactions between the particle size classes in these massive transport flows often produce evident phenomena of particle segregation capable of a significantly modification of the rheological properties of the material and therefore the flow properties. However, most studies on geophysical massive flows assume the simplified hypothesis of uniformly sized particles.

From a mechanical point of view, the flows of non-uniform granular mixtures are characterized by infiltration and diffusion processes, that produce the particle segregation especially in non-statistically stationary and homogeneous conditions while in stationary and homogeneous conditions they are characterized by a grains stratification.

These findings have drawn the attention to the need to have 1D or 2D shallow water models capable of taking these aspects into account for field applications. As known, these models require appropriate closure re-

lations, derived in of steady and homogeneous flow (i.e. uniform channel flow).

The objective of the thesis is to analyse in detail the flow of bi-dispersed mixtures of granular material in stationary and homogeneous conditions, i.e. uniform channel flow, and investigate the physical processes responsible for particles transfer.

For this purpose, a sequence of experimental investigations was carried out in a laboratory flume specifically designed to recirculate a bi-dispersed mixture of dry granular material (closed circuit system). A special weir at the end of the flume induced the formation of a uniform deposition layer on the flume bottom, in order to guarantee a sufficiently long stretch of uniform flow on the loose bed.

A specific optical measuring method was developed to measure from the transparent lateral walls of the flume the values of velocity and concentration of the two fractions. The innovation of this technique consists on the capacity to obtain, further the instantaneous values of the velocity of the single particles, also their concentration.

From these data we obtained the profiles of the time-averaged velocity and concentration of the two solid fractions. Moreover, the instantaneous values of fluctuating components of the data provided also the profiles of the second order correlations of the variables, such as the component of the granular temperature and Reynolds-like stresses and other second order terms involving the concentration fluctuations.

The results allowed to: i) prove the existence of a statistically stationary and homogeneous flow of a bi-disperse mixture; ii) evaluate the effects on the flow parameters with respect to the feeding rate and different flow percentage of the two grain classes; iii) define the role in the mass and momentum balances of the correlation between the fluctuating components

of the flow variables.

Furthermore, the experiments allowed to observe also in the binary mixture the presence of two types of regimes. In the case of low and intermediate discharges, the frictional regime prevails over the entire flow depth. For the higher flow rates there is a coexistence along the depth of the flow of two regimes: the frictional regime in the near-bed region and the collisional regime near the free surface.

Finally, the existence of a vertical velocity component of both phases, not counterbalanced by a diffusive term, leads to hypothesize the presence of secondary circulations in the flow.

Sommario

I fenomeni naturali di trasporto solido sono caratterizzati dalla presenza di un'ampia distribuzione granulometrica. Questa caratteristica è presente sia nei fenomeni naturali secchi, come le valanghe di roccia e neve, che bagnati, come le colate detritiche, dove vengono trasportati sia grandi massi che piccoli sassi.

Le interazioni tra le diverse classi di particelle in questo tipo di eventi producono la segregazione delle particelle, fenomeno capace di modificare in modo significativo la reologia delle proprietà del materiale e i parametri del campo di moto. Al contrario, la maggior parte degli studi sui fenomeni naturali di trasporto solido assume spesso l'ipotesi semplificativa di particelle a granulometria uniforme.

Da un punto di vista meccanico, i flussi granulari a granulometria non uniforme sono caratterizzati dai processi di infiltrazione e diffusione, che sono causa della segregazione delle particelle sopratutto in condizione di moto statisticamente non uniforme e omogeneo.

Vi è perciò la necessità di avere modelli monodimensionli o bidimensionali in acque basse che prendano in considerazione questi aspetti anche per applicazioni di campo. Questi modelli richiedono appropriate equazioni di chiusura, che derivano da condizioni di moto statisticamente

stazionario e omogeneo (moto uniforme).

L'obiettivo di questa tesi è di analizzare in dettaglio il flusso granulare composto da due classi granulometriche in condizione di moto uniforme e di analizzare i fenomeni fisici responsabili del trasferimento delle particelle all'interno del campo di moto.

A tale scopo, è stata condotta una serie di esperimenti in una canaletta di laboratorio, progettata per fare ricircolare in una circuito chiuso il flusso granulare secco composto dalle due diverse granulometrie. Un apposito stramazzo posto alla fine della canaletta induce la formazione di un deposito, in modo tale da garantire un tratto di moto uniforme sufficientemente lungo sul letto fisso di particelle.

Successivamente, è stato sviluppato uno specifico metodo ottico per misurare dalle pareti trasparenti della canaletta i valori di velocità e concentrazione delle due classi granulometriche del flusso granulare bifasico. La novità di questa tecnica consiste nella capacità di ottenere, oltre ai valori istantanei di velocità delle singole particelle, anche la loro concentrazione.

Attraverso i dati forniti dagli esperimenti è stato possibile ottenere i profili medi di velocità e concentrazione nel tempo delle due classi granulometriche. Inoltre, i valori istantanei e fluttuanti dei dati hanno fornito i profili di correlazione al secondo ordine delle variabili, come la temperatura granulare, gli stress 'Reynolds-like' e gli altri termini che includono le fluttuazioni delle concentrazioni.

I risultati hanno permesso di: i) testare l'esistenza della condizione di moto statisticamente stazionario ed omogeneo anche nella mistura bifasica; ii) valutare gli effetti sui parametri di flusso al variare della diversa portata e della diversa composizione della mistura; iii) definire il ruolo nella massa e quantità di moto della correlazione delle componenti fluttuanti delle variabili.

Inoltre, gli esperimenti hanno permesso anche di individuare nel flusso granulare bifasico la presenza di due tipi di regimi. Nel caso di portate basse ed intermedie, il regime frizionale prevale su tutto il tirante di moto uniforme. Diversamente, per portate più alte vi è una coesistenza dei due regimi: il regime frizionale prevale vicino al fondo mentre quello collisionale in superficie.

Infine, l'esistenza di una componente verticale delle velocità di entrambe le classi granulometriche, non controbilanciata da un termine diffusivo, porta ad ipotizzare l'esistenza della presenza di circolazioni secondarie all'interno flusso.

Acknowledgements

After almost four years of work, there are many people that I would like to thank who helped me with its realization.
At first, I would like to thank my supervisor Aronne Armanini, for the support and trust as well as for the scientific knowledge that he taught me in these years.
I want to express my gratitude to Michele Larcher and Michele La Rocca for the useful corrections and their availability on discussing the thesis revisions, that helped me in improving my work.
I would like to thank the technicians of the Laboratory of Hydraulics of Trento, in particular Lorenzo Forti. I thank Daniel Zugliani, colleague and friend, who was always available not only for scientific matters.
I am grateful to my colleagues Pepe, flatmate but also friend, for the serenity of the years lived together and the reciprocal support, and Mattia, for the happy moments shared during the PhD experience.
Then, I want to thank all the friends I have met in these years, from climbing to office mates. My staying in Trento would have not been the same without each of you.
Thank to my family, my parents and my sister, that support me in my choices and are always close to me in the difficult times.
Finally, I want to thank Matteo for always being there, despite everything.

Contents

List of Symbols

The physical quantities, in order of appearance, are indicated as T for time, M for mass and L for length.

x_i	spatial coordinate	$[-]$
t	variable for the time	$[\mathrm{T}]$
T	granular temperature	$[\mathrm{L}^2\mathrm{T}^{-2}]$
$\dot{\gamma}$	shear velocity	$[\mathrm{T}^{-1}]$
d	particle diameter	$[\mathrm{L}]$
λ	volume concentration	$[-]$
s	mean distance between grains	$[\mathrm{L}]$
c_*	packing concentration	$[-]$
φ	fraction angle	$[^\circ]$
μ_f	dynamic viscosity	$[\mathrm{ML}^{-1}\mathrm{T}^{-1}]$
τ	shear stress	$[\mathrm{ML}^{-1}\mathrm{T}^{-2}]$
p	normal stress	$[\mathrm{ML}^{-1}\mathrm{T}^{-2}]$
Ba	Bagnold number	$[-]$
$\overline{u}$	temporal average component of the velocity	$[\mathrm{L}^{-1}\mathrm{T}^{-1}]$

u_1	temporal average component of the velocity	$[\mathrm{L}^{-1}\mathrm{T}^{-1}]$
$f^{(1)}$	single distribution function	$[-]$
$f^{(2)}$	pair distribution function	$[-]$
$\overline{\Psi}$	single-particle property	$[-]$
r_i	position of the particle	$[\mathrm{L}]$
n	number of particle in a control volume	$[-]$
Φ_c	total contribution of the collisional forces	$[-]$
Ω	transfer contribution	$[-]$
χ	source-like contribution	$[-]$
$\mathcal{T}$	tensor of the granular stresses	$[\mathrm{ML}^{-1}\mathrm{T}^{-2}]$
β	single grain-size class of the particle	$[-]$
d^β	particle diameter of the grain size class β	$[\mathrm{L}]$
d^s	particle diameter of the small grain size class	$[\mathrm{L}]$
d^l	particle diameter of the large grain size class	$[\mathrm{L}]$
ρ_s	material density of the granular phase	$[\mathrm{ML}^{-3}]$
ρ_m	density of the particles mixtures	$[\mathrm{ML}^{-3}]$
c^β	concentration of the of the grain size class β	$[-]$
c^s	concentration of the small particles	$[-]$
c^l	concentration of the large particles	$[-]$
u^β	particle velocity of the grain size β	$[\mathrm{LT}^{-1}]$
g_0	distribution function	$[-]$
e	inelastic restitution coefficient	$[-]$
$f_{(i)}$	coefficient adopted in the kinetic theory	$[-]$

δ_{ij}	Kronecker delta	$[-]$
τ_{ij}^{fric}	frictional tangential stresses	$[\mathrm{ML^{-1}T^{-2}}]$
τ_{ij}^{coll}	collisional tangential stresses	$[\mathrm{ML^{-1}T^{-2}}]$
σ_2	normal stress	$[\mathrm{ML^{-1}T^{-2}}]$
a_{fr}	non-dimensional constant	$[-]$
p	confining pressure	$[\mathrm{ML^{-1}T^{-2}}]$
$\mu(I)$	dynamic angle ($\mu(I)$ model)	$[^\circ]$
I	inertial number	$[-]$
I_0	constant of the $\mu(I)$ model	$[-]$
φ_s	static friction angle ($\mu(I)$ model)	$[^\circ]$
φ_2	friction angle ($\mu(I)$ model)	$[^\circ]$
p^g	granular pressure (heuristic model)	$[\mathrm{ML^{-1}T^{-2}}]$
φ^{fric}	friction angle (heuristic model)	$[^\circ]$
I_s	inertial parameter	$[-]$
p^{coll}	collisional pressure	$[-]$
μ_I	tangential stress ($\mu(I)$ model)	$[\mathrm{ML^{-1}T^{-2}}]$
μ_s	static angle	$[^\circ]$
μ_2	dynamic angle	$[^\circ]$
τ_{ij}^{β}	granular tensor	$[\mathrm{ML^{-1}T^{-2}}]$
$\Xi_i^{\beta\kappa}$	vector of the external forces	$[\mathrm{MLT^{-2}}]$
g_i	volume force	$[\mathrm{MLT^{-2}}]$
F_i^{β}	forces exerted by the fluid on the solid	$[\mathrm{MLT^{-2}}]$
p^{β}	granular pressure of the phase β	$[-]$

T^{β}	granular temperature of the phase β	$[\mathrm{L}^2\mathrm{T}^{-2}]$
g_o^{β}	distribution function of the phase β	$[-]$
η_p	coefficient of kinetic theory	$[-]$
p^{β}	granular pressure of the phase β	$[-]$
μ	coefficient of the kinetic theory	$[^{\circ}]$
μ_b	coefficient of the kinetic theory	$[^{\circ}]$
$\mu^{\beta * - coll}$	coefficient of the kinetic theory	$[^{\circ}]$
$\Xi_i^{\beta\kappa}$	generic component of the interaction forces	$[\mathrm{MLT}^{-2}]$
$\xi^{\beta\kappa}$	coefficient defining the interaction forces	$[-]$
κ	grain size class	$[-]$
c'	fluctuating component of particle concentration	$[-]$
$\overline{c}$	average component of particle concentration	$[-]$
$\overline{u}$	average component particle velocity	$[\mathrm{LT}^{-1}]$
u'	fluctuating component of particle velocity	$[\mathrm{LT}^{-1}]$
ξ_2^{β}	diffusion coefficient	$[\mathrm{L}^2\mathrm{T}^{-1}]$
$[\Lambda]$	length scale	$[\mathrm{L}]$
$[\mathcal{U}]$	velocity scale	$[\mathrm{LT}^{-1}]$
f_D	pre-factor for the diffusion coefficient	$[-]$
$\mathcal{I}_2^{\beta}$	infiltration coefficient	$[\mathrm{LT}^{-1}]$
f_I	pre-factor for the infiltration coefficient	$[-]$
ϕ	concentration of each phase (chapter 2)	$[-]$
D	diffusion coefficient (chapter 2)	$[\mathrm{L}^2\mathrm{T}^{-1}]$
$\mathbf{F}^{\beta}$	segregation flux vector (chapter 2)	$[\mathrm{MLT}^{-2}]$

$n_{A,B}$	number of densities (chapter 2)	[−]
$m_{A,B}$	mass of species A and B (chapter 2)	[M]
$r_{A,B}$	radii of species A and B (chapter 2)	[L]
x	segregation function (chapter 2)	[−]
Q	measured discharge	[$L^{-3}T$]
P_T	weight of the collected material	[M]
t_c	recording time	[T]
V_β	particle volume of the phase β	[L^{-3}]
P_S	weight of the small particles in the control volume	[M]
P_L	weight of the large particles in the control volume	[M]
θ	slope of the loose bed	[°]
α	slope of the flume	[°]
u_i^β	time average velocity component	[LT^{-1}]
$\tilde{u}_i^\beta$	instantaneous velocity component	[LT^{-1}]
c_i^β	time average concentration component	[−]
$\tilde{c}_i^\beta$	instantaneous concentration	[−]
n_k	number of particles in a layer	[−]
C_{2D}	2D concentration	[−]
C_{2D}^*	2D packing concentration	[−]
C_{3D}	3D concentration	[−]
C_{3D}^*	3D packing concentration	[−]
W	channel width	[T]
$s_{1,2}$	measurement sections	[T]

n_t	number of frame	$[-]$
h_0	uniform flow depth	[L]
z_b	loose bed depth	[L]
V	volume of the particles in the control volume	$[L^{-3}]$
i_s	slope of the free surface of the granular flow	$[^\circ]$
P_β	volumetric partition of the grain size class β	$[-]$
P_S	volumetric partition of the small particles	$[-]$
P_L	volumetric partition of the large particles	$[-]$
Q_S^*	granular discharge of the small particles	$[\mathrm{L}^{-3}\mathrm{T}]$
Q_L^*	granular discharge of the large particles	$[\mathrm{L}^{-3}\mathrm{T}]$
Q_T^*	total granular discharge of the particles	$[\mathrm{L}^{-3}\mathrm{T}]$
u_1^β	longitudinal velocity of the grain size β	$[\mathrm{LT}^{-1}]$
u_2^β	vertical velocity of the grain size β	$[\mathrm{LT}^{-1}]$
t_1	first acquisition time step	[T]
t_2	second acquisition time step	[T]
$S_{1,2,3,4,5}$	section of measurements in the flume	[L]
c_r	relative concentration	$[-]$
τ_{12}^β	stresses frictional and collisional stress	$[\mathrm{ML}^{-1}\mathrm{T}^{-2}]$
$\overline{u'_1{}^\beta \; u'_2{}^\beta}$	Reynolds-like stresses	$[\mathrm{ML}^{-1}\mathrm{T}^{-2}]$
$\overline{u'_2{}^\beta \; u'_2{}^\beta}$	Reynold-like stresses	$[\mathrm{ML}^{-1}\mathrm{T}^{-2}]$

List of Figures

List of Tables

Introduction

Particles segregation is a universal phenomenon occurring in nature, such as in debris flows, snow, rock and ice avalanches, sediment transport in rivers, but also in many industrial processes, such as in chemical, food, powders and mining manufacture.

In granular flows particle segregation is a very complex event, as it is governed by a combination of mechanisms: the different geometry of the flow, the mechanical properties of the particles, their distribution, the environmental conditions, etc.

Attempts to define the mechanisms of the process have been enhancing in the past years and nowadays many studies on this topic are present in the literature.

Mainly two processes can be identified in segregation: the infiltration process and the random fluctuating sieve process [69]. In avalanches, the snow particles behave as a random fluctuating sieve, as the small particles percolate under the action of gravity, because they are more likely to fill the gaps that open beneath them [56, 69]. In dense frictional flows, squeeze expulsion is the predominant mechanism, as all the particles have an equal probability to be levered upwards, that results in a net flux of small particles at the base and large grains flux at the surface of the flow [69]. Thus,

segregation in granular flows as avalanches typically occurs in a vertical direction in inversely graded layers, with large particles above the fines, and brings the transport of the large particles toward the front, where they can be overrun, re-segregated, recirculated, and accumulated. At the same time the gravity-driven segregation leads to secondary lateral segregation, that with frictional or shape differences between the particles, leads to a strong feedback on the bulk flow [30].

Mechanisms of segregation are quite difficult to understand in their complexity and a reliable model that can predict the occurrence of segregation over the possible flow regimes is still missing. Moreover, the complexity is given by the difficulty on measuring the evolving particle-size distribution and quantitative data are still needed to calibrate and test the models.

This thesis fits into this complex context. The work deals with particle segregation in a granular flow composed of two size classes of grains and in dry condition.

With a general approach, first of all we tried to tackle the topic from a mathematical point of view. We wrote the equations of the mass and momentum balances of each particle-size class, also trying to take into account some of the most widespread hypotheses on the constitutive equations of the granular flows mechanics (chapter 1 and chapter 2).

Then, we analyse the process of segregation in a binary mixture running in a laboratory flume with transparent lateral walls. The experimental set-up and the measuring techniques are addressed in chapter 3.

Chapter 4 and chapter 5 present the analysis of the experiments. Chapter 4 describes as the statistically and stationary uniform flow condition is present also in the case of a binary mixture. Chapter 5 tackles the effects on the flow parameters of the feeding discharge with different flow rates. In chapter 6 the analysis of the experimental data is presented.

Chapter 1

Granular flows

This chapter addresses the problem of the granular flows composed by uniformly sized particles. Three types of regimes are identified. We examined the constitutive equations that according to different models can be adopted to explain the mechanics of the granular flows driven by gravity.

1.1 Introduction to granular flows

Many massive geophysical flows are classified as *granular flows*. These can be defined as an agglomerate of macroscopic particles that show specific features with respect to the standard state of the matter. In the analysis of the granular flow we distinguish two kinds of interstitial fluids. In debris flows, the interstitial fluid is liquid, that plays a key role on the mechanics of the flow. In dry granular flows, such as rock or snow avalanches, the interstitial fluid is air, that often can be neglected.

Generally granular flows do not have a similar behaviour neither to gas, fluid or solid, rather it is appropriate to consider them as another state of the matter (Jager [36]). Firstly, they differ from gases because the temperature has no influence on their motion and the interactions between the particles are dissipative both for frictional and collisional forces. Also, they differ from liquids as they segregate. Finally, they differ from solids as they result similar to them only in static condition, so the analogy is valid only if the slope of the material is under the friction angle of the granular mass [36]. Moreover they are characterized by different regimes, that depend on the concentration of the solid particles and the type of contact between the particles.

In granular flows the friction and the collision among the particles are the main cause occurring during the moving and stopping phase. The flow resistance is given by the collisions between the particles. Mainly, granular flows are characterized by the prevalence of the kinetic forces of collisional type and due to the particle collisions, the velocity field of the flow is rather variable and complex and it is not possible to define a laminar shear layer at a macroscopic phase. Besides, the granular flow analysis requires focusing on many aspects: the interactions between the particles and the interstitial

fluid, the interaction between boundary, particles and fluid, the interactions among particles of different grain-size classes.

Many geophysical phenomena have been studied in the light of the fluid mechanics of granular material. These phenomena are mostly gravity driven granular flows, with a wide particle-size dispersion. Among these, it is worth mentioning the interpretation through the principle of the mechanics of granular fluids of debris flows and snow avalanches: analysis initiated since many decades. Using a one-phase model for the analysis can properly describe the behaviour of the interstitial fluid (Chapman and Cowiling [20], Jenkins and Hanes [38]).

Bi-phase models are better suitable for the correct description of the physical mechanisms and many of these models are present in the literature. Armanini et al. [8] suggested treating the debris flows as a hyperconcentrated flow composed of two fluids: the interstitial fluid and the granular fluid. The interstitial fluid can be studied by applying the hydraulics laws and normally it is considered water at room temperature, which follows the Navier-Stokes equations. The granular flow corresponding to the solid phase can be treated as a continuum fluid with a proper rheological law, that can describe the interactions among the particles. The rheological law considers the two different mechanisms of the particle interaction, that can be instantaneous or long-lasting (Armanini et al. [8]).

1.2 Mechanics of dry granular flows

The particle dynamics becomes essential in granular flows. Mainly three types of flow regimes can be distinguished in granular flows driven by gravity according to the concentration of the material and the type of contact between the particles [48], even if several classifications are proposed, that

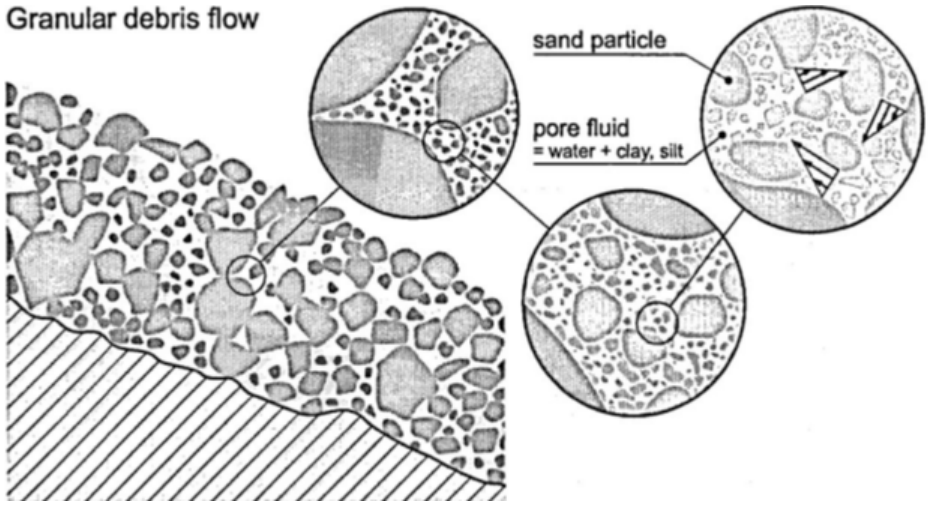

Figure 1.1: Schematic representation of a granular debris flow [35].

are typically more complex and less effective in describing the physical process.

- *The collisional regime:* nearly instantaneous collisions between particles characterize this regime and the most convincing constitutive equations are derived by the dense gas analogy (kinetic theory), which also takes into account the dissipative nature of granular flows.

- *The frictional or quasi-static regime:* the contacts among particles are quasi-permanent, and the concentration of the particle is close the packing concentration. In general it can be modelled by a Columbian friction model. In the literature the distinction between the quasi-static regime and the frictional regime is not clear yet.

- *The intermediate region:* it is an intermediate regime between the two, in which there are prolonged contacts alternating with short

contacts and collisions. The approach to this type of regime is still controversial. In this case both shear-dependent approaches, which treat the flow as that of a viscous fluid, and shear-dependent approaches, which use modified version of the Coulomb shear model, are used.

These aspects are very important to correctly define the dynamics and the kinematics of the granular flows. For each of these regimes specific rheological relations are proposed. These relations, inserted in the mass, momentum and energy balances allow to obtain an exhaustive and complete system of differential equation, that, with a numerical integration, gives the evolution of the flow field.

In this work we investigate whether similar regimes can be observed in a binary mixture and how segregation of particles of different size can influence and can be affected by them.

The main theories for the three different regimes are presented in the following sections.

1.3 Collisional regime

In the collisional regime, the instantaneous collisions between particles prevail over long-lasting contacts. Moreover, due to the rebounds of the particles, the volume concentration can be significantly lower than the maximum packing concentration that characterizes the material at rest. Often in this regime the motion is assimilated to that of a gas (granular gas Goldhirsch [27]). The particles are dispersed in a fluid and they move independently of each other. Collisions between grains are only instantaneous and binary in nature. We refer to *Bagnold* [11] for the first studies of the rheology of granular materials. In his experiments, he found that the normal and

shear stress are proportional to the shear rate and related by a Coulombian relation, that depends on the friction angle of the material. The main limitation of his theory is that a constant particle concentration is assumed across the flow depth. In order to overcame this limitation, the kinetic theory of dense gas is considered, as the molecules in gas can be assimilated to the particles in granular flows and both can move in every direction (Campbell [18], Goldstein and Shapiro [28], Goldhirsch [27]). These theories were expanded mainly by Jenkins and Richman [40], Jenkins and Hanes [38] and Jenkins and Savage [41], who consider mass, momentum and energy balance equations in order to derive a continuum model (macroscopic scale) starting from the individual particles (microscopic scale).

The Bagnold theory and the kinetic one differ mainly in the assumption on the scale velocity $[\mathcal{U}]$ which characterizes the apparent viscosity of the granular fluid. Bagnold assumes a scale velocity associated with the shear velocity $\dot{\gamma}$, i.e. $[\mathcal{U}] \propto \dot{\gamma} d$ (d is the particle diameter), while kinetic theory adopts the granular temperature T, that is $[\mathcal{U}] \propto \sqrt{T}$. The granular temperature T is the kinetic energy per unit mass of the fluctuating component of the particles velocity. This variable, which measures the agitation of the particles, also influences the pressure and, therefore, the state equation of the granular material.

1.3.1 Bagnold's theory

Bagnold [11] carried out a series of experiments on granular motions involving water and solid particles composed of wax, which therefore had similar density as water. He noted that the collision among particles generates a dispersive pressure that depends essentially on the mean distance between the grains s. This distance is expressed as a function of the *linear concentration* $\lambda = d/s$, where d is the particle diameter. For spherical particles

the linear concentration is related to the volume concentration:

$$\lambda = \frac{c^{1/3}}{c_*^{1/3} - c^{1/3}} \tag{1.1}$$

where c is the volumetric concentration of the particles and c_* is the maximum possible concentration, refereed to as the *packing concentration*.

Bagnold assumed that the dispersive pressure is function of this linear concentration. The relation between the shear stress τ and the normal stress p is of Coulombian type:

$$\frac{\tau}{p} = \tan\varphi \tag{1.2}$$

where φ is the friction angle of the material. Moreover, Bagnold defined a non-dimensional parameter, the *Bagnold number*:

$$\mathrm{Ba} = \frac{\rho_s \lambda^{1/2} d^2 \dot{\gamma}}{\mu_f} \tag{1.3}$$

where ρ_s the density of the solid material and μ_f the dynamic viscosity. This parameter represents the ratio between the apparent collisional stresses occurring due to the collisions among the grains and the viscous stresses appearing in the interstitial fluid.

Bagnold distinguishes the *grain inertia regime*, in which the viscous stress are greater than the dispersive pressure caused by the collisions, and the *macro viscous regime*, where the inter-granular collisions are rather significant. In his experiments with spherical particles, Bagnold found a different expression for the tangential shear stress and distinguished the grain inertia regime for $Ba < 40$ and the macro viscous regime for $Ba > 450$.

However, all the experiments on gravity driven granular motions, such as uniform motions in channels, show that the distribution of concentration

along the depth of the flow is not uniform, contrary to Bagnold's hypothesis. Experiments conducted on an erodible bed [6] also show that the concentration tends to zero at the free surface and monotonically increases towards the bed, where it assumes its maximum value.

1.3.2 Dense gas analogy (kinetic theory)

To overcome the limit of Bagnold's theory, the kinetic theory of gas was adopted to granular flows (Jenkins [37], Savage [66]). This theory assumes that an idealized granular material is flowing such that particles interact only through binary collisions with each other.

The main assumptions of the theory are:

- the gas is composed by a large number of small particles, that are in a constant random motion;
- the particles are constantly colliding each other and with the fixed walls of the container;
- the pressure derives by the collisions among the particles, that move at different velocities through a Brownian motion;
- the collision among the particles are binary.

The gas temperature is replaced with the concept of the granular temperature $T = (\overline{u_i' u_i'})/3$, where $\overline{u_i' u_i'}$ represents the average process of all the particles at each time and inside a defined control volume large enough with respect to the particles dimensions, $u_i' = u_i - \overline{u_i}$ represents the fluctuating component of the velocity vector and $\overline{u_i}$ the average component. The granular temperature changes in space and time and represents the kinetic energy of the collisional regime. The granular temperature can be generated in two different modes:

- *Collisional temperature generation:* the temperature derives from the transfer of momentum between particles when they collide and depends on the particles velocities and on the elastic coefficient of restitution;
- *Streaming temperature generation:* it is a mechanism similar to Reynolds turbulent stresses. Because of particles with different shear rates, these move from one layer to another by colliding with the particles that they meet [57]. This mode is dominant when the density is very low. The region governed by the the streaming temperature is often neglect.

In order to define the average process, the *distribution function* is introduced to express in probabilistic terms the position and the velocity of the particles in a certain range for an instant t. The *single-particle velocity distribution function* $f^{(1)}$ assumes a Maxwellian distribution:

$$f^{(1)}(r_i, u_i, t) = \frac{n}{(2\pi T)^{3/2}} \exp\left(\frac{(u_i - u_i')^2}{2T}\right) \tag{1.4}$$

where r_i is the position of the particle and u_i the velocity at each instant t.

The *ensemble average* for the generic single-particle property $\overline{\Psi}$ for n number of particles for unit volume is defined as:

$$\overline{\Psi} = \frac{1}{n} \int_{-\infty}^{+\infty} \Psi f^{(1)}(r_i, u_i, t) \mathrm{du} \tag{1.5}$$

As the particles interact with each other, the theory introduces also a *pair distribution function* $f^{(2)}$ to express the probability to find a pair of particles in a certain range of positions.

The kinetic theory defines the conservation equations starting from the Boltzmann equation, that has the following general formulation:

$$\frac{\partial f}{\partial t} + \frac{\partial r_i}{\partial t}\frac{\partial f}{\partial r_i} + \frac{\partial u_i}{\partial t}\frac{\partial f}{\partial u_i} = \frac{\partial f}{\partial t} + u_i \frac{\partial f}{\partial r} + \frac{F_i}{m}\frac{\partial f}{\partial u_i} = \Phi_c \tag{1.6}$$

where f is the distribution function. If the right hand side term was zero, the eq. (1.6) would express that the particle density is constant (the variation of the distribution function is zero). In our case, the trajectories of the particles are not continuous and the distribution function varies: the term Φ_c considers the contribution of the collisional forces.
The final system of constitutive equations of the model is derived by the Enskog's equation of change, that consists in the Boltzmann equation multiplied by the property Ψ and then the ensemble averaged process is applied:

$$\frac{\partial}{\partial t}(n\overline{\Psi}) + \frac{\partial}{\partial r_i}(n\overline{u_i\Psi}) - n\left(\frac{D\Psi}{Dt}\right) = \Phi_c \tag{1.7}$$

where D/DT represents the total derivative. The last term, Φ_c, represents the collisional transfer contribution Ω and the "source-like" contribution χ:

$$\Phi_c = -\nabla\Omega + \chi \tag{1.8}$$

By setting $\Psi = m$, $\Psi = m\vartheta$ and $\Psi = 1/2m\,\vartheta^2$ (m and ϑ are the mass and velocity of the particles respectively), it is possible to obtain the master equations for the granular flow, i.e. the hydrodynamics balance equations respectively for mass, momentum and energy:

$$\begin{cases} \dfrac{\partial \rho}{\partial t} + \dfrac{\partial\,(\rho\,u_i)}{\partial x_i} = 0 \\ \dfrac{\partial \rho\,u_i}{\partial t} + \dfrac{\partial\,(\rho\,u_i u_j)}{\partial x_j} = \rho\,g_i + \dfrac{\partial \mathcal{T}_{ij}}{\partial x_j} \\ \dfrac{3}{2}\rho\left(\dfrac{\partial T}{\partial t} + u_j\dfrac{\partial T}{\partial x_j}\right) = \dfrac{\partial}{\partial x_j}\left(f_4\rho_s\sqrt{T}d\dfrac{\partial T}{\partial x_j}\right) + \\ \qquad\qquad +\mu^{coll}\left(\dfrac{\partial u_i}{\partial x_j} + \dfrac{\partial u_j}{\partial x_i}\right)^2 - f_5\rho\dfrac{T^{1.5}}{d} \end{cases} \tag{1.9}$$

in which $\rho = c\,\rho_s$ is the density of the granular phase where c is the volume concentration of the solid grains and ρ_s is the density of the grain material;

μ^{coll} is a collisional dynamic viscosity, d is the diameter of the particles, u_i is i-th generic component of the velocity vector, g_i is the component of the volume force for unit mass acting on granular phase, which in the present case, is the gravity g, i.e. $g_i = -g\partial z/\partial x_i$, where z represents the vertical rising direction (opposed to the gravity vector).

$\mathcal{T}_{ij}$ is the tensor of the granular stresses:

$$\mathcal{T}_{ij} = -p\delta_{ij} + f_2\rho_s\sqrt{T}d\left(\frac{\partial u_i}{\partial x_j} + \frac{\partial u_j}{\partial x_i}\right) \tag{1.10}$$

where δ_{ij} is the Kronecker delta function and p is the isotropic collisional pressure of the granular phase, which is assumed to be dependent on the granular temperature:

$$p = f_1\rho T \tag{1.11}$$

The pressure relation is similar to the state equation of a gas $p = R\rho T$, where the thermodynamic temperature is replaced by the granular temperature. f_1, f_2, f_4 and f_5 are function of the granular volume concentration and of the inelastic restitution coefficient e. Extended kinetic theories were developed for *dense* granular flows by Jenkins [37] and Lun and Savage [69]. In table 1.1 the expression of these functions are reported according to [69] and [68].

In our approach, we neglected the interaction between the granular phase and the interstitial fluid, since its density is much smaller than that of particles. Besides, in the energy balance we have neglected the rotational energy and the spinning of particles.

One of the most important parameter of the kinetic theory is the *inelastic restitution coefficient*, that considers the not perfectly elastic collision among the particles. This coefficient e relates the normal component of the instantaneous velocity of the particles before and after collisions.

Table 1.1: Expressions of the different functions adopted in the kinetic theory equations, according to [69] and [67].

$$
\begin{aligned}
f_1 &= c\,(1 + 4c_{\,p}\,g_o) \\
f_2 &= \frac{5\sqrt{\pi}}{96\eta_p(2-\eta_p)}\left(1+\frac{8}{5}\eta_p\,c\,g_0\right)\left(\frac{1}{g_0}+\frac{8}{5}\eta_p(3\eta_p-2)c\right)+\frac{8/5}{\sqrt{\pi}}\eta_p c^2\,g_0 \\
f_4 &= \frac{25\sqrt{\pi}}{16\eta_p(41-33\eta_p)}\left(1+\frac{12}{5}\eta_p c\,g_0\right)\left(\frac{1}{g_0}+\frac{12}{5}\eta_p^2(4\eta_p-3)c\right)+ \\
&\quad +\frac{4}{\sqrt{\pi}}\eta_p c^2\,g_0 \\
f_5 &= \frac{12}{\sqrt{\pi}}c^2\,g_0(1-e^2) \\
\eta_p &= \frac{1+e}{2} \\
g_0 &= (1-c/c_*)^{-2.5c_*}
\end{aligned}
$$

Some authors extended the kinetic theories using different constitutive relations for p and $\mathcal{T}_{ij}$. The classical kinetic theory cannot be directly extended for granular flows with high concentration or with a different nature of interaction among the particles (e.g. the long-lasting contacts).

1.4 Quasi-static regime

The frictional or quasi-static regime is present when the concentration of the particles is close to the packing concentration and the contacts among the particles are long-lasting and it can involve also groups of particles. The tangential force are caused mainly by the friction between grains. Besides, sometimes the particles tend to form chains, due to the long-lasting contacts among them.

In granular flows driven by gravity the frictional regime can be observed in the lower part of the flow depth, where the concentration is close to the packing concentration. Armanini et al. [7] experimentally observed that this regime, which is generally predominant close to the loose bed, coexist with the collisional one, which is predominant in the free surface (Armanini et al. [5]). The rheological relations for this regime derive from the soil mechanics and they considered the visco-plasticity theory (Savage and Hutter [67], Pudasaini [63], Pitman and Le [60]). In this theory, the shear stress is proportional to the normal stress, which depends on the bulk density. Usually Coulomb-like laws with a shear independent behaviour are adopted for the quasi-static regime.

Johnson and Jackson [42] propose a Coulombian model for the frictional regime and, referring to a two dimensional flow along the axis x_1, x_2, the tangential stresses are expressed according to the Coulomb law:

$$\tau_{ij}^{fric} = \sigma_2 \sin\varphi \tag{1.12}$$

where σ_2 is the normal stress of the frictional part and φ is the friction angle. For the normal stresses, in particular Johnson and Jackson [42] propose:

$$\sigma_2 = \frac{a_{fr}}{(c_* - c)^n} \tag{1.13}$$

where a_{fr} is a non-dimensional constant and c_* is the packing concentration. Later Johnson [43] modified the expression assuming a minimum concentration c_{min} below which the frictional stress changing the definition of the normal frictional stress as:

$$\sigma_2 = \begin{cases} a_{fr}\dfrac{a - c_{min}}{(c_* - c)^n} & \text{if } c > c_{min} \\ 0 & \text{if } c \leq c_{min} \end{cases}$$

1.5 Intermediate regime

In a granular flow driven by the gravity, the quasi static or frictional and the collisional regime are both present in the flow motion and often there is not a clear separation between the two regimes.

In general most of the constitutive models in the literature consider the decomposition of the stress tensor in a rate independent and rate dependent contribution.

In its pioneering works, Savage and Hutter [67] expressed the stress tensor as a combination of a rate-independent Coulombian part and a rate-dependent part based on the dense gas analogy. Many other studies have proposed similar approaches, e.g. Savage [66], Johnson and Jackson [42], Johnson et al., [43], Louge, [50] and Louge and Keast, [51]. These models often assume that the flow is divided in different layers: a bulk flow and a boundary layer. The models defined different criteria for the solutions of the two types of flow, but actually the transition between the layers is gradual and not defined in a specific point as the authors pointed out. Aranson and Tsimring [2] and Bouchaud et al. [14] described the transition of the flow with a series of parameters and equations for the flow and shear stress, but again they consider a sharp division, differently from the real cases where rolling grains and static ones coexists.

More recently, GDR-MiDi group [26, 45] proposed an empirical model commonly referred as $\mu(I)$ model. The model derives from a series of experiments conducted by GDR-MiDi group and it is essentially based on the *inertial number*:

$$I = \frac{\dot{\gamma} d}{\sqrt{p/\rho_s}} \tag{1.14}$$

This non-dimensional number is the ratio between two time scales: the microscopic deformation scale ($\dot{\gamma}^{-1}$) and the inertial time scale ($\sqrt{d^2\rho_s/p}$),

where $\dot{\gamma}$ is the shear rate, d is the particle diameter and p the confining pressure. The *Inertial number* is equivalent to the square root of the Savage number.

The model assumes that the ratio between the normal and tangential stresses is a function of the Inertial number I:

$$\tau = \mu(I)p \tag{1.15}$$

where the parameter $\mu(I)$, according to a series of experiments, is given by:

$$\mu(I) = \mu_s + \frac{\mu_2 - \mu_s}{I_0/I + 1} \tag{1.16}$$

where μ_s and μ_2 are the tangent of the static angle and the dynamic angle of the flow respectively and I_0 is a constant depending on the properties of the flowing material. Through the $\mu(I)$ parameter, the model describes both the quasi-static regime ($I \to 0, \quad \mu(I) = \mu_s$ and the frictional regime ($I > I_0 \quad \mu(I) = \mu_2$).

As observed by Armanini et al. [8], the $\mu(I)$-model can be interpreted as a weighted combination of two Coulombian models:

$$(I_0 + I)\frac{\tau}{p} = I_0 \tan\varphi_s + I \tan\varphi_2, \tag{1.17}$$

One model is applied on the bed, with the static friction angle φ_s and the second one is applied at a somewhat arbitrary point far from the bed, where the friction angle φ_2 is assumed. I and I_0 can be interpreted as weighting functions. It can be observed that, while the first angle is a property of the material, the second angle is expected to be a property also of the flow field, while, according to the model, it should be known *ex ante*. However, the same research group [45] proposed a linear relationship between the inertial parameter and the particle concentration $c = c_* - (c_* - c_{min})I$, where c_*

is the random packing concentration and c_{min} the minimum concentration, that should also be known *ex ante*.

The $\mu(I)$-model is a structurally very simple model, nevertheless applied in the absence of a collisional regime, as observed by the same authors [44]. Therefore, it has the limit of applicability in conditions in which the concentration is reasonably constant.

A model that consider both the frictional and the collisional regime was proposed by Armanini et al. [8] and it is called *heuristic* model. According to these authors, the two regimes alternate in space and time, through a mechanism defined as *intermittency*, similar to that of a border of a turbulent boundary layer. The theory is based on the two-phase approach, in which each phase is defined as as a continuum and the kinematic properties of the flow are expressed by the *Savage number*, equal to the ratio between the shear independent stress and the shear dependent stress and coincides with the square of the inertia number I:

$$I_s = \frac{\rho_s(\dot{\gamma}d)^2}{p^g} \tag{1.18}$$

The tangential component satisfies two conditions: approaching the bed the flow tends to a pure Coulombian motion, while, on the other hand, for high values of I_s the frictional regime becomes zero. The tangential component for the frictional regime is expressed by the following formulation:

$$\tau^{fric} = p^g \tan\varphi^{fric} \frac{I_{s0}}{I_s + I_{s0}} \tag{1.19}$$

where p^g is the granular pressure, φ^{fric} is the friction angle of the material and I_{s0} is a parameter depending on the material properties. A similar formulation states the frictional pressure depending on the Savage number:

$$p^{fric} = p^g \frac{I_{s0}}{I_s + I_{s0}} \tag{1.20}$$

The model was experimentally tested in a uniform flow of a mixture of constant spherical particles and water. In figure 1.2 the friction angle along the non-dimensional vertical coordinate is plotted. We can observe that the friction angle tends to the static value close to the bed. In contrast, near the free surface the behaviour is similar to the one predicted by kinetic theory [8].

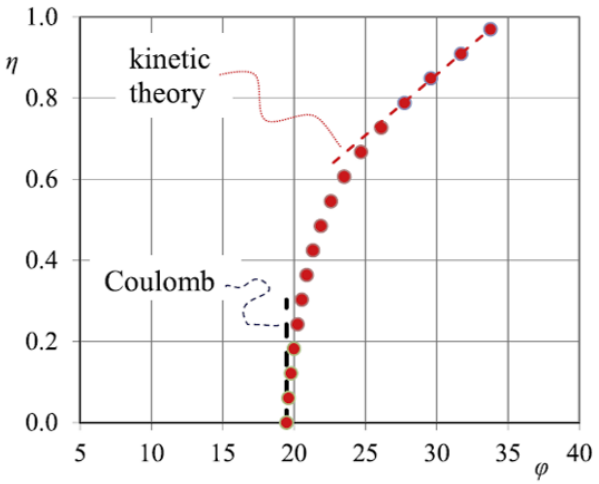

Figure 1.2: Distribution of the friction angle φ in a uniform channel flow mixture of spheres and water along the dimensionless flow depth η (Armanini et al. [8]).

Chapter 2

Segregation in granular flows

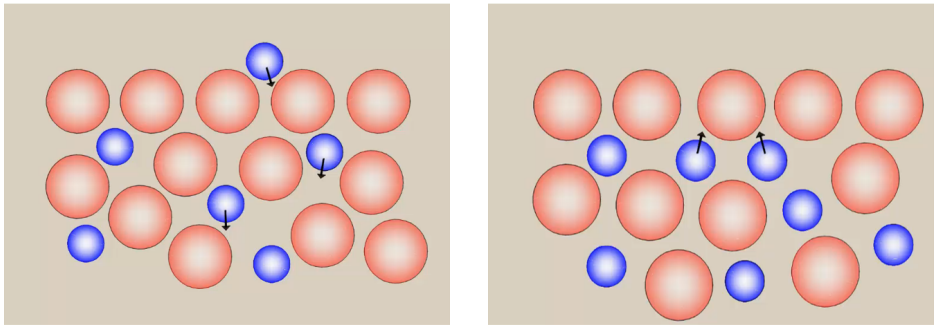

This chapter tackles the problem of particles segregation. The mechanisms governing the phenomenon are explained and a general approach to the mechanics of non-uniform granular transport is proposed along with the closure relations for a two-phases approach. The final part of the chapter explores some aspects of particles segregation processes with reference only to the conservation equation of the solid masses of the grain fractions.

2.1 Introduction

Segregation is a mechanism that involves all the particles of the mixture of granular flows of non uniformly sized particles. In general, materials segregate when they flow and are shaked, vibrated or sheared. We can observe this behaviour in the so-called "Brazil-nut" effect: the large particles rise to the top of a shaken container of mixed nut (Ottino and Khakar [59]). Snow avalanches or debris flow, with their widely dispersed grain size distribution, can be described as heterogeneous mixtures of particles of different size, density and shape (Rosato and Blackmore [64]) and then they are subject to segregation.

The presence of different phases, under the action of gravity as well as granular temperature gradients cause the phenomenon of particle-size segregation and particle grading. According to Bridgewater [**?**], the bulk solid evolves spatially in a non-uniform state, up to the complete separation of the phases. The consequences of this phenomenon are quite evident in the field observations of snow avalanche and debris flow deposits, as well as in many laboratory experiments (e.g. Bagnold [11], McElewaine and Nishimura [53], Vallance and Savage [76], Mandal and Khakhar [52], Lorenzini and Mazza [49]).

If we observe the snow avalanches, particle segregation becomes evident, with two superimposed layers: a snow cloud layer at to the surface and a dense snow flowing layer at the bottom. Usually the snow cloud moves faster and farther than the dense part and it may be the cause of serious damages in the run-out area [54]. Segregation acts differently in type of snow avalanches, resulting in a different grain distribution of the avalanche fronts since in the wet avalanches there is a larger production of large grains than in dry ones [12]. In case of fast-moving dry snow avalanches, field ob-

servations show that the bigger particles arrive at the top of the flow and they are afterwards transported to the front due to the high velocity at the surface. The well-sorted granular mixture in the font of dry avalanches indicates the vertical segregation (Bartlet and McArdell [12]). The mobility feedback influences the avalanche run-out distance, that is a critical parameter in the hazard mapping, as the avalanche run-out distance is increased by the formation of the lateral levees (Van der Vaart et al. [78]).

The effects of segregation are observed also during the development of a debris flow. A vertical grading moves the largest blocks near the free surface and the coarser particles to the front. At the same time a lateral grading forms lateral levees (Ottino and Khakahr [59], Goujon et al. [29], Pouliquen et al. [62]) that again have a strong influence on the deposition.

The bed-load sediment transport in rivers also exhibit a grain segregation, which, however, is quite different from that of massive granular flows. In rivers, the grain size of the material transported as bed-load is finer than that which makes up the bed (also called bed-layer), while the material below this layer is thinner. This phenomenon is known as dynamic armoring (Armanini [4]). Frey and Church [24] tried to applied a segregation mechanism to the bed load in rivers.
Last but not least, segregation mechanism is also observed in industrial process, as it represents the main problem causing the non-uniformity of the product (Hill [34]).

Segregation is widely studied, as the difficulty on measuring the distribution of the particle during the flow motion cannot be neglected. Literature and experiments on granular flows are quite numerous, but understanding the mechanisms between the bulk mobility and size-segregation is still an open issue, also in order to predict correctly the behaviour of the avalanches and debris flows [78].

2.2 The mechanisms of segregation in a granular flow mixture

Segregation is a combination of mechanisms, which makes this phenomenon so complex to analyse [16]. The phenomenon is influenced by many variables: the property of the particles and their distribution, the environmental conditions, the shape, the geometry, the elasticity and the density of the particles, the morphology of the flow field and the friction among the particles. The two more relevant aspects of segregation in the granular flows are the *size* and the *density* of the granular particles, but size-segregation has a predominant aspect [64].

In its pioneering work, Bridgwater and co-workers [16, 22] performed a series of experiments developed by considering the behaviour of a layer of particles subjected to a shear strain under normal condition of packing and normal stress. He found that the mechanics of segregation is influenced mainly by the void fraction created by the particles movement. Moreover, Bridgwater established that the most important parameter controlling segregation is the grain-size ratio. According to the rates of strain existing in the failure zone, different types of particle segregation are distinguished: (i) *inter-particle percolation*: the particles percolate due to the opening and the closure of the voids created by the motion of the particles; (ii) *particle migration*: the particles of larger dimensions tend to go in the direction of the increasing shear stress; (iii) *free surface segregation*: near the surface the largest particle float and the smallest one sink.

In granular flow mixture the predominant segregation process is given by the difference in the size of the particles while the density difference is less important (Bridgewater and co-workers [16], Vallance and Savage, [76]). Vallance and Savage [76] conducted experiments with different den-

sities of the particles but same diameter and found that denser particles are segregated to the bottom. However, they underline that particle density-segregation is weaker than particle size-segregation, except at high-inclination angles [30]. These works shows also that the gravity is the principal force in driving mechanisms for segregation in dense sheared flow, particle size-segregation decreased with viscous interstitial fluid.

Savage and Lun [69] investigate the mechanisms of size segregation during the relatively slow flow of dry particles of equal mass density down a rough inclined chute. With these gravity-driven chute flow experiments, similar to Bridgwater's [16], they identified the mechanisms responsible for the particle transfer: the random fluctuating sieve and the squeeze expulsion. Xiao et al. [80] found that the same mechanisms can be identify in case of density segregation. In figure 2.1, obtained by [80], the two particle transfer mechanism are identified: the first row of pictures is representative of the *kinetic sieving* where the steel particle falls into a void generated by surrounding particles; the second row of pictures refers to the *squeeze expulsion* where a ceramic particle is squeezed up into a void in the surrounding particles.

2.2.1 Random fluctuating sieve

This mechanism occurs when the smaller grains percolate due to gravity through the smallest cavities formed by the largest particles. Savage and Lun [69] defined this process as "a gravity-induced, size-dependent, void-filling mechanism". The contact force and the void spaces in the flow motion are continually changing, so at each instant the void spaces is redistributed. If a void space is large enough, a particle from the layer above may fall into it [69] (see first row of pictures in figure 2.1).

This process is sometimes defined as *percolation* or *kinetic sieving* and it was observed firstly by Middleton [56]. The particles have equal probability to be squeezed and the mechanism maintains constant the solids volume fractions of the mixture [26]. Gray [30] pointed out that this mechanism can be direction preferential, as the gravity force is essential for the small grains to fall into the gaps among the larger grains.

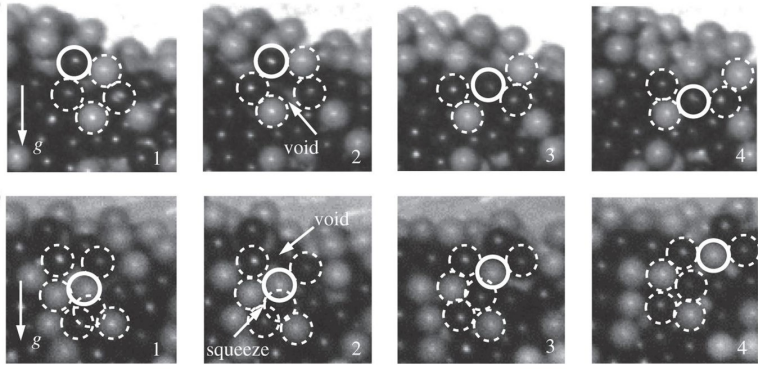

Figure 2.1: Experimental observation of density segregation of 3 mm steel and ceramics particles [80].

2.2.2 Squeeze expulsion

In this case the particles are squeezed upwards, due to imbalances in contact forces on an individual particle, as in the second row of picture in figure 2.1. Savage and Lun [69] assumed that this mechanism is not size preferential neither there is preferential direction for the transfer between layers, since it happens when the instantaneous forces acting on individual particle are imbalanced, so that a particle is squeezed out of its layer and goes to the close one. The authors assume that this mechanism is not size preferential

and there is no a preferential direction for the transfer between layers.

2.3 General approach to mechanics of non-uniform granular transport

Most of existing models for segregation in bi-disperse mixtures present in the literature show a similar structure based on the mass-balance equation, that results in an advection-diffusion equation.

Let us consider a granular flow composed by a mixture of n grain-size classes of particles, each of them denoted the index β. The dynamic of the each single class fraction β is described by the Cauchy equations, already introduced in section 1.2, for the uniform granular material [13]:

$$\begin{cases} \dfrac{\partial \rho^\beta}{\partial t} + \dfrac{\partial \left(\rho^\beta \, u_i^\beta\right)}{\partial x_i} = 0 \\ \dfrac{\partial \rho^\beta \, u_i^\beta}{\partial t} + \dfrac{\partial \left(\rho^\beta \, u_i^\beta \, u_j^\beta\right)}{\partial x_j} = \rho^\beta \, g_i - \dfrac{\partial p^\beta}{\partial x_i} + \dfrac{\partial \tau_{ij}^\beta}{\partial x_j} + \sum_1^n \Xi_i^{\beta\kappa} + F_i^\beta \end{cases} \tag{2.1}$$

where $\rho^\beta = c^\beta \, \rho_s$ is the density of the single class where c^β is the volume concentration of the class β and ρ_s is the material density of the grains; u_i^β is the generic component of the velocity vector of the class; g_i is the component of the volume force (per unit mass) acting on each class, which, in the present case, is the vector of the gravity acceleration g, i.e. $g_i = -g\partial z/\partial x_i$, where z represents the vertical rising direction; τ_{ij}^β and p^β are the granular tensor of the internal stresses and the granular pressure among the particles of the same class respectively; $\Xi_i^{\beta\kappa}$ is the component of the vector of the forces exerted by the other classes on the grain size class β. F_i^β is the component of the forces exerted by the interstitial fluid on class β. Since in our case the interstitial fluid is composed of air with a density much lower

than the solid particles and a speed similar to the solid phase, this term will henceforth be neglected.

2.3.1 Rheological relations

As already done in chapter 1 for the homogeneous material, the tangential stress and the pressure can be expressed as the sum of two contributions, a collisional and a frictional part.

The same assumptions are considered valid for the non-homogeneous case. The shear stress of each grain-size class β is:

$$\tau_{ij}^{\beta} = \tau_{ij}^{\beta-coll} + \tau_{ij}^{\beta-fric} \tag{2.2}$$

The frictional or quasi-static regime is present when the concentration of the particles is close to the packing concentration and the contacts among the particles are long-lasting and can involve also a group of particles. For the frictional regime, the theories presented in chapter 1 can be extended also in case of non-homogeneous material.

By following the authors [37, 10] that extended the theory for inelastic shearing of disks to spheres, the dense gas analogy provides appropriate constitutive relations for the collisional component.

We will present in the next pages the constitutive relations for each individual class for the collisional regime valid in case of dilute granular flow.

Pressure. The constitutive relation for granular pressure is:

$$p^{\beta-coll} = f_1^{\beta}\, T^{\beta} \tag{2.3}$$

with:

$$f_1^{\beta} = 1 + 4\,\eta_p \sum_{\beta=1}^{n} c^{\beta} g_o^{\beta} \tag{2.4}$$

where T^β is the granular temperature of each grain size β $T^\beta = (\overline{u_i' u_i'})^\beta/3$ and g_o^β is the radial distribution function of each grain size β. We highlight the similarity between this constitutive relation and that for the homogeneous material (Table 1.1).

Granular shear stresses. The collisional shear stress, in analogy with the procedure used in the kinetic theory for a mono-granular material, is [13]:

$$\tau_{ij}^{\beta-coll} = \mu^{\beta-coll}\left(\frac{\partial u_i^\beta}{\partial x_j} + \frac{\partial u_j^\beta}{\partial x_i}\right) \tag{2.5}$$

with:

$$\begin{aligned}\mu^{\beta-coll} \;=\; & \frac{2+\alpha}{3}\left[\mu^{\beta*-coll}\frac{1}{g_o^\beta\,\eta_p(2-\eta_p)}\left(1+\frac{8}{5}\eta_p\sum_{\beta=1}^{n}(c^\beta\,g_o^\beta)\right)\times\right.\\ & \left.\left(1+\frac{8}{5}\eta_p(3\eta_p-2)\sum_{\beta=1}^{n}(c_\kappa\,g_o^\beta)\right)+\frac{3}{5}\eta_p\mu_b\right]\end{aligned} \tag{2.6}$$

where:

$$\mu^{\beta*-coll} = c^\beta\,\rho_s\,g_o^\beta\,T^\beta\frac{\mu}{\rho_s\,T^\beta\left(\sum_{\beta=1}^{n}c_\beta g_o^\beta\right)}$$

$$\mu = \frac{5}{96}\rho_s\,d^\beta\left(\pi\,T^\beta\right)^{1/2} \tag{2.7}$$

$$\mu_b = \frac{256}{5\pi}\mu\,c^\beta\left(\sum_{\beta=1}^{n}c^\beta g_o^\beta\right) \tag{2.8}$$

$$\tag{2.9}$$

Agrawal et al. [1] recommend to use $\alpha = 1.6$.

Inter-classes forces. These forces are the interactions between the generic class κ and the class β. According to Benyahia et al. [13] the generic component of this force vector between the single class and other particle classes is:

$$\Xi_i^{\beta\kappa} = \xi^{\beta\kappa}\rho_s\left(u_i^{\kappa} - u_i^{\beta}\right)|\mathbf{u}^{\beta} - \mathbf{u}^{\kappa}| \tag{2.10}$$

with the coefficient $\xi^{\beta\kappa}$:

$$\xi^{\beta\kappa} = 3(1+e)\left(\frac{\pi}{2} + c^{\kappa\beta}\frac{\pi^2}{8}\right)\frac{\left(d^{\beta} + d^{\kappa}\right)^2}{2\pi\left(d^{\beta 3} + d^{\kappa 3}\right)}\rho_s {g_o}^{\kappa} \tag{2.11}$$

where d^{β} is the diameter of the grain size class β, d^{κ} the one of the grain-size class κ and e the elastic restitution coefficient of the particles.

Dissipation of kinetic energy. The rheological terms concerning the equation of the kinetic energy of the grains (Eq.2.13) is:

$$f_5^{\beta} = c^{\beta}\frac{48}{\sqrt{\pi}}\eta_p(1-\eta_p)\left(\sum_{\beta=1}^{n} c^{\beta} g_o^{\beta}\right) \tag{2.12}$$

where n is the number of grain classes. We underline that this term is analogous to that of the mono-granular material (table 1.1).

2.3.2 Kinetic energy balance

As already stated, in order to close the problem, it is necessary to write the kinetic energy balance as a function of the granular temperature, that is the crucial parameter in the collisional regime accounting for the collisions of the particles. Similarly to homogeneous granular fluids, the velocity scale

of the diffusion processes of the single class is represented by the granular temperature of the class, i.e. T^β.
By following a procedure analogous to that tackled in section 1.3.2 (chapter 1), the kinetic energy balance of the single class β is:

$$\frac{3}{2}\rho_s\left(\frac{\partial c^\beta T^\beta}{\partial t}+\frac{\partial c^\beta u_i^\beta T^\beta}{\partial x_j}\right)= \\ =\frac{\partial}{\partial x_i}\left(k_\beta\frac{\partial T^\beta}{\partial x_i}\right)+\tau_{ij}^\beta\frac{\partial u_i^\beta}{\partial x_j}+\Pi_f^\beta-f_5^\beta\rho_s\frac{(T^\beta)^{1.5}}{d^\beta} \quad (2.13)$$

where T^β is the granular temperature of the each single grain size class β, k_β is the diffusion coefficient of the granular temperature. The term Π_f^β represents the kinetic energy exchange between the fluid and the size class β. However in our case it can be neglected for the same reason as F_i^β (component of the forces exerted by the interstitial fluid on class β).
The balance equation reduces to:

$$\frac{3}{2}\rho_s\left(\frac{\partial c^\beta T^\beta}{\partial t}+\frac{\partial c^\beta u_i^\beta T^\beta}{\partial x_j}\right)= \\ =\frac{\partial}{\partial x_i}\left(k_\beta\frac{\partial T^\beta}{\partial x_i}\right)+\tau_{ij}^\beta\frac{\partial u_i^\beta}{\partial x_j}-f_5^\beta\rho_s\frac{(T^\beta)^{1.5}}{d^\beta} \quad (2.14)$$

The above relations (for pressure, granular shear stress, inter-classes forces) are the closure relations to the system 2.1. By adding the kinetic energy balance equation for the granular temperature, the system results close and complete.

2.4 Simplified models of particles segregation

In this section we describe simplified models for segregation. The first section presents a general approach considering Reynolds decomposition. The following ones present some of the relevant works in the literature.

2.4.1 Mass balance of the solid phases

We consider the mass conservation equation of the single class β (Eq. 2.1) for the two dimensional case where the axes are x_1 and x_2:

$$\frac{\partial c^\beta \rho_s}{\partial t} + \frac{\partial (c\rho_s u)^\beta}{\partial x_i} = 0 \tag{2.15}$$

where ρ_s is the density of the solid phase and c^β is the volume fraction of each solid class β. Since the solid phase density is constant, it can be neglected from each terms so the mass balance equation for each solid phase β reduces to:

$$\frac{\partial c^\beta}{\partial t} + \frac{\partial (cu_i)^\beta}{\partial x_i} = 0 \tag{2.16}$$

We assume that the state variables of the governing equations, so the concentration of the particles c^β and the velocity u^β, are equal to the sum of an average variable and a fluctuating variable (Reynolds' decomposition):

$$\begin{aligned} c^\beta &= \overline{c^\beta} + c'^\beta \\ u_i^\beta &= \overline{u_i^\beta} + u_i'^\beta \end{aligned} \tag{2.17}$$

with the average value considered as:

$$\overline{c^\beta} = \frac{1}{T} \int_{t_0+\frac{T}{2}}^{t_0-\frac{T}{2}} c^\beta dt$$

for $T \to \infty$. The decompositions (2.17) are inserted in the mass balance equation (2.16) and the resulting equation is then averaged. After some simple mathematical manipulation the resulting equation is:

$$\frac{\partial(\overline{c^\beta} + \overline{c'^\beta})}{\partial t} + \frac{\partial(\overline{c^\beta}\,\overline{u_i^\beta} + \overline{c'^\beta u_i'^\beta})}{\partial x_i} = 0 \tag{2.18}$$

The average of the fluctuating terms can be neglected as it is zero for definition of fluctuation and T is greater than the time scale of the fluctuations, so the result is:

$$\frac{\partial \overline{c^\beta}}{\partial t} + \frac{\partial(\overline{c^\beta}\,\overline{u_i^\beta} + \overline{c'^\beta u_i'^\beta})}{\partial x_i} = 0 \tag{2.19}$$

In the case of a statistically homogeneous flow in the direction $i = 1$ and in the hypothesis that the axis x_2 is vertically upward oriented, eq. (2.19) reduces to:

$$\frac{\partial \overline{c^\beta}}{\partial t} + \frac{\partial(\overline{c^\beta}\,\overline{u_2^\beta} + \overline{c'^\beta u_2'^\beta})}{\partial x_2} = 0 \tag{2.20}$$

The term $\overline{c'^\beta u_2'^\beta}$ in the eq. (2.20), assuming the *convection-diffusion hypothesis*, is defined as:

$$\overline{c'^\beta u_2'^\beta} = -\xi_2^\beta \frac{\partial c}{\partial x_2} + I_2^\beta \tag{2.21}$$

where ξ_2^β is the *diffusion coefficient* in the x_2 direction and I_2^β is the *infiltration coefficient*. These two terms express the diffusion and infiltration processes occurring in segregation. The diffusion process describes the kinetic sieving mechanism while the infiltration process is related to the percolation mechanism of the particles.

With the diffusive-convective hypothesis the mass balance equation (2.19) becomes:

$$\frac{\partial \overline{c^\beta}}{\partial t} + \frac{\partial}{\partial x_2}\left(\overline{c^\beta}\,\overline{u_2^\beta} - \xi_2^\beta \frac{\partial \overline{c^\beta}}{\partial x_2} + I_2^\beta\right) = 0 \tag{2.22}$$

where $\overline{c^\beta}$ is the average concentration of the particle class β.

2.4.1.1 The diffusion coefficient

The diffusion mechanism is responsible for the transfer among different grain size classes in the granular mixture. It acts on the velocity of the particles causing the mechanism of the kinetic sieving and it occurs mainly due to the particles agitation. This diffusive flux:

$$-\xi_2^\beta \frac{\partial c}{\partial x_2} \tag{2.23}$$

is proportional to the *diffusion coefficient* ξ_2^β with dimension $[\mathrm{L}^2\mathrm{T}^{-1}]$. Its definitions is not trivial and in many cases it is considered constant and calibrated according to numerical and physical granular flow experiments.

The diffusion process, in general, is scaled respect to a *length scale* $[\Lambda]$ and a *velocity scale* $[\mathcal{U}]$:

$$\xi_2^\beta = \mathrm{f_D}[\mathcal{U}][\Lambda] \tag{2.24}$$

where f_D is a pre-factor that can be or not a constant. Ottino and Khakhar [59] assumed f_D as a function of the particles restitution coefficient e. Sometimes ξ_2^β is kept as a constant (Wiederseiner et al.[79], Gray and Chugunov [32]). In particular Schlick et al. [70] compared the results by assuming ξ_2^β constant and by assuming as a function of the shear stress. They found that considering ξ constant gives good results for computing the segregation flux, but the value of the constant seems depending on the boundary conditions.

Most of the work in literature consider $[\mathcal{U}]$ equal to $\dot{\gamma}d$, where $\dot{\gamma}$ is the shear rate (Bridgewater [16], Campbell [18], Utter and Behringer [15], Tripathi and Khakar [75]). Sometimes the velocity scale is defined as $\sqrt{T}$, where T is the granular temperature (Arnarson [2], Larcher and Jenkins, [47]). Dolgunin and Ukolov [21]) assume for $[\mathcal{U}]$ the intensity of the fluctuating longitudinal component of particle velocity $(\overline{u_x' u_x'})^{1/2}$.

As length scale $[\Lambda]$ the particle diameter is generally assumed (Utter and Behringer [15], Gray et al. [30], Fan et al. [23], Van der Vaart et al., [77]).

2.4.1.2 The infiltration coefficient

The infiltration process expresses the percolation mechanism and has dimension of a velocity $[LT^{-1}]$. It is assumed as:

$$\mathcal{I}_2^\beta = \mathrm{f_I}\, u_2 \tag{2.25}$$

where u_2 is the *percolation velocity* along the vertical direction and $\mathrm{f_I}$ a segregation rate coefficient. Dolgunin e Ukolov [21] define the *infiltration coefficient* as a reflection of the influence of the particle non-uniformity on the segregation intensity depending on the conditions of the particle interactions in the flow. The *percolation velocity* accounts for the relative motion between each grain-size class in the vertical direction.

Dolgunin and Ukolov [21] express the infiltration coefficient depending on the velocity of the particle in the vertical direction, determined experimentally, and $\mathrm{f_I}$ equals to a segregation force M that depends on the physical and mechanical properties of the bulk particles and the particle diameter.

Fan et al. [23] and Shlick at al. [70] assume the infiltration coefficient proportional to a constant value S (length scale), the percolation velocity equal to the shear rate $\dot{\gamma} = \partial u_2/\partial x_2$ and $\mathrm{f_I} = (1 - c^\beta)$ where c^β is the concentration of each grain-size class.

Van der Vaart [78] and Wiederseiner et al. [79] consider the infiltration coefficient as the product between a velocity u_2 (the maximum segregation speed or the average velocity of the bulk solid) and $\mathrm{f_I} = c^\beta(1 - c^\beta)$.
In conclusion, by assuming $\sqrt{T^\beta}$ as velocity scale and the above Fan et al.

expression for the infiltration coefficient, the mass balance equation for the solid phase β results:

$$\frac{\partial \overline{c^\beta}}{\partial t} + \frac{\partial}{\partial x_2}\left(\overline{c^\beta}\,\overline{u_2^\beta} + d^\beta\sqrt{T^\beta}\frac{\partial \overline{c^\beta}}{\partial x_2} + \overline{u_2^\beta}\,\overline{c^\beta}(1-\overline{c^\beta})\right) = 0 \tag{2.26}$$

2.4.2 Advection-diffusion equation models

The earliest continuum model for the description of segregation was developed by Bridgwater and the key elements are still present in the more recent theories (Gray and co-workers [30, 31]). It is based on the mass balance equation and consists of a spatial one-dimensional time-dependent advection-diffusion equation, with a shear rate dependent segregation flux. In the recent multi-dimensional models, the main elements of the original theory are still present but differ for the relation chosen for the segregation flux (linear, quadratic or cubic).

The model captures the interactions between advection, segregation and diffusion in size bi-disperse granular materials and it is based on the Peclet number, that represents the exchange in segregation between the advetction and the diffusion (Gray and Chugonov [32], Fan et al. [23], Schlick et al. [70]). The steady state non-dimensional segregation-remixing balance equation in a dimensionaless form has the general expression:

$$\frac{\partial \phi^\beta}{\partial t} + \nabla\cdot(\phi\mathbf{u})^\beta + \nabla\mathbf{F}^\beta = \nabla\cdot(D\nabla\phi^\beta) \tag{2.27}$$

where ϕ is the concentration of each phase, $\mathbf{F}^\beta$ is the segregation flux vector for the phase β and D is the diffusion coefficient, equal for all phases. The model considers the sum of the concentration of the phases, or species, as:

$$\sum_\beta \phi^\beta = 1 \tag{2.28}$$

In this approach the voids are included in the definition of the concentration ϕ. Eq. (2.27) can be solved analytically obtaining the concentration profile of the species. The model was tested with experiments by Wiederseiner et al. [79] and with numerical simulation by Thornton et al. [73]. Van der Vart [77] underlined the asymmetry in the segregation flux.

The problem of this model is represented by the segregation flux function as a definitive form that makes sense of is still lacking. The complexity is due to its dependencies on many variables, such as gravity, mean particle size, particle size ratio, shear rate, frictions of the grains, local volume fraction.

2.4.3 Segregation in dense inclined flows

A large contribution on segregation in granular flows was given by Larcher and Jenkins in [46, 47, 39]. They studied dry granular flows composed of two types of rigid spheres, flowing down an inclined, rigid and bumpy bed with no side-walls.

The hypothesis of their works are steady and uniform condition in all direction except the direction normal to the free surface, a fully developed flow, the collisions among particles dissipative but with not much dissipated energy and particles similar in size and mass. The particles of species A and B have radii r_A and r_B, masses m_A and m_B, number of densities n_A and n_B and concentration c_A and c_B.

The governing equations are based on the mass, the momentum and the energy balance of the two species composing the mixture. To predict the concentration of the mixture c_M and the profile of the mixture velocity the kinetic theory is applied. The pressure of a species comes from particles that transfer energy in collisions: $p_A = (n_A + K_{AA} + K_{AB})T_{AB}$, where T_{AB} is the granular temperature of the mixture $T_{AB} = (n_A T_A + n_B T_B)/(n_A + n_B)$;

K_{AB} considers the dependence of the collisional transfer of momentum between different particles and depends on the radius of each species, the concentration and the radial distribution function g_{AB}.

For the description of the parameters involved, the authors consider Enskog's assumption for the collisional frequency in a dense gas and employed the Chapman-Enskog procedure to obtain the Boltzamnn equation for the single particle velocity distribution function.

The result of the procedure consists in writing the expression of the particle interaction depending on the chemical potential μ and the thermal diffusion coefficient K. The expression proposed for the segregation function is $x = n_A - n_B/2n_A + n_B$ and with this expression the concentration of the particles c_A and c_B is computed accordingly. The mixture velocity profile, the shear stress, the pressure, the rate of collisional dissipation are found integrating the momentum balance of the mixture in the direction of the flow. The prediction of this theory is compared to the results of the numerical simulations by Tripathi and Kahakhr [75], with a good correspondence.

Later Larcher and Jenkins [47] improved their theory considering the mass balance of the mixture and the difference in the velocities vector. This quantity depends on the diffusion coefficient D_{AB}, the gradient of the mixture pressure, the kinetic energy of velocity fluctuations and the granular temperature of the mixture . The profile of the granular temperature of the mixture was obtained by momentum balance of the mixture across the flow and by using the hypothesis that in dense flows the mixture concentration is uniform across the flow. The time-dependent segregation equation was solved and compared to experiments (Wiedereseiner at al. [79], Savage and Lun, [69]) and numerical simulations (Thornton et al. [73]).

A good agreement was found and this allows the authors to state that

in case of steady and uniform flow the major role in segregation is given by granular temperature gradients and by density differences in case gravity is present. The flow evolves towards segregation and the perfect mixing is possible only for peculiars radii and density ratio.

The authors underline how segregation depends on the ratio between the depth of the flow and the average particle size, the slope of the bed where the mixture is flowing, the coefficient of restitution and the volume fraction of the species. The limit of the theory is an underestimation of the diffusion and segregation rate, that produces a prediction of sharper segregation profile in the steady state in numerical simulation and slower segregation in experiments.

Chapter 3

Laboratory set-up and measurement technique

The experiments concern the flow of a dry bi-disperse granular mixture in a free surface channel. The displacements of each individual particle were measured with a high-speed camera through a transparent side-wall.

An algorithm developed ad hoc gave the time evolution of both the granular instantaneous Eulerian velocity and concentration and, by time integration, the average profiles of velocity, concentration and granular temperature of both classes of grain. The tests were repeated for different flow rates and size partition of the mixture.

3.1 Laboratory set-up and measurement devices

In the literature, the mechanics of infiltration and segregation of polydisperse mixtures of granular materials are generally studied through two types of experiments: the flow driven by gravity down a chute and the flow in shear boxes, annular shear cells or rotating drums.

Our experiments concern the flow in a flume, where the granular binary mixtures run in a closed-circuit system. The set-up consists of a free surface channel ending with a weir with two vertical slits. The channel is 3.50 m long and 10 cm wide, but the width could be increased up to 15 cm. The slope of the channel can be regulated from 0° to 50° with a proper hydraulic piston system.

At the beginning of each experiment a fixed volume of particles was inserted in the flume. The granular mixture was recirculated through an auger lateral to the flume, that took up the particles and deliver them in a hopper. The hopper was equipped by a controlling gate, from which the particles flowed down in the flume. Both the auger frequency and the opening gate could be set manually and varied in each test.

At the end of each test a certain volume of recirculated material was collected and measured in order to obtain the flow rate (section 3.1.3). To avoid that the solid particles become electrostaticlly charged, a metal cable was positioned on the auger to eliminate the charge. In the measuring

section two led lights were installed on a support to properly illuminate the flow field for the high speed camera recording. Figure 3.1 shows the set-up.

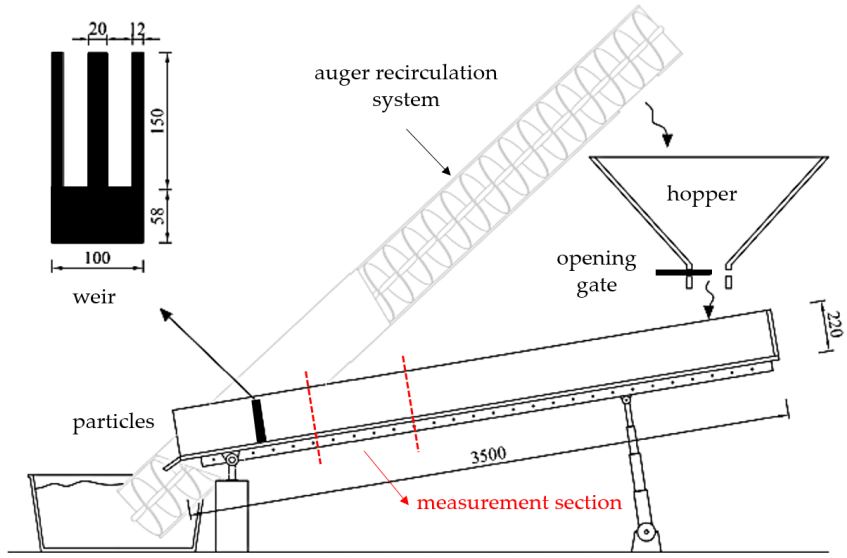

Figure 3.1: The laboratory set-up: the granular mixture is recirculated by the auger and lateral to the flume the flow field is measured by a high speed camera. The measures are expressed in millimetres.

3.1.1 The granular material

The mixture was composed of spherical particles of different diameters, but the same density. The diameter of the smaller class was $d_S = 0.75\,\text{mm}$ while that of the larger class was $d_L = 1.14\,\text{mm}$. Both classes were composed of

not-expanded polystyrene, with a material density of $\rho_s = 1035\,\mathrm{kg/m^3}$.

The particle inelastic restitution coefficient e was measured experimentally by dropping a particle from a certain height onto a perspex surface and measuring the maximum rebound height, obtaining $e = 0.91 \pm 0.01$, measured already by [65].

The friction angle was estimate by measuring the free surface slope of a heap that forms naturally by pouring grains on an horizontal plane. The friction angle of the small particles ranges about $21^\circ \pm 5^\circ$ and for the large particles $25^\circ \pm 5^\circ$.

Before each test, the two solid fractions were sieved to obtain particle size classes with the lowest possible dispersion. Fig. 3.2a shows the large fraction and Fig. 3.2b the small one. The colour was an important property because in the camera acquisition the two fractions could be distinguished thanks to their different colours only. For this purpose, the small particles are black, while the large ones are white. In the table 3.1 the main properties of each granular material are summarized.

Table 3.1: Properties of the granular material used in the experiments to reproduce the binary mixture.

particles properties	**small fraction**	**large fraction**
density ρ_s $[\mathrm{kg/m^3}]$	1035	1035
mean diameter d_m $[mm]$	0.75	1.14
colour	black	white
friction angle φ $[^\circ]$	21 ± 5	25 ± 5
inelastic restitution coefficient e	0.91 ± 0.01	0.91 ± 0.01

(a) Large fraction: white spherical particles of diameter d_L=1.14 mm.

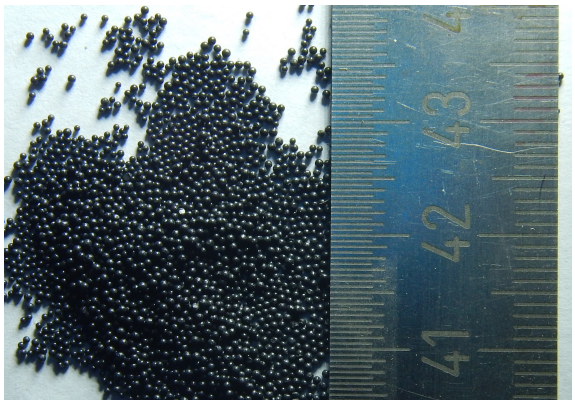

(b) Small fraction: black spherical particles of diameter d_S=0.75 mm.

Figure 3.2: The granular material.

3.1.2 Acquisition set-up

Lateral to the flume, in correspondence to the measurement section, the high speed camera on a tripod was positioned. The camera was equipped with different lens, but in the experiments lenses from 45 mm to 60 mm were used. The high speed camera (a Phantom VEO) is able to record up to 7000 fps. The choice of a lower resolution corresponded to a faster recording. In our work, for high discharges the maximum frame rate used was 3000 fps and for lower discharge the acquisition frequency was set to the minimum value of 1000 fps, so a longer record and larger imagesize were obtained.

Along with the camera, two led lights (spotlight GSVTEC, model Multiled QT) were positioned on the side of the camera. The choice of the type of lighting system was found after a series of test comparing other lighting systems (section 3.2.1).

A preliminary procedure to regulate the acquisition system was needed before each experiment. Through an external software regulating the camera options, the exposure time, the shutter and the exposure index were calibrated along with the two led lights, in order to eliminate as much as possible the noise and the reflections in the image. These parameters had to be set in each experiment, as it was crucial to obtain images in which both the small and the black particles are visible as better as possible.

The high speed camera was tilted to obtain images parallel to the flow field with the lens perpendicular to the plastic wall. The adjustable distance between the side walls of the channel was kept constant in all tests. Fig. 3.3 shows the camera Phantom VEO with the two led lights.

The frame rate was adjusted in order to give particle displacement in two subsequent frames not greater than the radius of the largest particles. If this was not satisfied, we increased the frame rate of the camera.

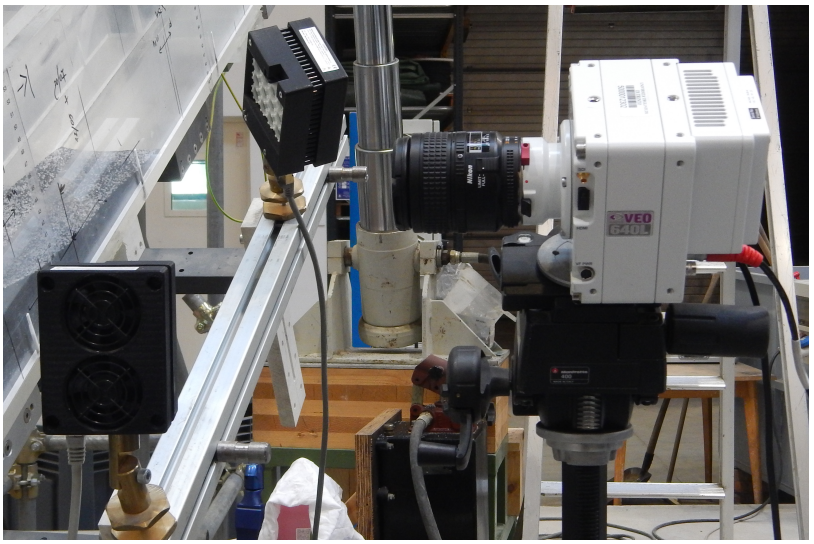

Figure 3.3: Laboratory equipment. The high speed camera positioned on the tripod and in front of to the plastic flume ready to record the experiment.

3.1.3 Measurements

The solid discharge was measured by collecting the total volume of the flowing particles in the recording time $t_c = 10 \sim 20\,\mathrm{s}$. The weight P_T of the collected material was measured and then the two fractions were separated in order to obtain the volume $V_\beta = V_S, V_L$ of the recirculating material of each grain size class.

If ρ_s is the density of the particles material and t_c the collecting time, the granular discharge is:

$$Q = \frac{P_T/\rho_s}{t_c} \tag{3.1}$$

In such a way the volumetric partition P_β of each grain-size class is:

$$P_\beta = \frac{V_\beta}{\sum V_\beta} = \begin{cases} P_S = \dfrac{V_S}{V_s + V_L} \\ P_L = \dfrac{V_L}{V_S + V_L} \end{cases} \tag{3.2}$$

The slope of flume was kept constant in each experiment (about 29°), whereas the slope of the free surface changed depending on the flow condition. They were measured by a proper inclinometer, but the slope of the free surface (together with the bed slope) was also measured by the recorded frames of the tests.

The duration of each test ranges between 30 and 60 minutes. In table 3.2 the measured data in each experiment are reported alongside with the unit of measure.

Table 3.2: Measured data in each test.

data	**definition**	
P_S	weight of the small particles in the control volume	[kg]
P_L	weight of the large particles in the control volume	[kg]
t_c	recording time of discharge measurement	[s]
θ	slope of the loose bed	[°]
α	slope of the flume	[°]

3.2 The optical method

An imaging technique was used to analyse the flow field. The frames acquired during the tests were evaluated with an *optical method*, which detected the black and the white pixels in each image, allowing to distinguish

the pixels belonging to the two grain size classes. The measurement method was defined as an optical method because is based on the detection of the particles in each single image.

The method is similar to the technique used in [65], but developed for two different classes of particles in a dense environment.

The optical method is implemented in a code developed in *Python* language. Each set of frames of a test is insert in the code, which are a series of text files. These outputs were successively analysed through specific algorithms, that we developed. At the end the longitudinal velocity, the vertical velocity, the concentration and the granular temperature of the small and large particles in SI unit are obtained.

3.2.1 Set-up of the lighting system

The method adopted to measure particle speed and concentration is derived from a previous procedure [65] aimed at making measurements with uniformly sized particles. We therefore substantially modify the original method to make it suitable for measurements with bi-dispersed particles. We used a standard configuration system to record the tests.

The optical method used is very sensitive to how the light illuminates the image. The lighting system must provide:

- high contrast between the particles and the other noisy elements that can be present during the acquisition procedure (dust on the wall, scratches,...);
- uniform light on the entire picture (low bright gradient in vertical and horizontal direction);
- high contrast between the black and white particles;

- low reflection of the light on the particles and on the plastic wall;
- equal precision of the visibility for both of the small and large particles (good resolution and illumination);

In order to obtain a good lighting system that satisfies all the above conditions we try different configurations both in position and types of light. For simplicity we have done some preliminary tests in a smaller channel, by inserting a very thin strip of small led-lights on the internal face of lateral transparent wall of the flume, but this arrangement did not guarantee a sufficiently uniform lighting. We then tried to illuminate with two or more incandescent lamps, positioned outside the flume near the camera, but also this configuration provided insufficient light intensity to distinguish the two classes of particles (Fig. 3.4). Next, we used two powerful led lights, initially facing outwards on a white parabolic surface aimed to reflect the light on the flume more evenly (Fig. 3.5). This arrangement, however, did not lead to any improvement in image quality. The best solution was to illuminate the measuring area directly with two LEDs positioned outside to the flume and pointing to it with an angle of about 20° (Fig. 3.6).

3.2.2 Particle detection

The first step in this procedure of the optical method, once the experiment is recorded, is identifying the individual particles. At first, the user has to select the Region of Interest (ROI) in each image. The original frame is cropped according to the interested area. This allows to exclude non representative zones, such as broken particles (noisy pixels). The following step consists in adaptively equalizing, de-noising and filtering the image. This is performed in three different steps, visible in figure 3.8.

Figure 3.4: First two configurations of the lighting system in a smaller flume. On the left the strip of led-light is inserted in the flume. On the right the flume is lighted up by a series of lamps.

1. Adaptive histogram equalization is applied to the image. This technique is used to improve the contrast of the images. It differs from ordinary histogram equalization in the sense that the adaptive method computes several histograms, each corresponding to a distinct section of the image, and uses them to redistribute the lightness values of the image. It is therefore suitable for improving the local contrast and enhancing the definitions of edges in each region of an image. This is performed using the CLAHE technique [61].

2. A de-noising operation is applied on the image using the non-local de-noising technique [17].

3. A bilateral filter operation is then applied to smooth the image [74]. A bilateral filter is a non-linear, edge-preserving, and noise-reducing smoothing filter for images. It replaces the intensity of each pixel

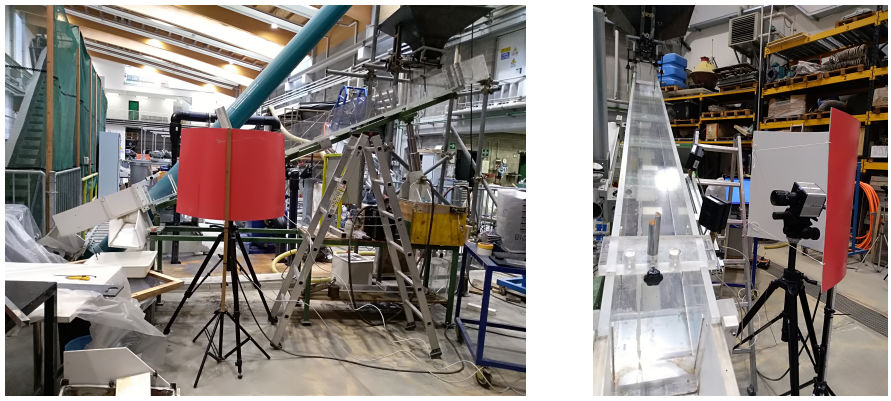

Figure 3.5: Lighting tests: parabolic paper positioned behind the camera in order to reflect the light onto the channel wall.

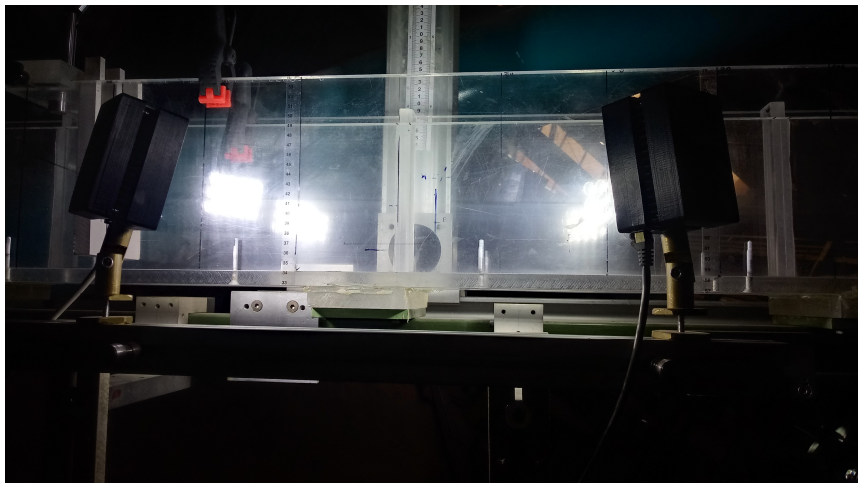

Figure 3.6: Final lighting set-up: two led lights tilted towards the plastic flume.

with a weighted average of intensity values from nearby pixels.

Otsu thresholding [58] is then applied to obtain a binary mask, as the one shown in Fig. 3.8. It is used to automatically perform clustering-based image thresholding, or the reduction of a gray level image to a binary image. The algorithm assumes that the image contains two classes of pixels following bi-modal histogram (foreground pixels and background pixels). It then calculates the optimum threshold separating the two classes so that their combined spread (intra-class variance) is minimal, or equivalently (because the sum of pairwise squared distances is constant), so that their inter-class variance is maximal. From this last type of image it will be possible to detect the position of the particles.

The watershed algorithm is then applied on the binary mask obtained. The watershed algorithm is a classic algorithm used for segmentation and is especially useful when extracting touching or overlapping objects in images, such as the particle or the coins in Fig. 3.9. This algorithm is composed of different steps. The first step in applying the watershed algorithm for segmentation is to compute the Euclidean Distance Transform (EDT). As the name suggests, this function computes the Euclidean distance to the closest zero (i.e., background pixel) for each of the foreground pixels. A peak is defined as a point that maximizes the average distance from zeros. The algorithm allows to set the minimum distance between two peaks. If the algorithm detects two or more peaks with the same intensity at a lesser distance with respect to the minimum, it will output both of them. The watershed algorithm returns a matrix of labels, an array with the same width and height as the input image. Each pixel value has a unique label value. Pixels that have the same label value belong to the same object.
Ideally there should be a label for each of the particles in the image. However, this is not our case, since our images are much more noisier and

present a much greater deal of occlusions with respect to the coins example. We define c_1 and c_2 as the centres of two particles, being $(x_1;\, y_1)$ and $(x_2;\, y_2)$ their pixel coordinates. The particles are spheres with diameters d_β and radius r_β in pixel dimensions. The distance between the centre of two spheres is the Euclidean distance d:

$$d = \sqrt{(x_2 - x_1)^2 + (y_2 - y_1)^2} \tag{3.3}$$

If two centres are at a distance lesser than the radius, a new centre c_3 will be initialized in the midpoint and the centres c_1 and c_2 will be discarded from the set of centres C_0 . After, it is checked if the particles overlap with each other. Overlapping particles are two particles whose centres c_1 and c_2 respect the following condition:

$$0 < d(c_1, c_2) < 2r_\beta \tag{3.4}$$

If a particle present overlapping parts with one or two other particles, it is listed as a weak match. If a particle does not overlap, it is listed as a strong match. After the detection step has been performed, each image has a set of weak matches and a set of strong matches. To determine if the weak matches are real particles or not, the correlation between set of consecutive frames is exploited. Let's take two consecutive frames, f_1 and f_2, with their sets of strong matches, S_1 and S_2, and weak matches, W_1 and W_2. Let's take a strong match $s_i \in S_1$ and a weak match $w_j \in W_2$, we move weak matches to strong matches array if the following condition is satisfied:

$$d(s_i; w_j) < r \tag{3.5}$$

At the opposite, we discard weak matches that satisfy the following condition:

$$d(s_i; w_j) > r \tag{3.6}$$

In this way the particles inside the weak match are associated to the strong one or disregarded (so the detected particle is not a true particle). With this settings we simply plot a circle with radius r entered on each point present in the strong matches array and if a weak particle falls inside this circle becomes a strong one. After this operation is performed on all the consecutive frames, we produce an equivalent image for each frame which will be used to compute the density and velocities of balls at later stages. The explained step are performed both for the black and for the white particles, or better for black and white pixel.

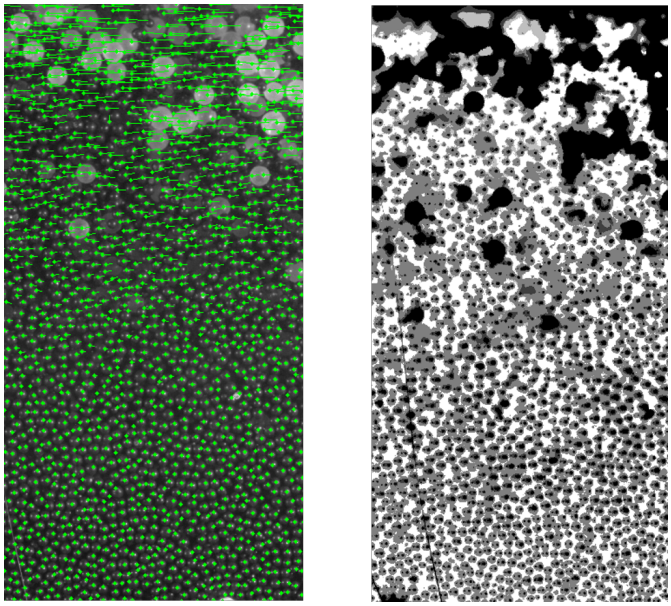

Figure 3.7: Application of the optical method. On the left trajectories of the particles displacements used to calculate the velocity and on the right binary mask of the detected particles used to calculate the concentration.

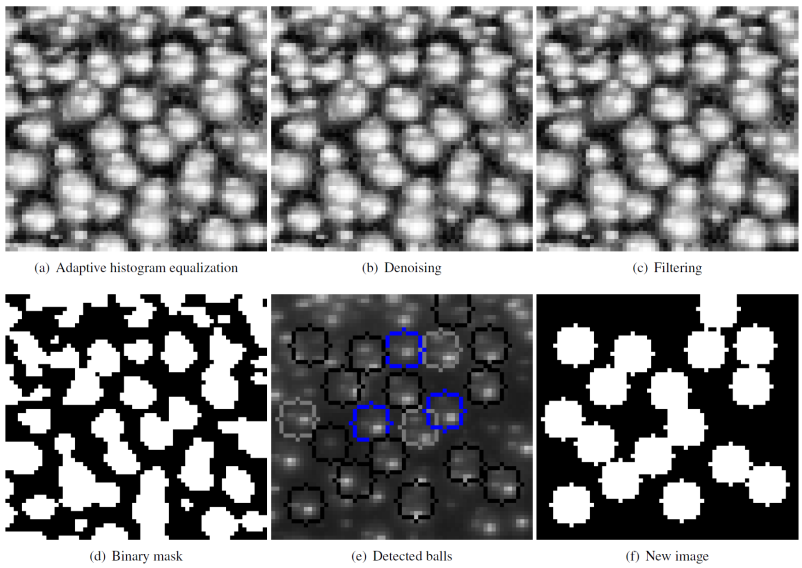

(a) Adaptive histogram equalization (b) Denoising (c) Filtering

(d) Binary mask (e) Detected balls (f) New image

Figure 3.8: Main steps of the optical method for the detections of the spherical particles.

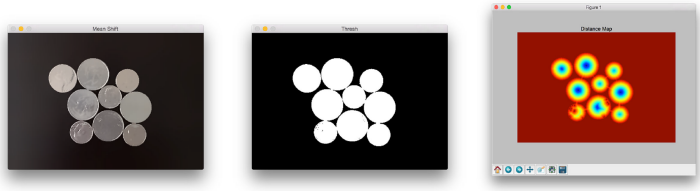

(a) Filtered image (b) Binary mask (c) Watershed visualization

Figure 3.9: Example of the application of the watershed algorithm to detect coins.

3.2.3 Application of the optical method

The optical method tracks the particles across multiple frames and saves the resulting average displacements of the detected features across a series of frames (Fig. 3.7). The optical method needs a user, who selects i) the Region of Interest (ROI), that reduces the whole frame to the interested area; ii) the Region of Measure (ROM), that allows to select the section of measure only. To perform these steps, it is necessary to detect the coordinates $(x_1,\ y_1)$, $(x_2,\ y_2)$ of the Region of Interest and the coordinates $(x_3,\ y_3)$, $(x_4,\ y_4)$ of the Region of Measure, that usually consists in a rectangle with height equal to the flow depth. The width of the ROM has to satisfy two conditions: i) it cannot be too small, as in this case only few particles would be detected; ii) at the same time the width cannot be really large, as we are interested in the the average distribution of the particle along the flow depth only. The coordinates have to be insert in the code manually by the user. The other important parameter is the choice of the number of layers. The region of interest is divided in n horizontal strips, with height h_{layer} and width w_{layer} (Fig. 3.10b). The particle detection is performed in the entire region of interest of the frame, but the concentration and the velocity of the particle are computed for each single layer only. The outputs of the optical method refers to the average coordinate of the i_{th}-layer of each frame. The number of layers is proportional to the height of the region of measure and a single layer must have a width at least equal to $h_{layer} = 2\,d_l$, where d_l is the diameter of the *large* particles. The algorithm provided the output respect to the system of reference of the image in pixel/frame along the average vertical coordinate y_m of each layer. Therefore the data obtained by the optical method have to be post-processed by an algorithm that converts the unit of measures to the SI unit system and rescales the dimension with respect to the reference system of the channel flow.

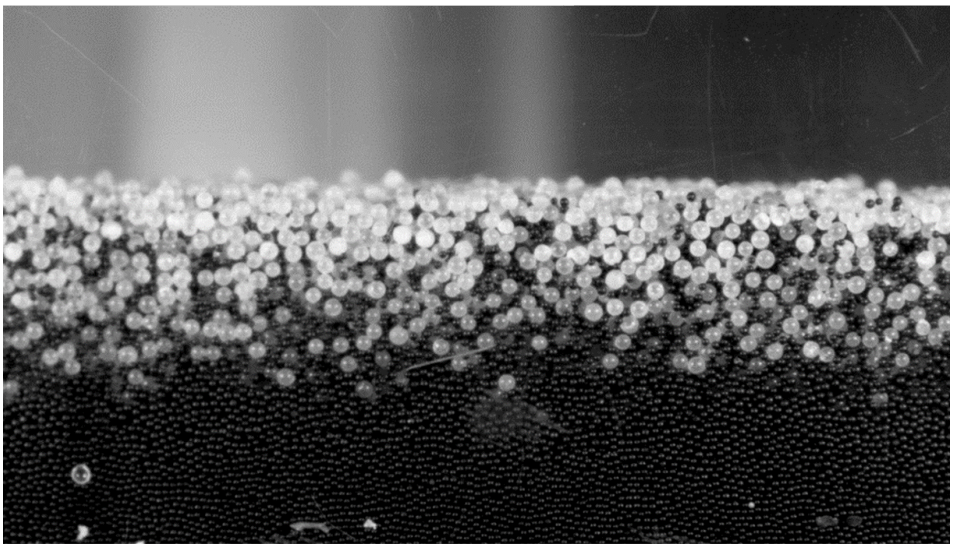

(a) Example of a single frame analysed by the optical method.

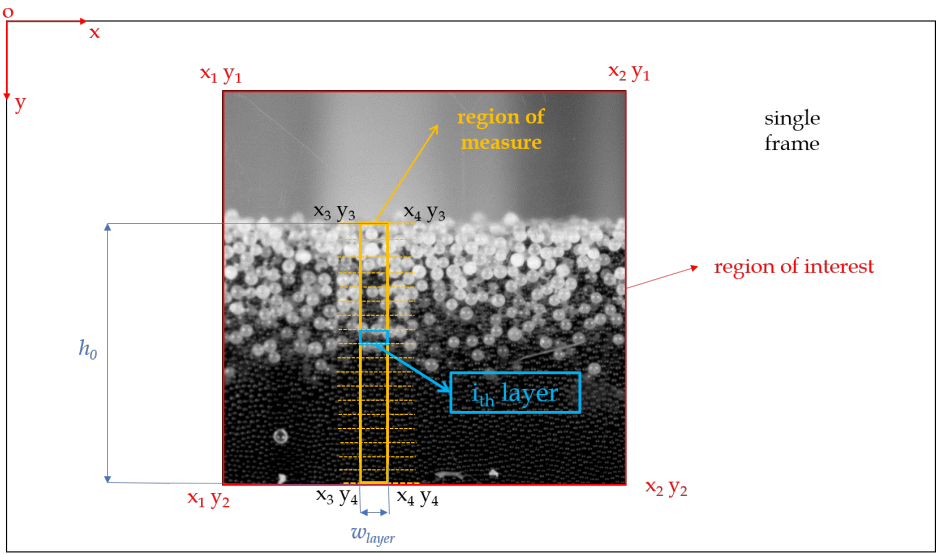

(b) Selection of the Region of Interest and the the Region of Measure of a single frame.

Figure 3.10: Example of the measurement technique on a single frame.

3.3 Measurements of velocity and concentration

The optical method is used in order to obtain the longitudinal and vertical component of the velocity, the concentration and the granular temperature of the flowing particles. These values are measured from the transparent side-wall both for the small and large particles. A *Matlab* code gives the above variables in the proper units, referenced to a fixed coordinate system.

3.3.1 Velocity measurements

As explained in Section 3.2, through the optical method we know the instantaneous velocity component of each particle in each layer. The calculation of granular velocity is based on the measurements of the displacement between two consecutive frames of the particles in each layer. The first calculated value is the *instantaneous velocity* $\mathbf{u}_\mathbf{p}^\beta$ of the small and large particles contained in each single layer.

In each frame and for each size class, the *i-th* component of the instantaneous granular velocity (at time t) of the layer is defined as the average of the velocity components of the individual particles:

$$\widetilde{u}_i^\beta = \frac{\sum_{k=1}^{n_k} \left((u_p)_i^\beta \right)_k}{n_k} \tag{3.7}$$

where n_k is the number of particles of each class contained in the single layer in each frame. Fig. 3.11 shows the individual particle velocity (blue and light-blue arrows) and the instantaneous velocity of each layer (red and purple arrows).

The time averaged granular velocity component of each class is there-

fore:

$$u_i^\beta = \frac{\sum_{t=1}^{n_t} \left(\tilde{u}_i^\beta\right)_t}{n_t} \tag{3.8}$$

where n_t is the number of frames considered for each layer. The instantaneous Eulerian velocity vector of the single class is obtained. We underline that with *vertical velocity* we refer to the direction normal to the bed.

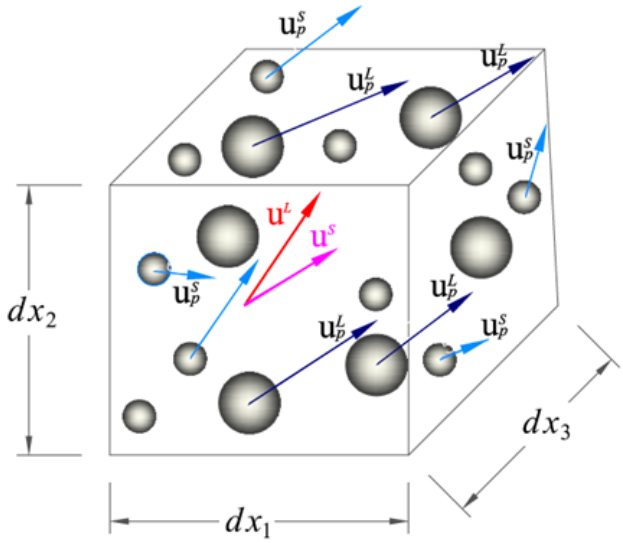

Figure 3.11: Velocity vector of the small and large particles in the control volume. The red and purple arrows represent the average velocity of the particles.

3.3.2 Concentration measurement

The instantaneous concentration of each grain-size class β is calculated by measuring the number of pixels contained respectively in the black and

white areas of each single frame in each layer. In each layer of a single frame there are n^w number of white pixels, n^b number of black pixels and the number of total pixels is:

$$n^{tot} = n^w + n^b + n^v \tag{3.9}$$

where n^v is the number of the pixels of the voids. The pixels in the background are treated as voids.
The 2D instantaneous concentration of each grain size class β is therefore:

$$\widetilde{c}^{\beta}_{2D} = \frac{n^{\beta}}{n^{tot}} \tag{3.10}$$

This is a 2D concentration. For each spherical particles, with some algebra (Rossi [65]), it is possible to obtain the three dimensional instantaneous concentration $\tilde{c}^{\beta}$ as a function of $\widetilde{c}^{\beta}_{2D}$, C^{*}_{2D} and C^{*}, where $\widetilde{c}^{\beta}_{2D}$ is the instantaneous $2D$ concentration, C^{*}_{2D} is the $2D$ packing concentration and C^{*} is the $3D$ packing concentration, i.e.:

$$\widetilde{c}^{\beta}_{3D} = C^{*}_{3D}\left(\frac{\widetilde{c}^{\beta}_{2D}}{C^{*}_{2D}}\right)^{3/2} \tag{3.11}$$

where for spherical particle $C^{*}_{3D} = 0.7405$ and $C^{*}_{2D} = 0.906$.
As for the velocity, the time averaged concentration in the single layer is:

$$c^{\beta} = \frac{\sum_{t=1}^{n_t} \widetilde{c}^{\beta}}{n_t} \tag{3.12}$$

with n_t the number of frames of the single grain size class.

3.3.3 Granular temperature measurement

The granular temperature represents the specific particle kinetic energy. In a two dimensional flow, for each layer and each grain size class, the granular

temperature T^β is defined as:

$$T^\beta = \frac{1}{2}\sum_{t=1}^{n_t}\left((u_1'^\beta)^2 + (u_2'^\beta)^2\right)_t \tag{3.13}$$

where:

$$(u_i'^\beta)_t = (\widetilde{u}_i^\beta)_t - (u_i^\beta)_t \tag{3.14}$$

is the fluctuating part of the granular velocity component. The index t represents the single frame. In the next chapter 4, the granular temperature, expressed in $\mathrm{cm}^2/\mathrm{s}^2$, is calculated both for the small and large particles along the uniform flow depth.

3.4 Validation of the optical method

To verify the accuracy of the optical method and, if necessary, to calibrate it, we made a series of comparisons between the measurements taken with the automatic procedure and those performed with a manual method.

In the second method a certain number of consecutive frames was first selected. The spherical particles were identified by circles and in each frame and in each layer the centres of the large and small particles were identified. At the end the coordinates of the centres were measured. In this way it was possible to obtain the displacements and, consequently, the time average components of the particle velocity $u_i^\beta = (u_1, u_2)^\beta$.

Fig. 3.12 shows a sketch of the procedure. The horizontal strip is divided in a certain number of layers. In each layer, that is a rectangular, we identified the large and white particles (yellow, purple, blu and green circles in the figure), the small and black particle (light blues circles in the figure) and the void space (red strips in the figure).

The manual results were compared to the values obtained for the same

set of frames with the optical method. Moreover, the manual velocity was computed by two different operators, with the purpose of reducing the error in the identification of the particles centres. The procedure was developed both for the small and large particles. Table 3.3 report the errors found.

In order to estimate the accuracy of the measurement of concentration we compared the automatic measure with a manual measure similarly to the one adopted for the velocity. Instead of directly locating the coordinates of the particles centres, we calculated in each layer the surface area A^β occupied by the small and large particles. In addition, we calculated the total void surface in each frame. The instantaneous concentration of each grain size class β is given by the ratio (in each layer) by the areas occupied by the particles of the class β and the total area. Tab. 3.3 shows the evaluation of the errors.

The estimation error on the concentration of small particle is rather high. A further comparison analysing only this variable was conducted to estimate precisely the error. In particular, for the small particles whose average concentration was affected by a systematic error, we rescaled the average concentration value on the base of the average concentration based on the manual method.

Table 3.3: Estimated errors on the variables computed by the optical method.

variable	**error**
longitudinal velocity large particles	2%
vertical velocity large particles	6%
longitudinal velocity small particles	2%
vertical velocity small particles	8%
concentration small particles	20%
concentration large particles	11%

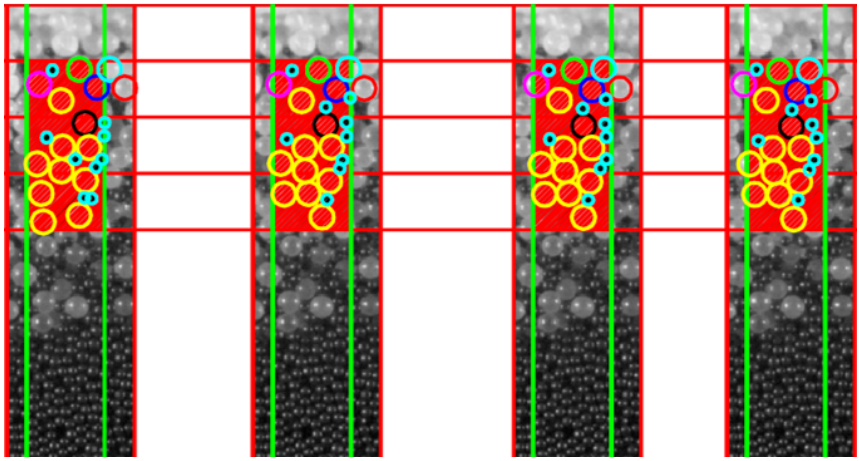

Figure 3.12: Sketch of the manual procedure to compute the velocity and the concentration.

3.5 Determination of the bed and the free surface elevation

The distributions along the flow depth of the granular velocity and granular temperature, which we will present and discuss in the next chapters, show that these profiles have an asymptotic trend approaching to zero as we proceed towards of the loose bed (static bed generated in the experiment, as it will be explained in the next Chapter chapter 4). This fact makes problematic the definition of the bed elevation.

We solved this ambiguity by identifying therefore the position of the bed in correspondence to the layer in which the velocity of the small particles is 1% of the maximum velocity, following a convention already introduced in Armanini et al. [3], Nucci [57] and Meninno et al. [55]. We highlight that

this threshold does not influence noticeably the calculation of the depth averaged velocity.

We have a similar problem for the identification of the free surface. Since we know that the concentration of the small particles near the free surface is approaching zero due to the collisional regime, we identified the position of the free surface with the first layer in which the particle concentration of the small particles is less than 0.01.

Figure 3.13 shows the identification of the bed and the free surface on a single frame of a test.

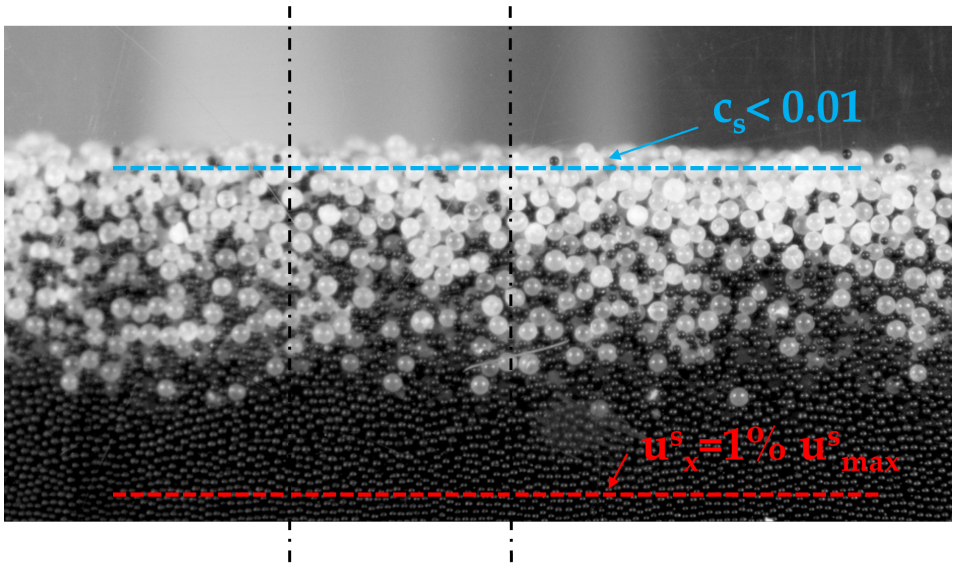

Figure 3.13: Identification of the bed and the free surface.

Chapter 4

Stationarity and homogeneity in a channel flow

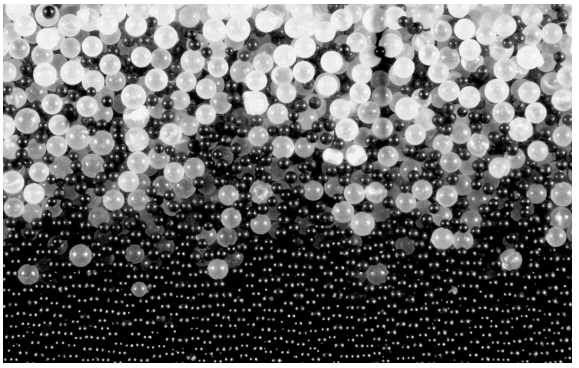

This chapter analyses the conditions that allow the formation of a flume stretch in which the bi-dispersed dry material can be considered statistically stationary and homogeneous (uniform channel flow). These conditions are checked through the measure of the flow parameters in different sections and in different times. The invariance of these parameters in time and in the

longitudinal direction demonstrates the statistically stationarity of the flow.

4.1 Uniform channel flow condition of dry granular mixture

Let us consider a long rectangular channel inclined by an angle θ with respect to the horizontal direction. When the flume is fed by a constant liquid discharges, a steady non-uniform flow profile is established. With a proper choice of boundary conditions, at a certain distance from the end of the channel the statistically and homogeneous flow condition is obtained. We refer to this condition as *uniform channel flow*. The free surface becomes parallel to the channel bottom and the flow depth depends on the flow rate. In case of sediment transport, feeding with solid and liquid discharges a rectangular channel controlled by a weir downstream generates a deposit over which the flow can be considered uniform. In this case the slope of the free surface depends on the sediment characteristics and on the solid and liquid flow rates (Armanini and Rossi [9]).

Let us now analyse the case of dry granular material. By feeding with semi-elastic solid particles a sufficiently long channel, closed downstream by a weir, a steady granular flow similar to that of sediment transport in water is obtained. This was also observed in recent works by Mennino et al. [55], in the case of homogeneous material, where three stretches on the channel are identified: a decelerated, an accelerated and a uniform flow stretch.

4.2 Experimental procedure

In all the tests conducted, we noticed upstream of the weir the formation of a loose static bed layer over which the granular materials was flowing. After a certain time, the flow becomes steady and the flow depth, defined as the distance between free surface and bed, was not constant along all the flow. In each test, however, a sufficiently long stretch of the channel was formed in which the free surface and the bed elevation exhibited a linear trend and the flow depth was constant, as shown in Figure 4.1. We aimed therefore to check whether in this stretch the uniform flow condition was achieved. We measured velocity, concentration and granular temperature in different sections (Fig. 4.2) of the flume at different times.

The measures were performed from the transparent side-wall of the flume. By following the procedure described in chapter 3 the granular discharge of each grain-size class was taken. We measured the flow depth h and the bed elevation z_b (Fig. 4.1).

We tested three different partitions of the feeding discharge between the classes: i) $P_S = 25\%$ and $P_L = 75\%$, ii) $P_S = P_L = 50\%$ and iii) $P_L = 25\%$ and $P_S = 75\%$, as summarized in Table 4.1. In this convenient to define a dimensionless discharge of the two classes with respect to the channel width W, the particle diameter of the class d^β and the gravity acceleration g:

$$Q^*_\beta = \frac{Q_\beta}{W d_\beta \sqrt{d_\beta g}} \tag{4.1}$$

where Q_β is the granular discharge of the single grain-size class measured at the end of the experiment in the control volume. The definition (4.1) considers the mobility scale d_β and the width W of the rectangular channel for the lateral effect. The total granular discharge is therefore:

$$Q^*_T = Q^*_S + Q^*_L \tag{4.2}$$

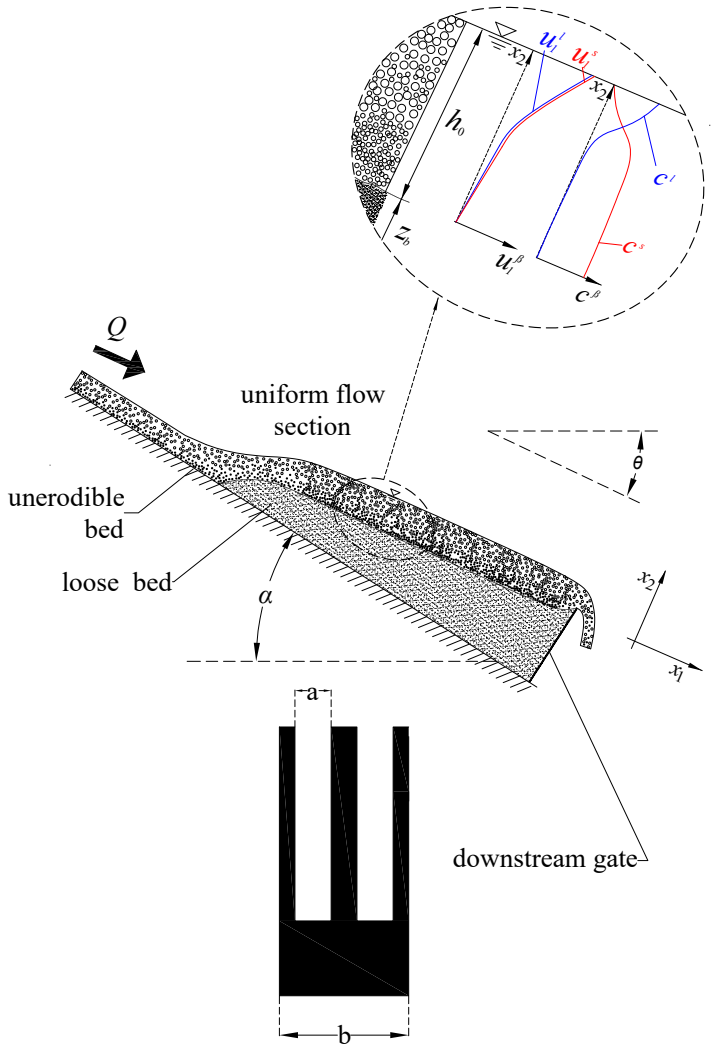

Figure 4.1: Sketch of the dry granular mixture flowing over the loose bed.

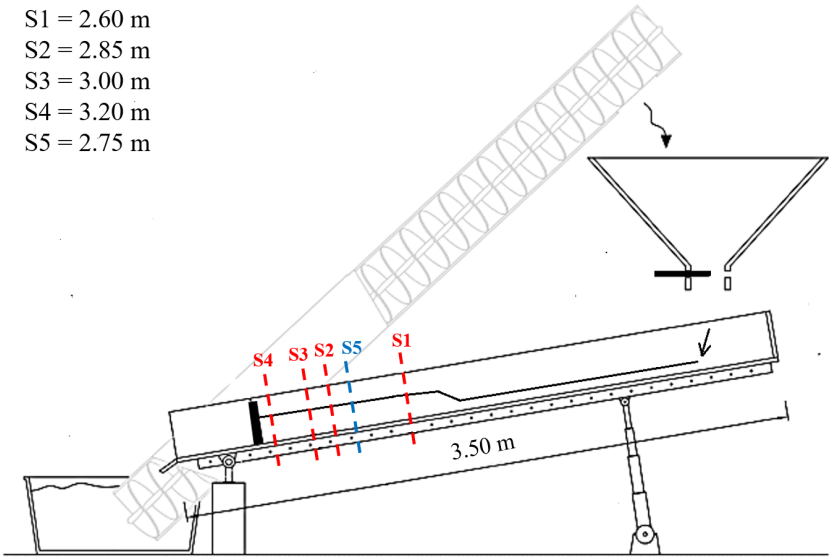

Figure 4.2: Section of measurement for the uniform flow channel tests.

Table 4.1: Summary of all the tests conducted for the uniform channel flow conditions. The sections of measurement refer to Figure 4.2.

Test	Q_T^* [-]	P_S [%]	P_L [%]	sections of measurement
T1	20	50	50	5
T2	120	75	25	5
T1	200	25	75	5
H0	80	50	50	1, 2, 4
H1	20	50	50	2, 3
H2	30	50	50	2, 3
H3	50	50	50	2, 3
H4	120	75	25	2, 3
H5	200	25	75	2, 3

4.3 Statistically stationary condition

The first experiments where addressed to check the existence of the statistically stationary condition. A central location with respect to the flume was chosen in order to minimize the influence of the longitudinal gradient of the variables. We chose the section S5, at 2.75 m from the beginning of the flume (Fig. 4.2), to verify the possible temporal variation of the variables and therefore determine the time necessary to reach a statistically stationary condition.

We want to underline that the present tests are aimed at determining the possible stationarity of the flow, while the homogeneity has been verified with a series of tests described in section 4.4.

After some preliminary series of tests, we determined the necessity to an adaptation time (t_1), ranging between 30 and to 60 minutes, to reach the stationarity. We performed a series of measures of velocity, concentration and granular temperature profiles after this time.

Figures 4.3, 4.4 and 4.5 show the results for the two time steps that are compared in the same graphs for the two grain size classes (large and small particles). In the graphs the normal coordinate x_2 is made dimensionless with respect to the flow depth h, that is $\eta = x_2/h$ (Fig. 4.1).

We can notice that the velocity and the concentration profiles result almost coincident in all the three tests, even if the concentration profiles of the two classes measured in different times are not perfectly superimposed. We believe that these differences are attributable to the lower accuracy of the concentration measurement with respect to that of velocity and granular temperature measurements.

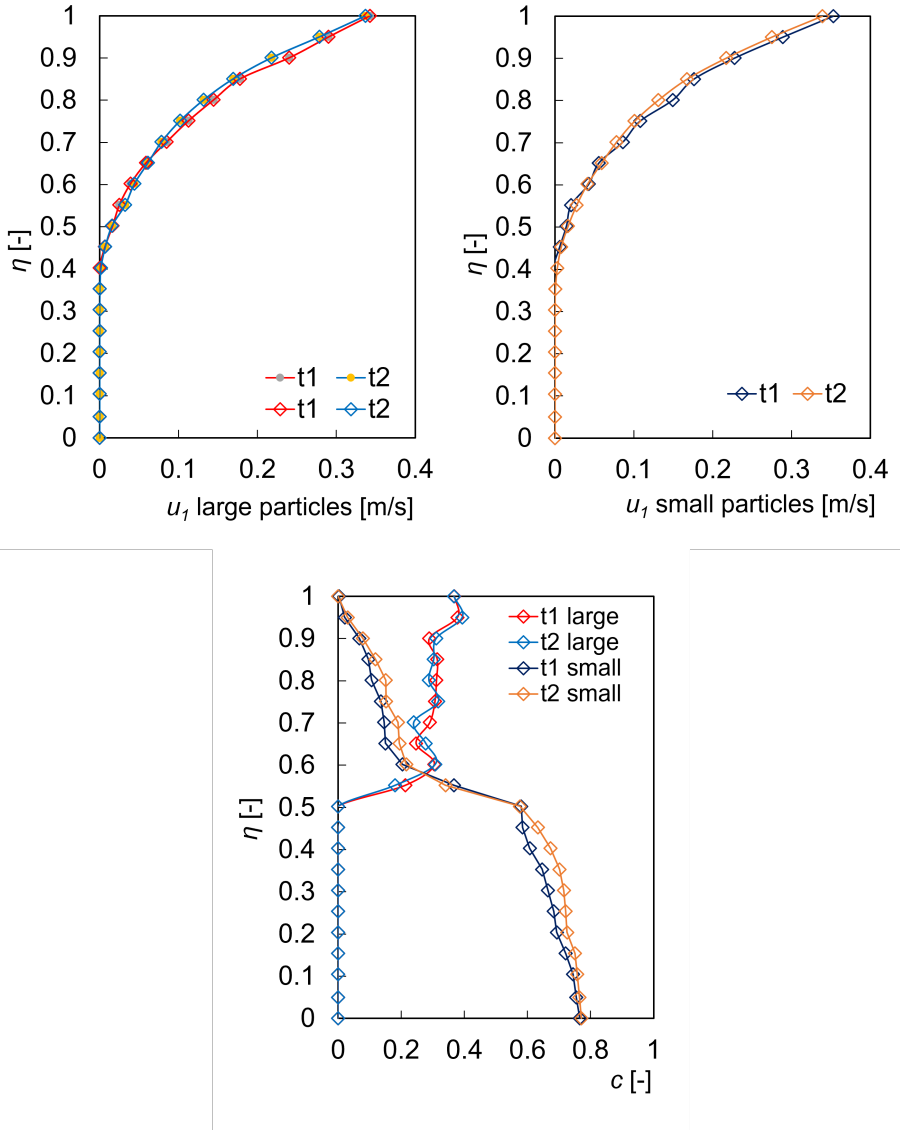

Figure 4.3: Test T1. Profiles of velocity and concentration in section S5 in two time steps with $Q_T^* = 20$; $P_S{=}P_L = 50\%$.

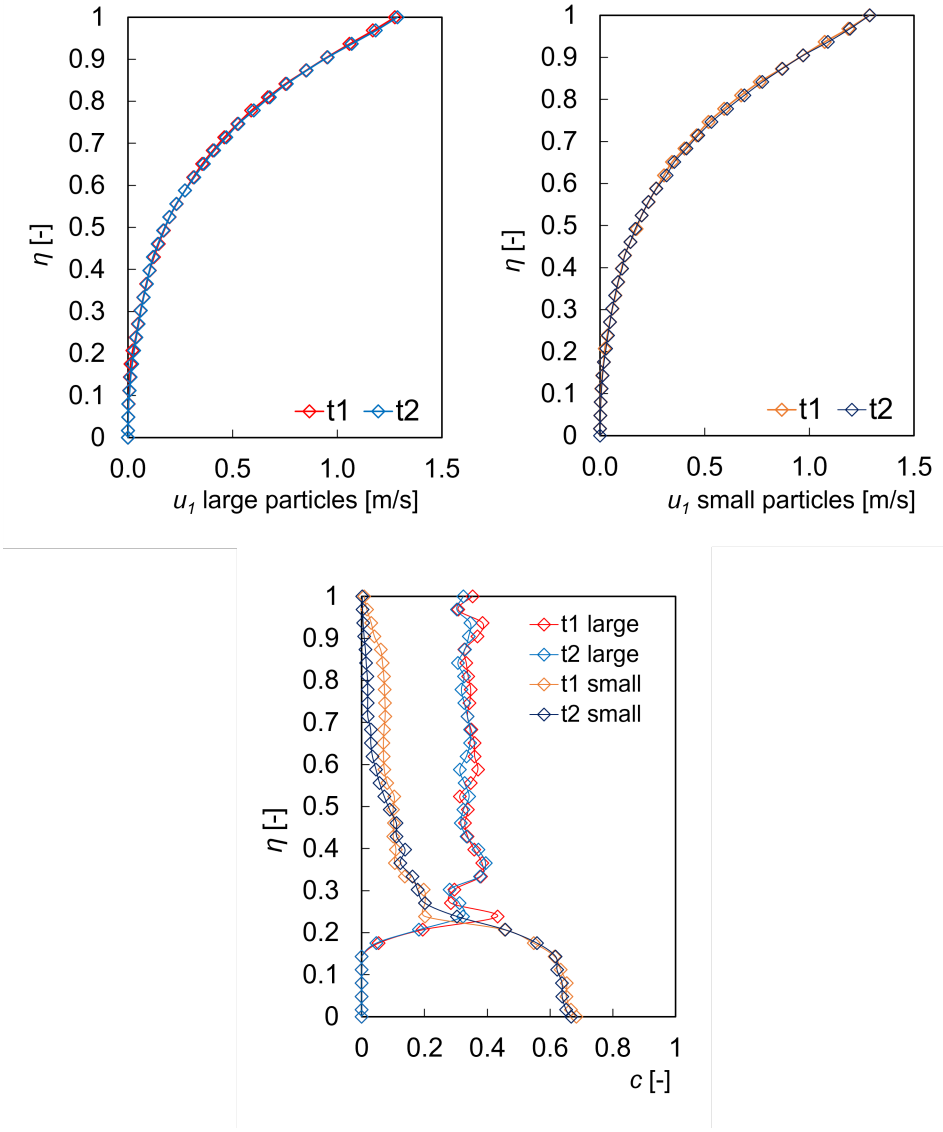

Figure 4.4: Test T2. Profiles of velocity and concentration in section S5 in two time steps with $Q_T^* = 120$; $P_S = 75\%$ and $P_L = 25\%$.

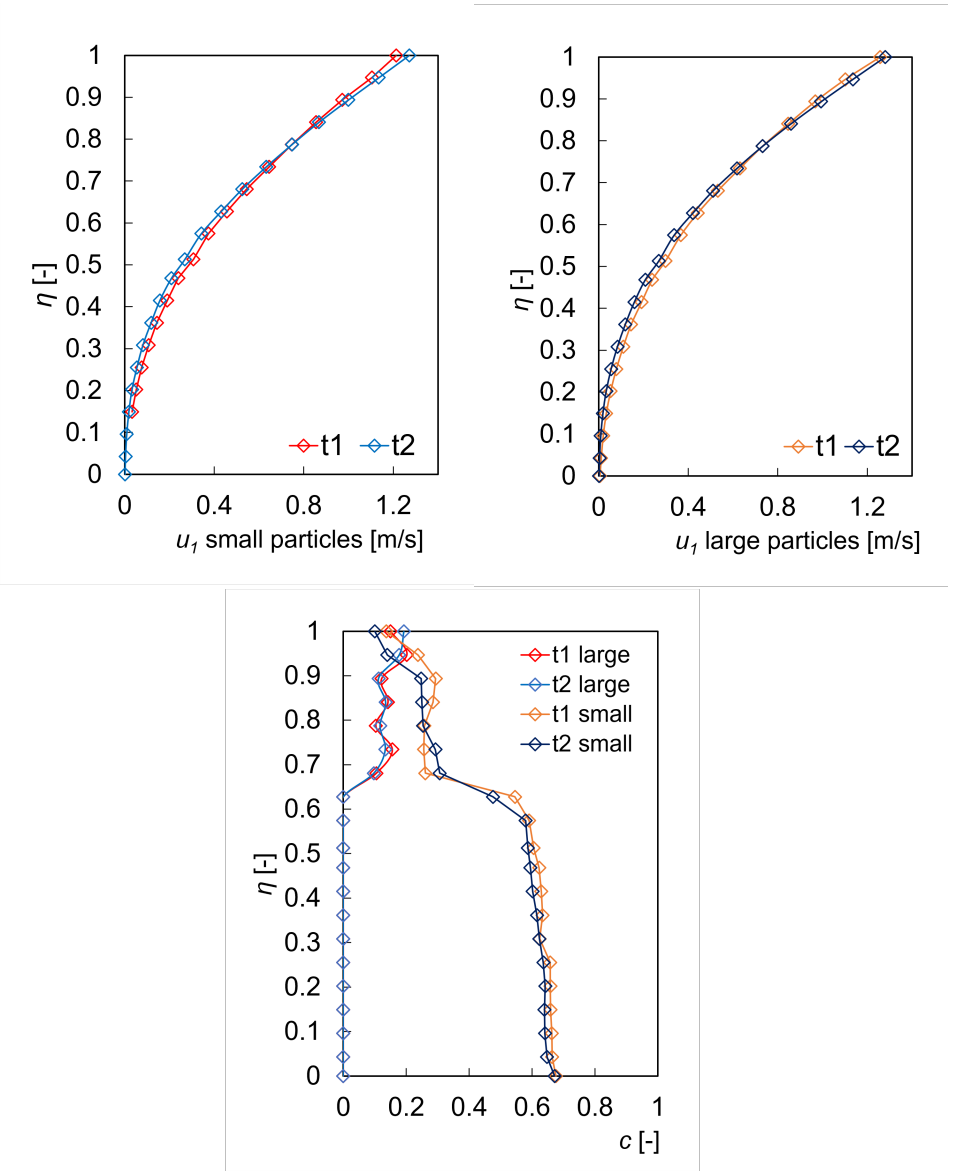

Figure 4.5: Test T3. Profiles in section $S5$ in two time steps with $Q_T^* = 200$; $P_S = 25\%$ and $P_L = 75\%$.

Table 4.2: Data for stationary condition tests.

Test	Q_T^*	P_S	P_L	h [cm]	t_1 [min]	t_2 [min]
T1	20	50	50	1.50	30	60
T2	120	75	25	3.00	45	90
T3	200	25	75	3.30	60	120

4.4 Statistically homogeneous stretch

After the existence of the statistically stationary condition was verified, we checked the existence of the statistically homogeneous condition: we investigated the time average profile of the variable in different sections of the flume (Sections S1, S2, S3 and S4 of Figure 4.2).

4.4.1 Results in sections 1, 2 and 4

At first, we performed the simultaneous measure in sections S1, S2 and S4 (Fig. 4.2). In this case the tests were carried out with volumetric partition of the granular mixture equal to $P_S = P_L = 50\%$ and $Q_T^* = 80$, the same previously adopted to check the flow stationarity. Figures 4.6 and 4.7 show the velocity, the concentration and the granular temperature profiles. The general flow condition are reported in Table 4.3, where z_b is the depth of the loose bed from the bottom of the channel. In general, we can see that the profiles of velocity, concentration and granular temperature in the three sections are different. In particular the concentration profiles show that an evident stratification of the two classes is present in all the sections, with the large particles flowing mainly near the free surface while the small particles flowed mainly near the static bed. However an intermediate layer in which the two classes were mixed is present in all the sections too.

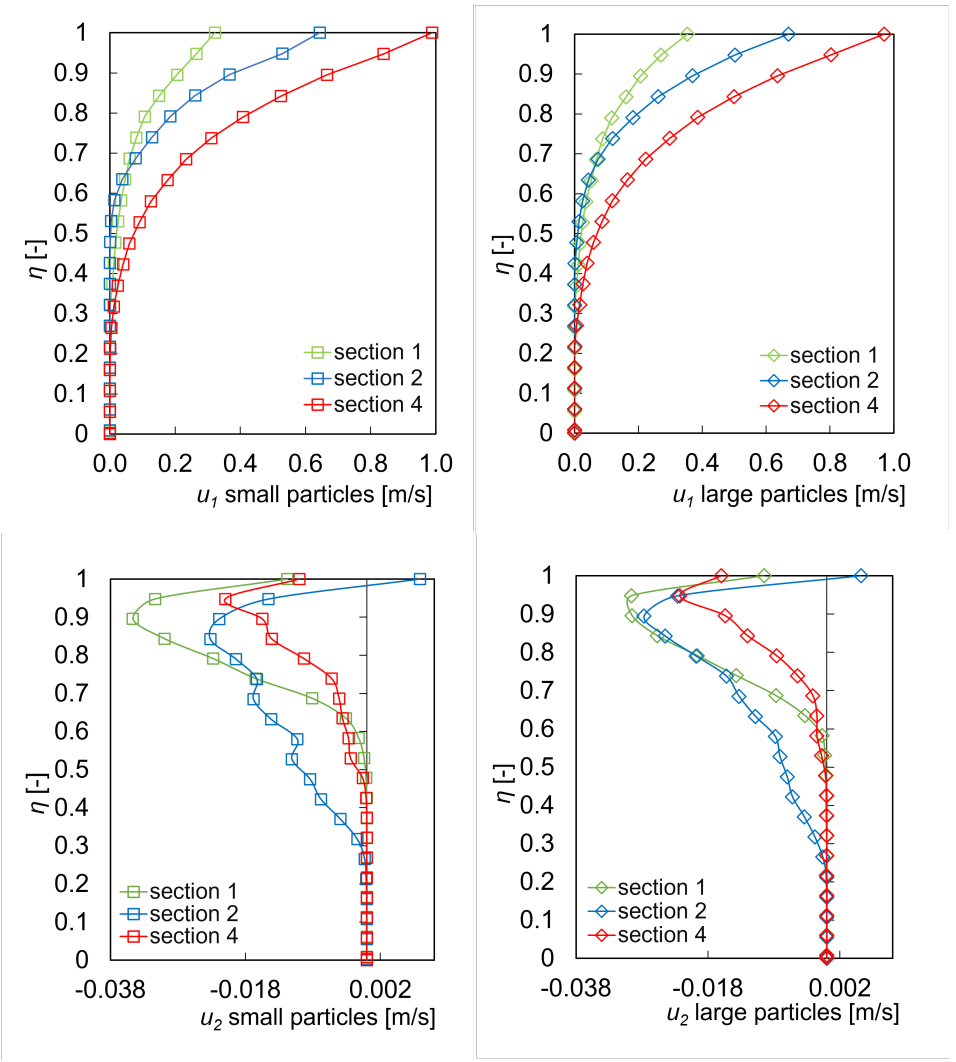

Figure 4.6: Test H0. Velocity profiles in sections 1, 2 and 4 of the flume (Fig. 4.2).

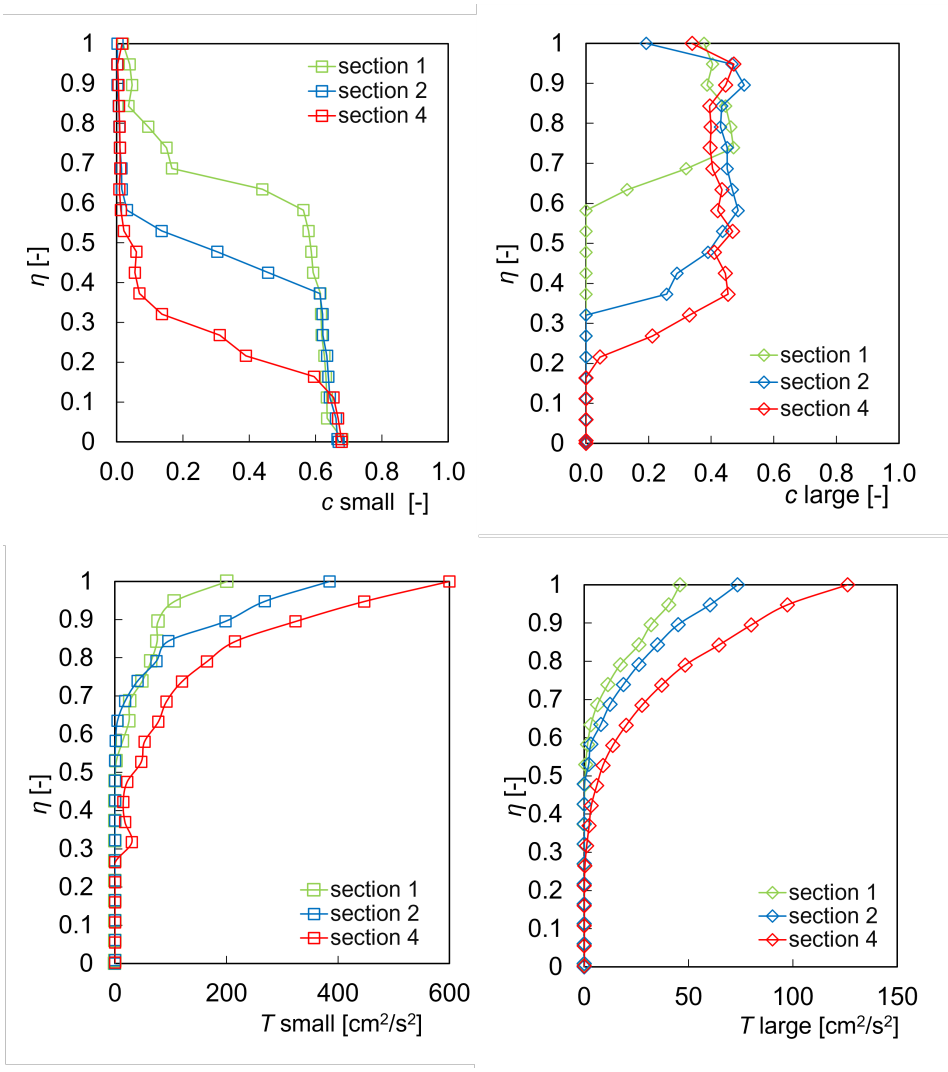

Figure 4.7: Test H0. Concentration and granular temperature profiles in sections 1, 2 and 4 of the flume (Fig. 4.2).

Table 4.3: Data for the homogeneous test H0 in 3 Sections of Fig. 4.13.

Test H0	**section** $S1$	**section** $S2$	**section** $S4$
distance [m]	2.60	3.20	3.00
h_0 [cm]	1.70	2.50	2.00
z_b [cm]	4.00	4.50	5.10

4.4.2 Results in sections 2 and 3

Since the profile in Sections S1, S2 and S4 are not constant (i.e the flow is not statistically homogeneous), we introduced a further measuring sections between the section S1 and S2 (Fig. 4.13).
We performed and analysed five new tests, defined H1, H2 H3, H4 and H5, which data are summarized in table 4.4. In test H1, H2 and H3 we kept constant the grain classes volumetric partition ($P_S = 50\%$ small and $P_L = 50\%$large), but changed the discharge ($Q_T^* = 20 - 30 - 50$). In the tests H4 and H5, instead, we checked different volumetric partition and different discharges: $P_S = 75\% - P_L = 25\% - Q_T^* = 120$ and $P_S = 25\% - P_L = 75\% - Q_T^* = 200$. Figures from 4.8 to 4.12 show that there is not an appreciable variation of the flow variables between section 2 and section 3. The gaps on the concentration profiles are considered acceptable due to the error on the measuring method. The overlapping of the profiles confirms the achievement of the statistically stationary condition. In this case the longitudinal velocity of the two phases result really similar for both the small and the large particles. We might conclude that the flow between the flow section 2 and section 3 can be considered statistically stationary and homogeneous (uniform channel flow) in all respect.

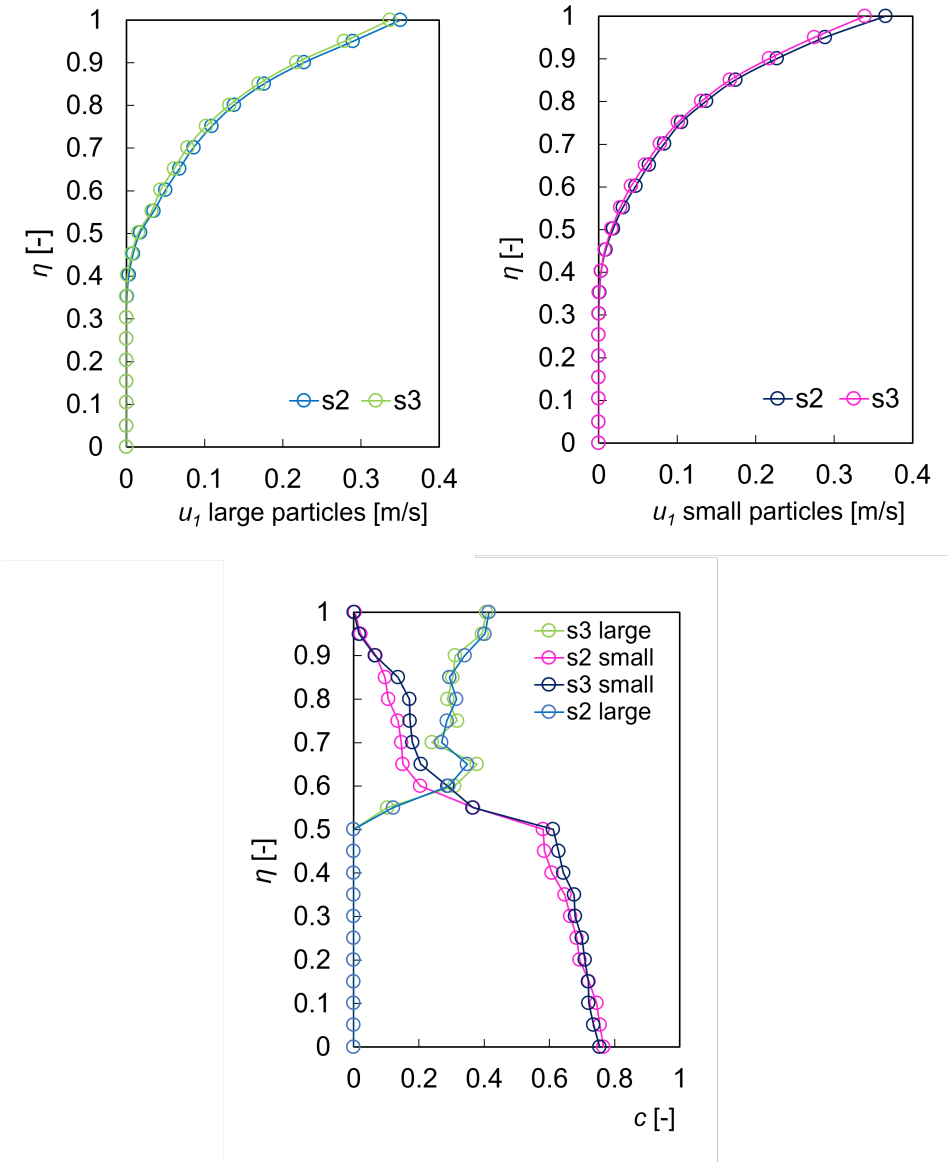

Figure 4.8: Test H1. Longitudinal velocity and concentration profiles in sections S2 and S3 of the flume (Fig. 4.2).

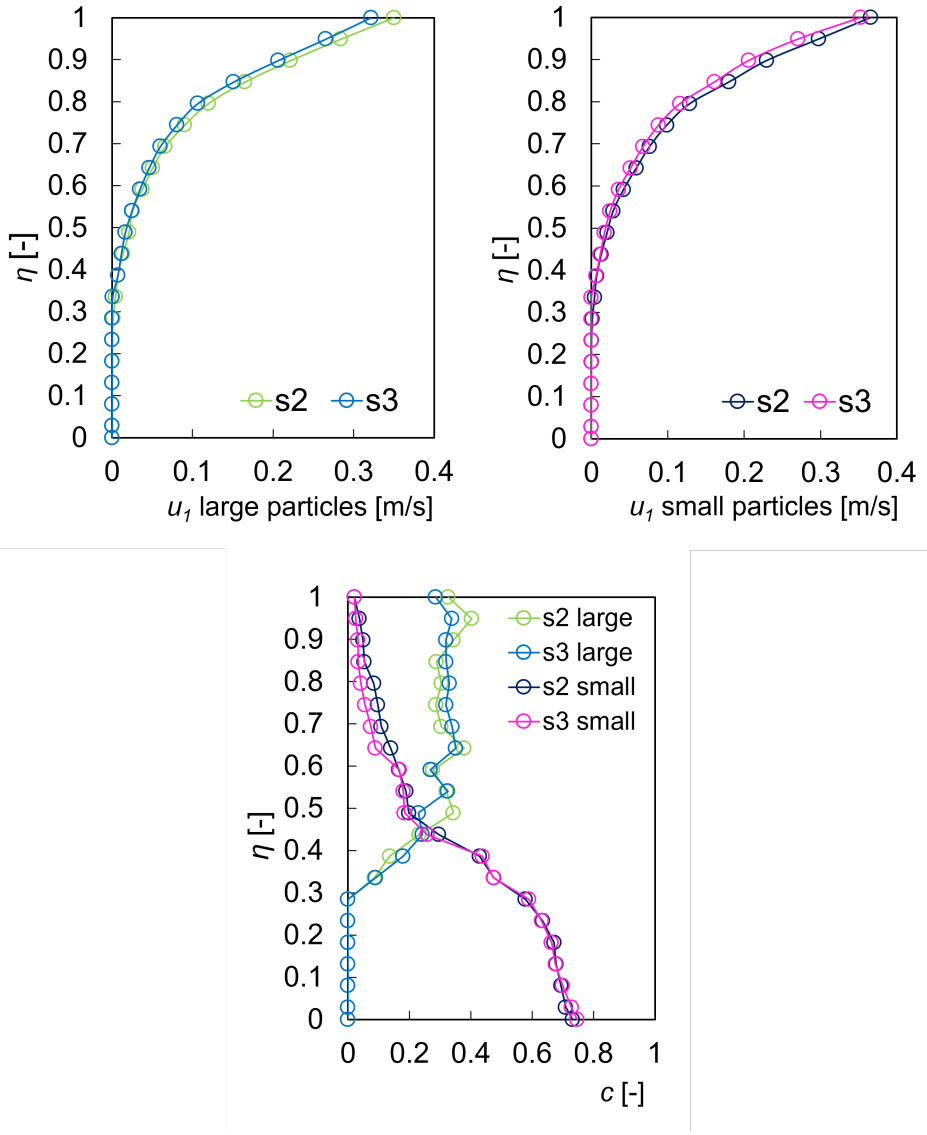

Figure 4.9: Test H2. Longitudinal velocity and concentration profiles in sections S2 and S3 of the flume (Fig. 4.2).

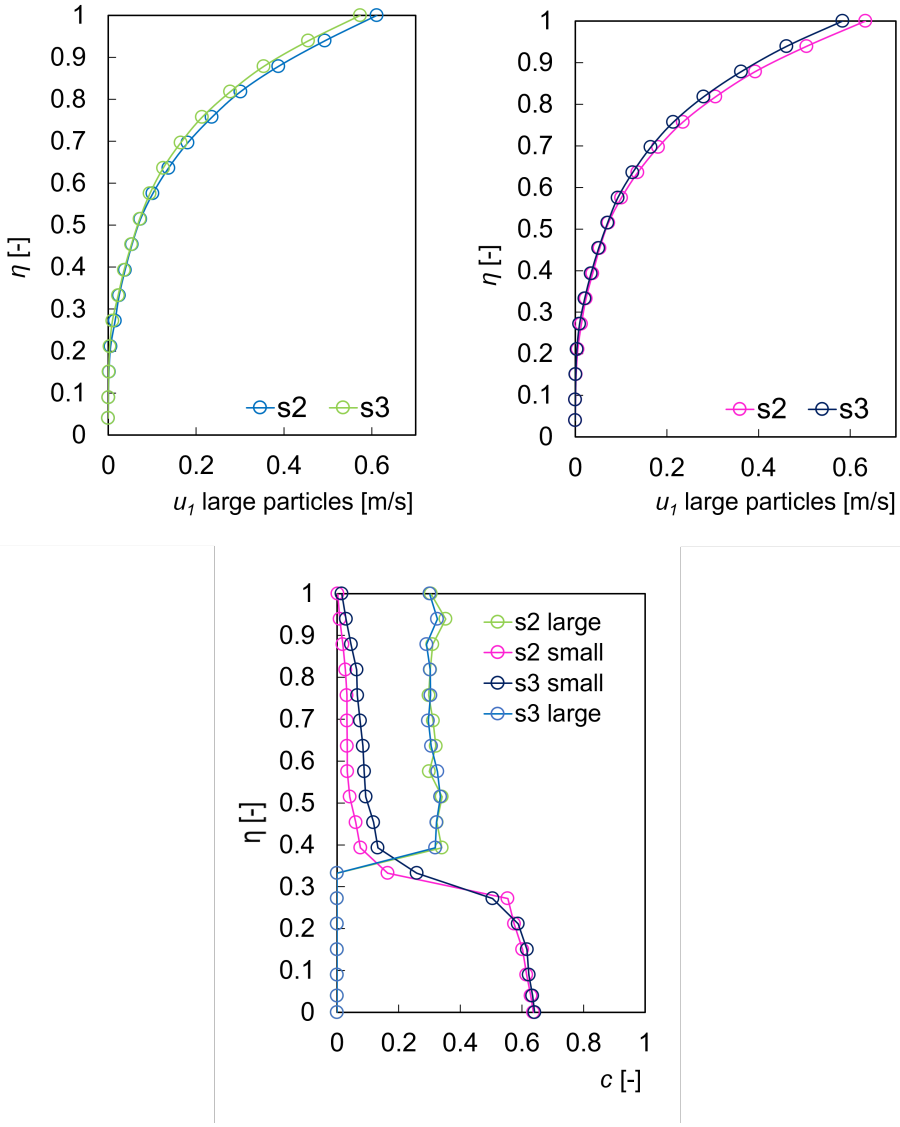

Figure 4.10: Test H3. Longitudinal velocity and concentration profiles in sections S2 and S3 of the flume (Fig. 4.2).

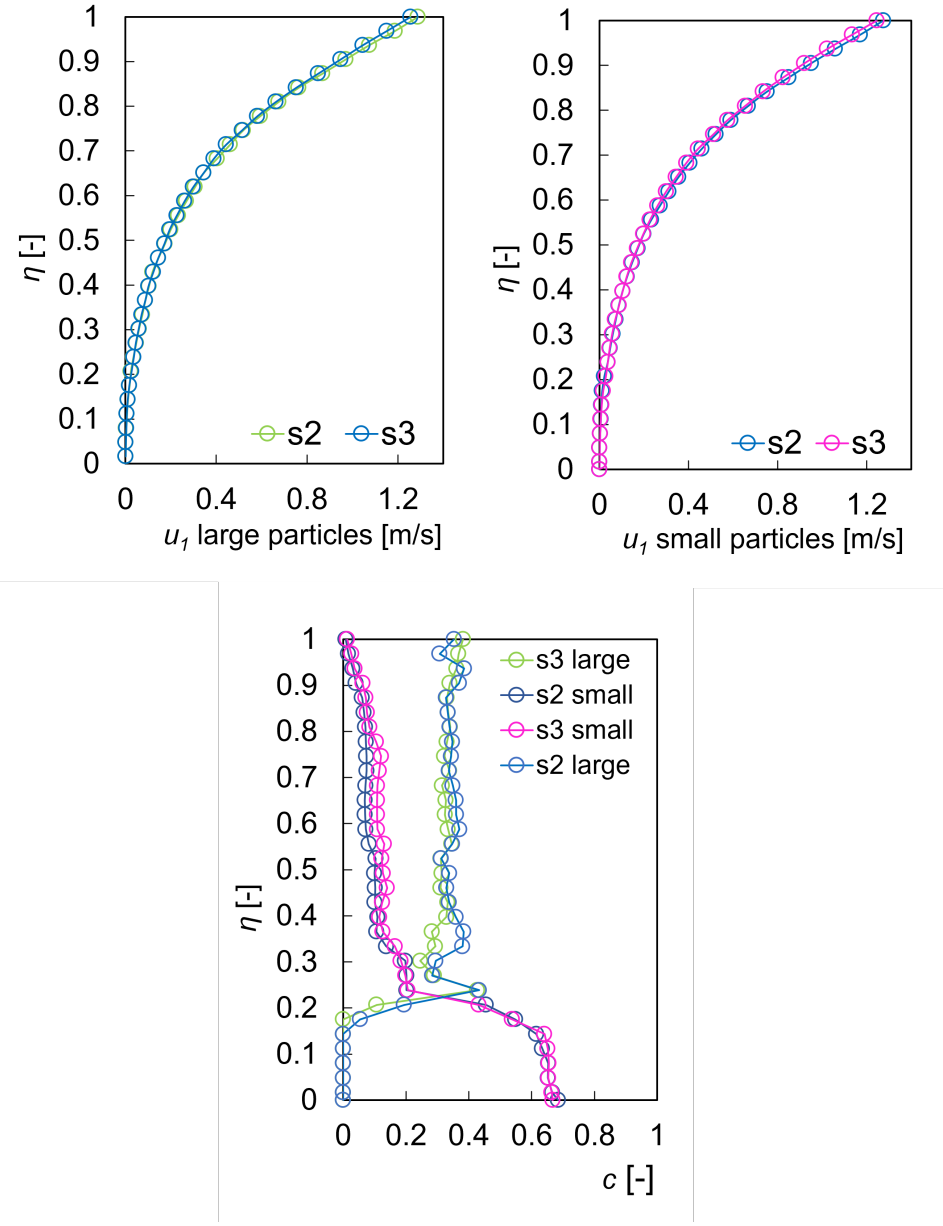

Figure 4.11: Test H4. Longitudinal velocity profile and concentration profiles in sections S2 and S3 (Fig. 4.2).

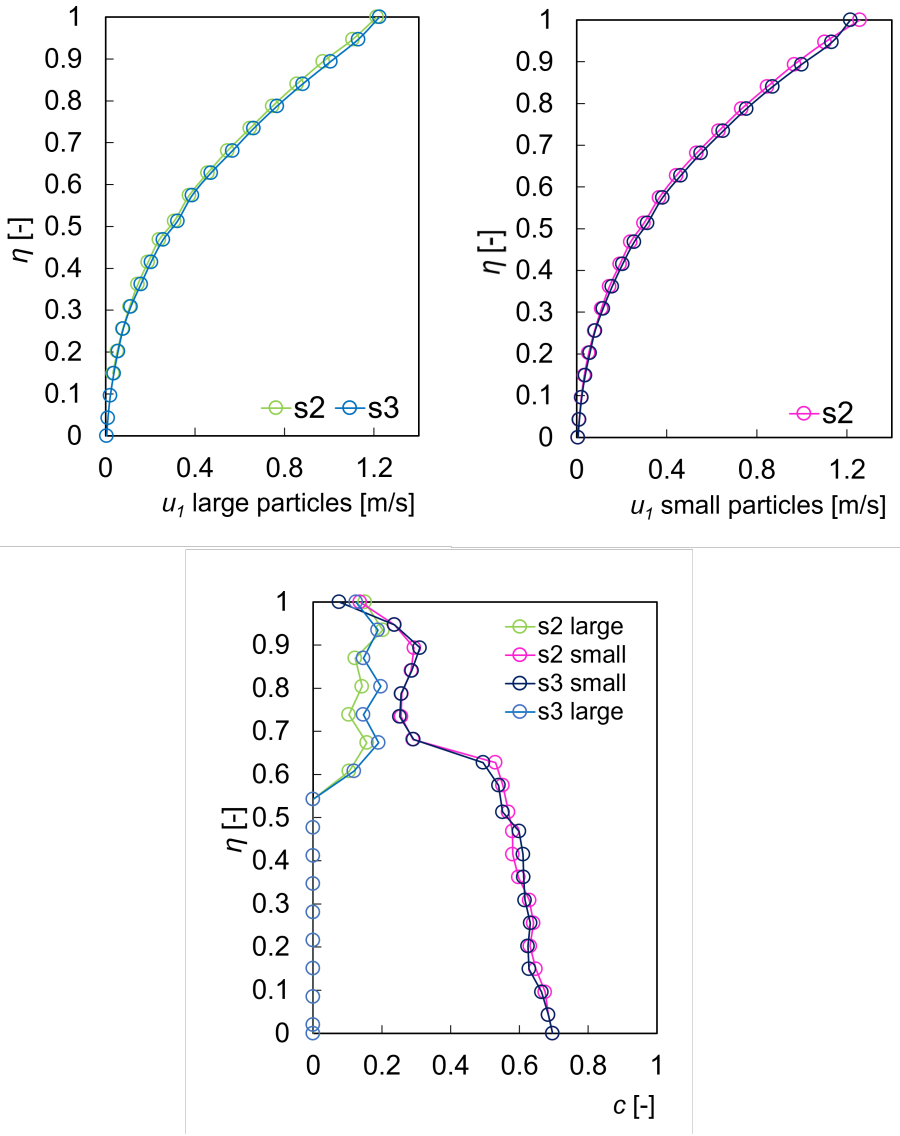

Figure 4.12: Test H5. Longitudinal velocity profile and concentration profiles in sections S2 and S3 (Fig. 4.2).

Table 4.4: Data for homogeneous condition tests in sections $S2$ and $S3$ (Fig. 4.2).

Test	Q_T^*	$P_S[\%]$	$P_L[\%]$	h_0 [cm]	z_b [cm]	z_t [cm]
H1	20	50	50	1.50	3.00	4.50
H2	30	50	50	2.00	4.00	6.00
H3	50	50	50	2.50	4.50	7.50
H4	120	75	25	3.00	4.50	7.50
H5	200	25	75	3.30	4.00	7.30

4.5 Conclusions

The previous tests were finalized to check the existence of a sufficiently long stretch of the channel in statistically stationary and homogeneous condition, already observed in uniform dry granular flows by [55] and [65], also for a binary mixture.

Moreover, in these works three different types of flow were identified along the flume: a decelerated, an accelerated and a uniform flow stretch. In our case, we observed the same features.

We identified the three type of flow on the loose bed: a decelerated part, a uniform flow sections in a stretch proportional to the granular discharge, then, immediately upstream of the weir, an accelerated section (Fig. 4.13). Therefore we can conclude that the granular mixture shows the same characteristics also in case of a bi-disperse mixture. We noticed, besides, that the uniform flow depth depends mainly on the feeding discharge. This consideration is valid as the slope of the surface depends on the discharge only [55, 65, 3]. With greater values of the slope of the flume, but maintain-

ing the discharge constant, the loose bed slope and the flow depth do not change since the volume of the deposit varies until the same properties are reached.

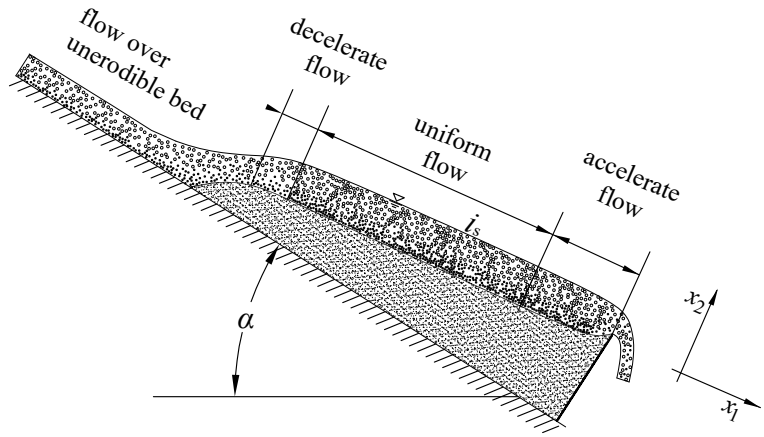

Figure 4.13: Three different flowing conditions are identified in the channel.

Chapter 5

Uniform channel flow results

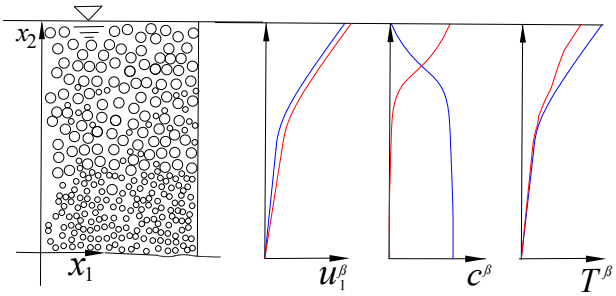

In this chapter the results of the tests concerning the uniform flow are presented. The first part examines the effect of the volumetric particle partition on the velocity, concentration and granular temperature average profiles. The second part tackles the problem of the influence of the discharge on the flow regime.

5.1 General remarks

The chapter aims at analysing the general features of the flow in the central reach of the flume in which the flow is statistically homogeneous and stationary (uniform channel flow).

In the uniform flow stretch, the flow regime results stratified, with the large grain-size class in the upper part of the flow depth and the small grain-size class at the bottom (Fig. 5.1). This configuration is reached in all the tests, independently from the percentage of the two grain-size classes composing the mixture and the flow rate. Consequently, the loose bed results composed mainly by the small grain-size class. Sometimes the large particles percolate downward in the loose bed, but the quantity is negligible respect to the black particles, also in experiments with high volumetric partition of the large grain-size class. Between the two layers of different particles, there is a mixing layer in which both the two grain-size classes are present. In addition, on this reach the slope of the free surface is parallel to the bed slope, i.e. the flow depth is constant.

Let us remember that in the tests we will always refer to the dimensionless flow rate $Q_T^* = Q_S^* + Q_L^*$, with $Q_\beta^* = Q_\beta / W d_\beta \sqrt{d_\beta g}$, where Q_β is the measured discharge (chapter 4).

The control volume is represented by the selected section of the frame and the ensemble of the particles the volume of the two grain size classes (Fig. 3.10, chapter chapter 3). The profiles of velocity, concentration and granular temperature refer to this control volume.

With *volumetric partition* we refer to the percentage of each single grain-size class respect to the total binary mixture. The total volume of the granular mixture is V_{tot} and it is composed:

$$V_{tot} = V_{small} + V_{large} \tag{5.1}$$

In this definition, used to distinguish the different initial mixture, we are not considering the voids. The total volume V_{tot} is that of the control volume chosen for the discharge measurement, as the volumetric partition P_β is measured at the end of each test respect to this control volume:

$$P_\beta = \frac{V_\beta}{V_{tot}} \tag{5.2}$$

Numerous tests were carried out to control precisely the percentage of the two grain-size classes in the flowing mixture. We highlight that with *vertical direction* we refer to the normal direction to the loose bed.

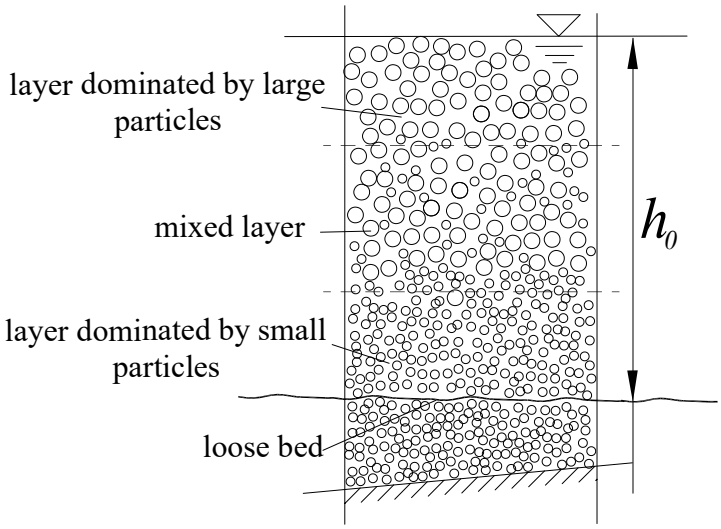

Figure 5.1: Different regions in the uniform flow stretch.

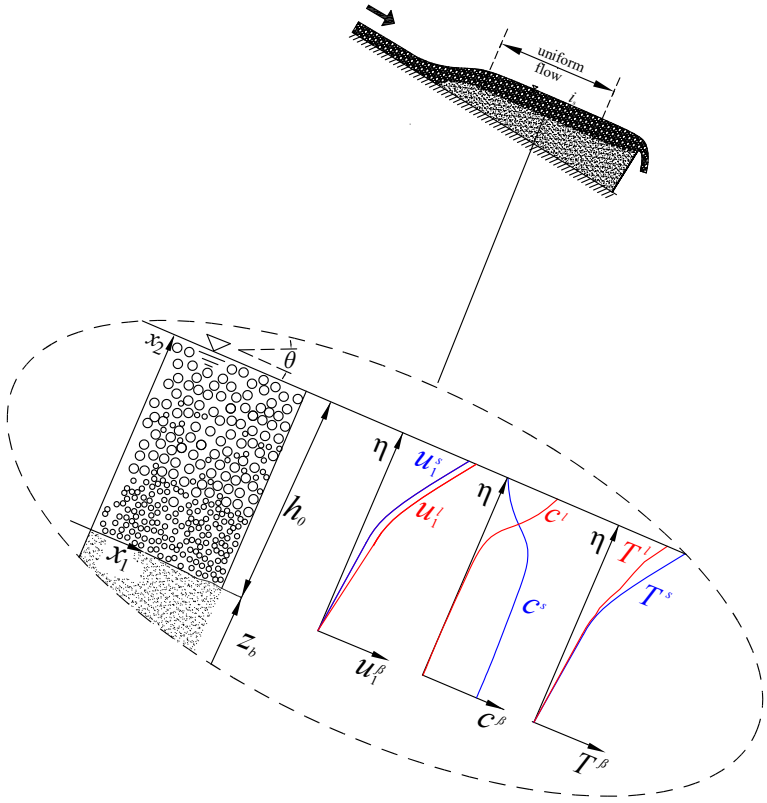

Figure 5.2: Scheme of the average temporal profiles in the uniform flow sections, of longitudinal velocity, concentration and granular temperature of the two grain size classes, *s* and *l*, along the adimensionless flow depth η, from the side-wall.

5.2 Velocity, concentration and granular temperature distributions

We did different tests to analyse how the flow regimes changes in relation to the volumetric partition of the mixture P_β and the total granular discharge Q_T^*. Different combinations of volumetric partition composing the discharge were tested:

- $P_S = 0$ and $P_L = 100\%$
- $P_S = 25\%$ and $P_L = 75\%$
- $P_S = 50\%$ and $P_L = 50\%$
- $P_S = 75\%$ and $P_L = 25\%$
- $P_S = 100\%$ and $P_L = 0\%$

Some preliminary tests were necessary to obtain the desired percentage. These combinations were tested with a low flow rate ($Q_T^* = 50$) and a high flow rate ($Q_T^* = 200$). In addition, for the combination $P_S = 50\%$ and $P_L = 50\%$ the tests were repeated for numerous flow rates to deeply analyse the effect of the discharge.

In the following analysis we made the vertical coordinate x_2 dimensionless with respect to the uniform flow depth h_0 (Fig. 5.2). Table 5.1 shows the features of the tests in steady uniform flow condition. In the following sections the results for each case are presented.

Table 5.1: Summary of all the tests conducted in the uniform flow section.

Test	$Q_T^* [-]$	$P_S [\%]$	$P_L [\%]$
B1	50	100	0
B2	200	100	0
W1	50	0	100
W2	200	0	100
P1	50	75	25
P2	200	75	25
P3	50	25	75
P4	200	25	75
Q1	16	50	50
Q2	32	50	50
Q3	40	50	50
Q4	50	50	50
Q5	70	50	50
Q6	80	50	50
Q7	90	50	50
Q8	150	50	50
Q9	200	50	50

5.2.1 Tests with uniform sized material

In order to have some information about the behaviour of the single class of particles, some tests were conducted with the small particle only or with the large particle only, which data are summarized in Tab. 5.2.

We analyse the results of the mixture composed by small particles. Figure 5.3 shows respectively the profile of longitudinal velocity, concentration and granular temperature for small particle for $Q_S^* = 50$ (low discharge), while Figure 5.4 shows the same variables for $Q_S^* = 200$ (high discharge).

The velocity profile for the low discharge ($Q_S^* = 50$) shows a concave distribution up to the top layer. For the high discharge test, the velocity profile shows an inflection point with a convex trend near to the free surface. The two different configurations suggest that at higher discharges the flow presents a layer dominated by collisional regime, as already observed by Mennino et al. [55] and Armanini et al. [8].

The concentration profiles (central plot of Figures 5.5 and 5.6) show that the concentration decreases systematically moving toward the free surface, exhibiting a strong change in the decreasing rate near to the free surface. As expected, the concentration gradient in the lower part of the flow depth are higher at higher discharge. As regards the granular temperature, the gradients in this case are much higher at higher flow discharges.

Figure 5.5 and Figure 5.6 show the same variables for the test with large particles only. One of the most evident difference between large and small particle variables profiles is in the granular temperature profile, which is notably larger for the large particles. The inflection point in the longitudinal velocity profile is more evident as well. These differences suggest that the collisional component of the flow is more important for the larger particles. In addition, the longitudinal velocity increases with the discharges.

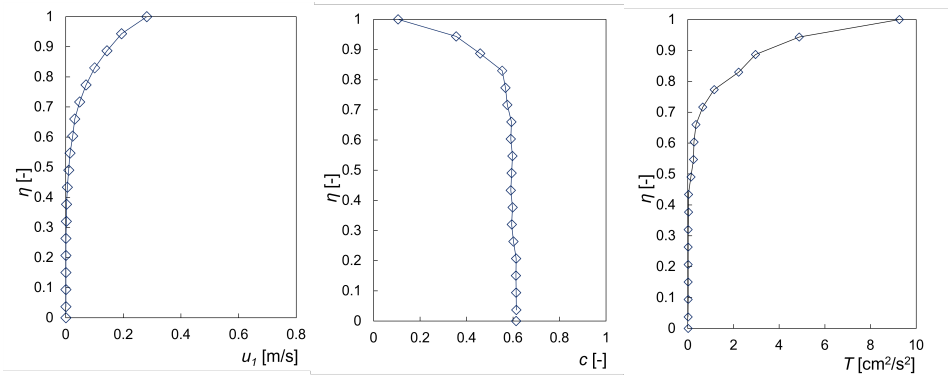

Figure 5.3: Test B1. Profiles of longitudinal velocity, concentration and granular temperature (small particles, $Q_T^* = 50$) .

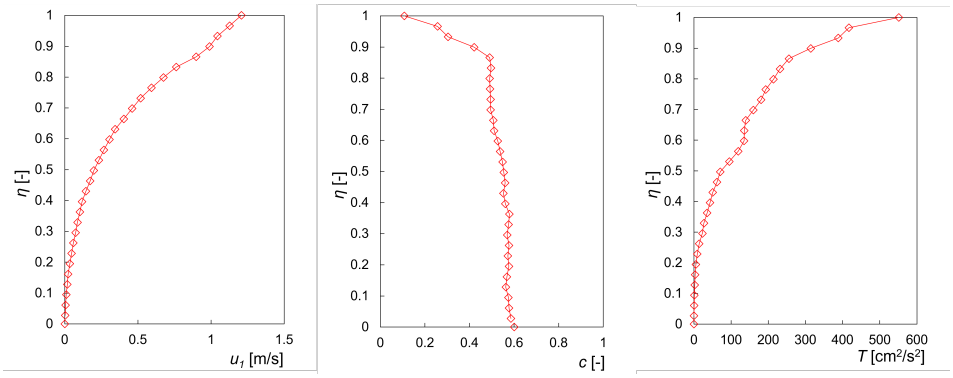

Figure 5.4: Test B2. Profiles of longitudinal velocity, concentration and granular temperature (small particles, $Q_T^* = 200$).

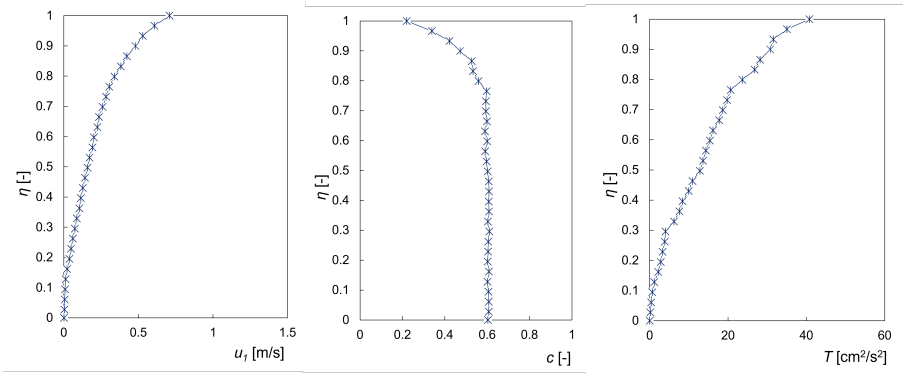

Figure 5.5: Test W1. Profiles of longitudinal velocity, concentration and granular temperature (large particles, $Q_T^* = 50$).

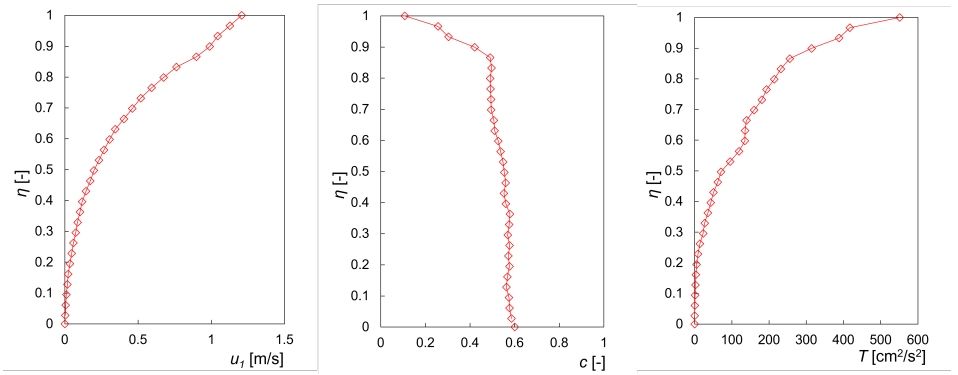

Figure 5.6: Test W2. Profiles of longitudinal velocity, concentration and granular temperature (small particles, $Q_T^* = 200$).

Table 5.2: Summary of the the uniform sized test in the uniform flow section.

Test	$Q_T^*[-]$	$P_S[\%]$	$P_L[\%]$	h_0 [cm]
B1	50	100	0	1.20
B2	200	100	0	2.00
W1	50	0	100	1.50
W2	200	0	100	2.30

5.2.2 Tests with granular mixture $P_S = 75\%$ and $P_L = 25\%$

In this case the granular mixture is composed mainly by small particles. We conducted a test, defined as test P1, with the low discharge $Q_T^* = 50$ and a second one, defined as P2, with the high discharge $Q_T^* = 200$, which main properties are reported in Table 5.3.

Figure 5.7 shows that the components of the velocity nearly coincides between the two classes. The Figure 5.9 confirms that with the higher discharge also the profiles of the velocity component of the two fractions coincide. The intensity of the longitudinal velocity component is higher at higher discharges as well as the vertical component and this means that the the granular discharge influences the value of the velocity vector. In these tests we did not observe the inflection point in the longitudinal velocity distribution nor for the higher discharge. The vertical velocity distribution shows that for both the classes a downward flux is present. We will discuss this downward flow in the next section.

Figure 5.8 and Figure 5.10 show the profile of the concentration and granular temperature for both classes and for the test P1 and P2 respectively. The concentration profiles show a marked (as already mentioned) tendency to stratification, with the larger particles concentrated in an upper

layer and well mixed with the small ones, while the lower layer is composed by the small particles only. However, even in the upper layer, between these two layers there is a mixed layer showing a smooth transition between the two.

In Figure 5.8 and Figure 5.10 we reported also the total volume concentration, defined as the sum of the concentration of the two classes. These profiles present a trend similar to that of single classes profile: in the lower part of the profile the concentration tends to decrease nearly linearly moving upwards, with a stronger negative gradient near the free surface.

The right plot of Figure 5.8 and Figure 5.10 show the granular temperature profile of the two classes for both the flow rates. The granular temperature profile shows a different behaviour for the two grain-size classes. Also in this case the smaller class exhibits an higher granular temperature with respect to the larger particles. This difference is likely due the larger relative mean path of the small grain size class.

Table 5.3: Data of the tests P1 - P4.

Test	$Q_T^*[-]$	$P_S[\%]$	$P_L[\%]$	h_0 [cm]
P1	50	75	25	1.50
P2	200	75	25	3.00
P3	50	25	75	1.20
P4	200	25	75	2.90

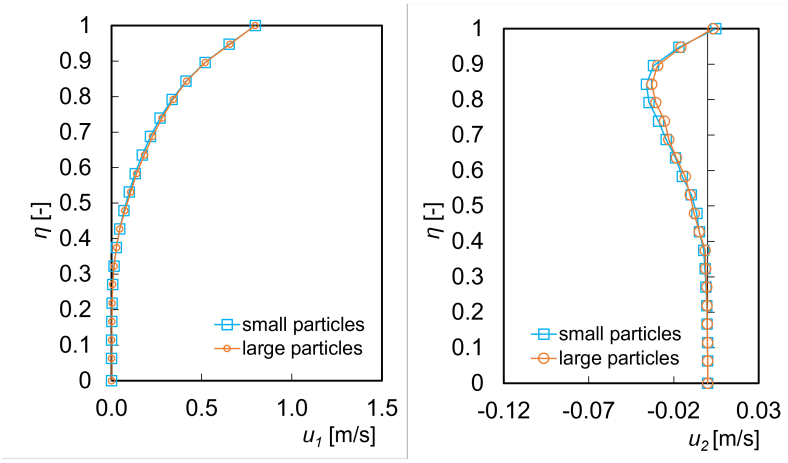

Figure 5.7: Test P1. Velocity profiles.

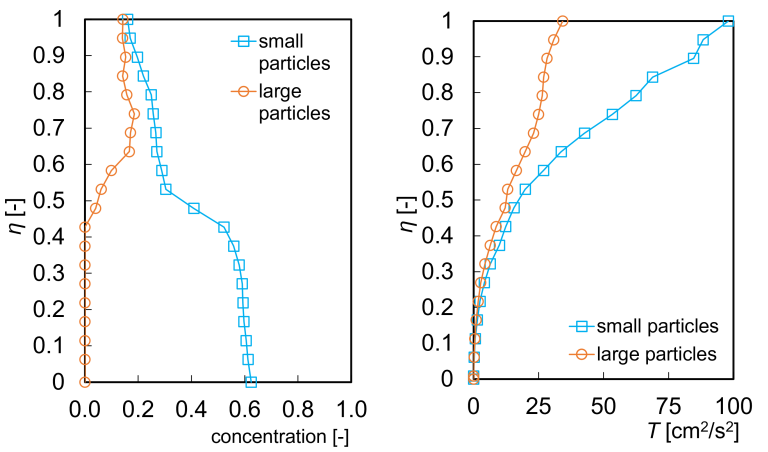

Figure 5.8: Test P1. Concentration and granular temperature profiles.

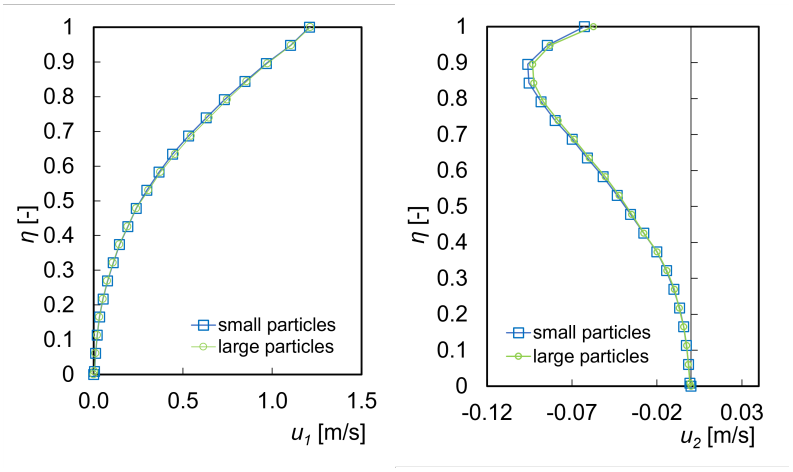

Figure 5.9: Test P2. Velocity profiles.

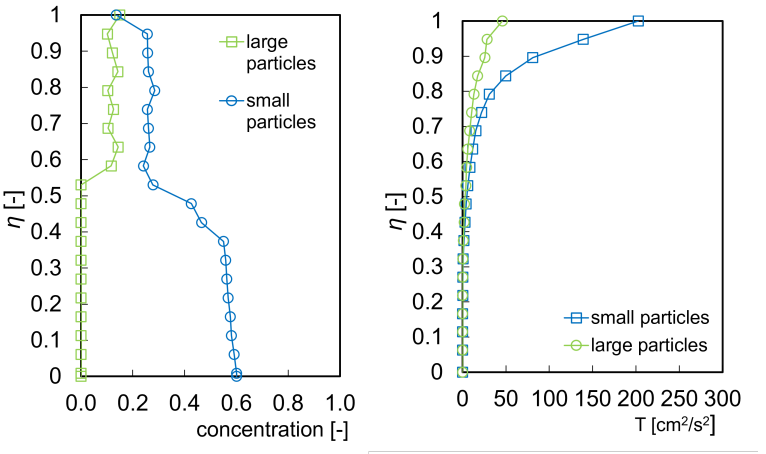

Figure 5.10: Test P2. Average concentration and granular temperature profiles.

5.2.3 Tests with granular mixture $P_S = 25\%$ and $P_L = 75\%$

In this case the mixture is composed mainly by large particles. Figure 5.11 shows the profile of the longitudinal and normal velocity component for both classes. Figure 5.13 shows the same profile for the higher discharge ($Q_T^* = 200$).

As regard the velocity profiles, both in longitudinal and vertical direction, the same considerations of the case of the previous granular mixture are valid. The velocity vectors of the two grin-size classes coincide. The longitudinal velocity profile in case of high discharge shows a shiny kink at the top layer, whereas the profile for low discharge is concave. This result suggests the existence of a top layer dominated by collisions in case of high discharge. Again the vertical velocity profiles are not equal to zero and they indicate the presence of a small vertical motion downward, of both the two grain-size classes.

Moreover, we can notice that the mixed layer increases with the discharge, as in case of high discharge test, the thickness of the small particles decreases. From Figure 5.12 and Figure 5.14 we can see that the granular temperature profiles of the two grain-size class have a similar trend independently from the discharge. Again here the granular temperature of the small particles is greater than that of the large particles.

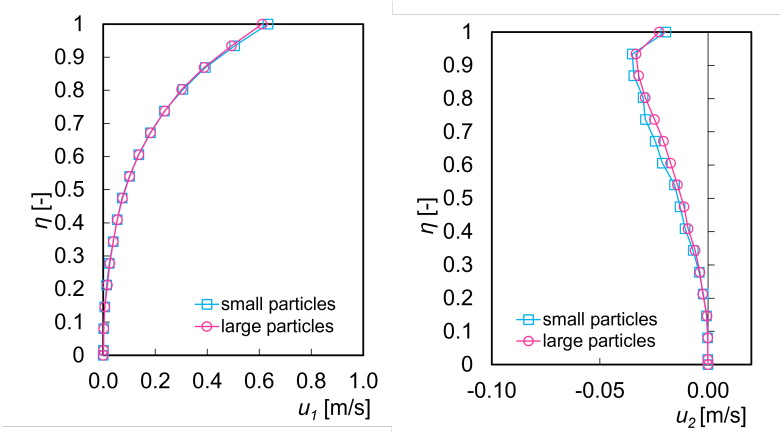

Figure 5.11: Test P3. Velocity profiles.

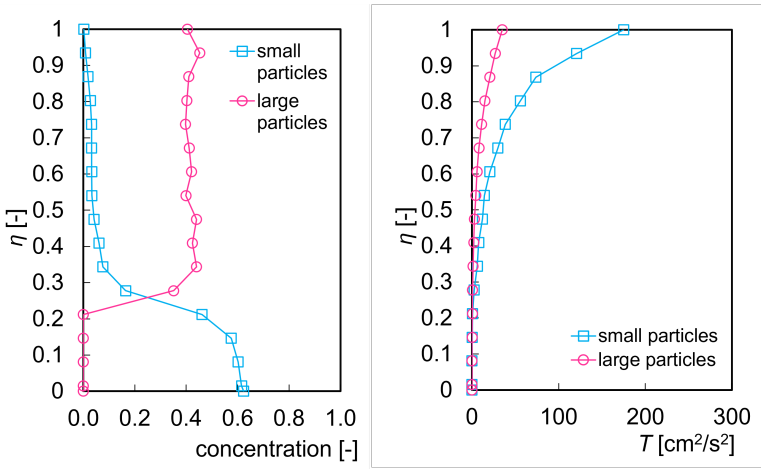

Figure 5.12: Test P3. Concentration and granular temperature profiles.

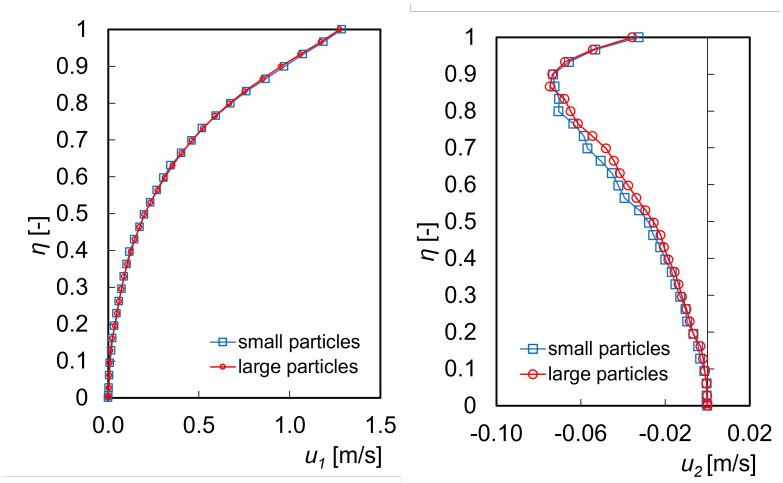

Figure 5.13: Test P4. Velocity profiles.

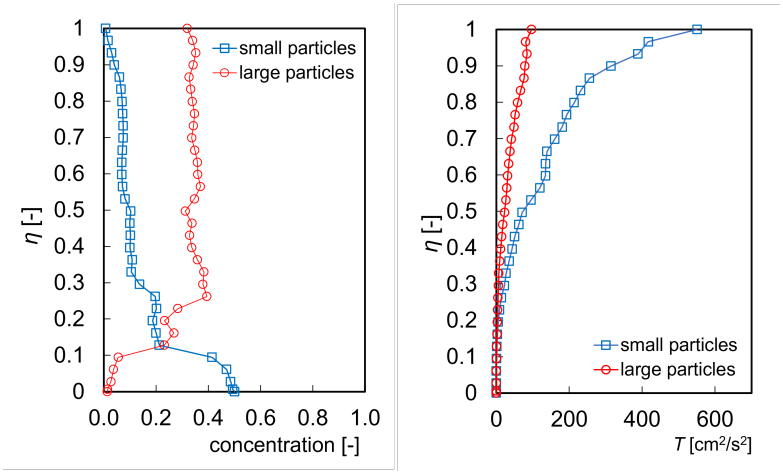

Figure 5.14: Test P4. Concentration and granular temperature profiles.

5.2.4 Tests with granular mixture $P_S = P_L = 50\%$

We performed the tests with $P_L = 50\%$ and $P_S\% = 50\%$ even with more discharges in order to better highlight the effect of the discharge on the flow field.
In particular, we conducted nine tests with the following dimensionless total granular discharges: $Q_T^* = 16 - 32 - 50 - 70 - 80 - 110 - 150 - 220$.

By taking into account the previous results and the role the collisional regime, we grouped these tests in three groups:

- low discharge: $Q_T^* = 16 - 32 - 40$;
- intermediate discharge: $Q_T^* = 50 - 70 - 80$;
- high discharge: $Q_T^* = 110 - 150 - 200$;

In the next sections we show the results of the tests according to this division. The data of the tests are reported in Table 5.4.

Table 5.4: Data for tests with same volumetric partitions.

Test	Q^* [-]	$P_S[\%]$	$P_L[\%]$	h_0 [cm]
Q1	16	50	50	1.00
Q2	32	50	50	1.25
Q3	40	50	50	1.50
Q4	50	50	50	2.20
Q5	70	50	50	2.37
Q6	80	50	50	2.50
Q7	110	50	50	2.60
Q8	150	50	50	3.10
Q9	200	50	50	4.00

5.2.4.1 Velocity profiles

Figures 5.15, 5.16 and 5.17 report the longitudinal and normal velocity profiles for the different discharge classes. In general the longitudinal velocity profiles exhibit at the beginning a downward concavity. After, its trend changes according to the different flow rates. In particular, analysing the results in Figures 5.15, 5.16 and 5.17, we can see that for very low and intermediate discharges the trend is concave up to the top layer. The low discharge test (Fig. 5.15) presents a lower velocity with respect to the others. Moreover, we can notice that the velocity of the two grain-size classes has exactly the same trend, both in the longitudinal and vertical directions. As regard the high discharge tests (Fig. 5.17), we can see that there is not a large difference between the velocity test with $Q_T^* = 110$ and the $Q_T^* = 150$, but there is a strong difference between the tests with discharge $Q_T^* = 150$ and $Q_T^* = 200$. An inflection point is present in both the cases and we can observe that the maximum values of the vertical velocity are between $\eta = 0.8 - 0.9$. In the next chapter we will explain this downward flux more in detail. The vertical velocity is not null, although the values are pretty small. The profile underlines a transversal gradient and it displays the presence of a downward displacement of the particles. This can suggest the presence of secondary circulations close to the walls or due to diffusive terms. Secondary circulations were already found in the work by Rossi [65]. The intermediate discharge tests (Fig. 5.16) show a behaviour between the two other cases, again the longitudinal velocity profiles of the two grain size classes coincide, but the inflection point is not present yet. We can observe that both the longitudinal and the vertical velocity maximum value increase with the discharge (e.g. the maximum longitudinal velocity in the low discharge case is equal to 0.5 m/s, whereas in the high discharge tests it arrives up to 1.20 m/s.)

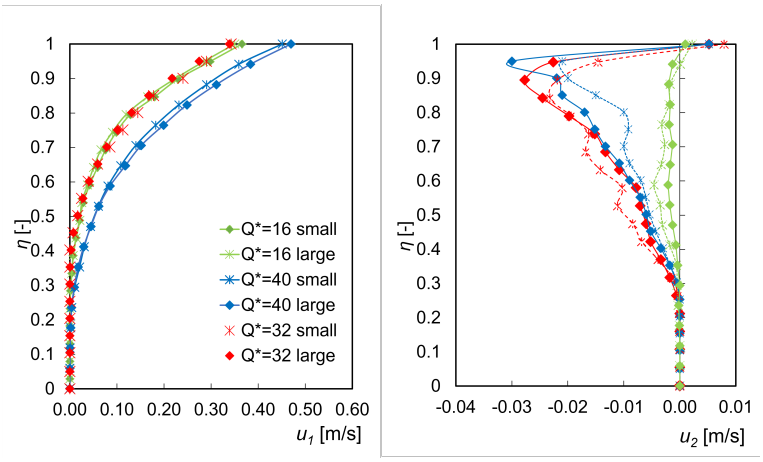

Figure 5.15: Velocity profiles for the group of low discharges $Q_T^* = [16 - 40]$

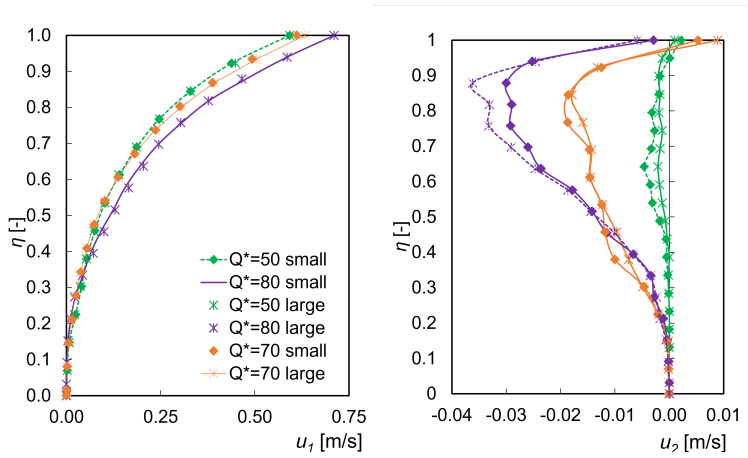

Figure 5.16: Velocity profiles for the group of intermediate discharges $Q_T^* = [50 - 80]$

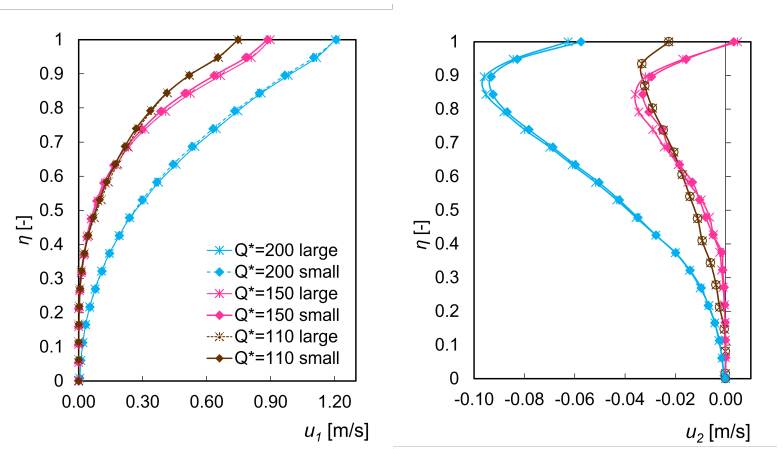

Figure 5.17: Velocity profiles for the group of high discharges $Q_T^* = [110 - 200]$.

5.2.4.2 Concentration profiles

Figures from 5.18 to 5.20 report the average concentration profiles. From the graphs we can see that there is a strong tendency to stratification. If we observe Fig. 5.18, we can see that with the lowest discharge $Q_T^* = 16$ the stratification results much more marked and the layer with no large particles arrives nearly up to the middle of the flow depth ($\eta = 0.5$). In contrast, for the highest discharge ($Q_T^* = 50$) the layer of small particles results much smaller, up to $\eta = 0.15$.

There are not remarkable differences for the concentration of the large particles in this test. We can notice that for intermediate discharges (Fig. 5.19), in the case of $Q_T^* = 50$ and $Q_T^* = 70$, the upper layer dominated by large particles is larger with respect to the low discharge tests (Fig. 5.18). For the high discharge case (Fig. 5.20), the concentration profiles exhibit

the existence of a lower layer in which the large solid fraction is not present and the flow depth of this layer does not depend on the discharge. In the upper part of the flow we can see the presence of layer dominated by the small particles, that decreases with the discharge. In addition, the profiles show that the gradients of the total concentration are considerably higher for $Q_T^* = 200$, reporting an important dominance of the collisional regime, as it will be better explained in the next chapter.

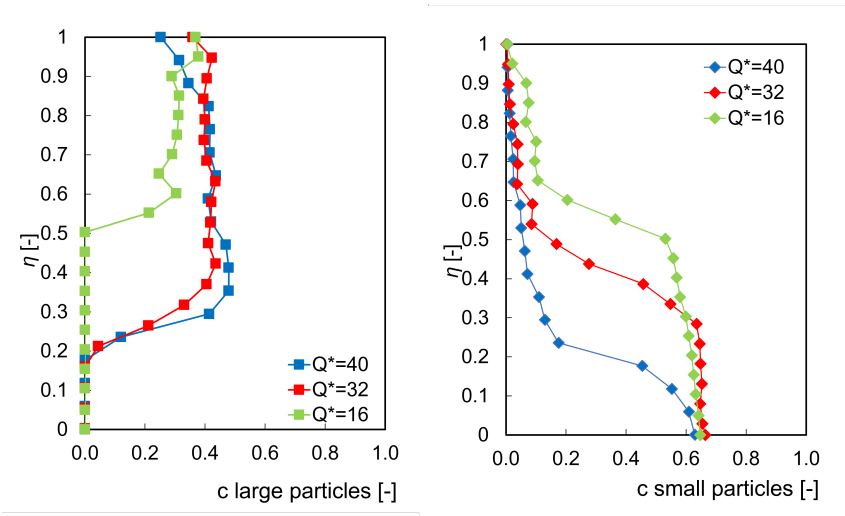

Figure 5.18: Concentration profiles for the group of low discharges $Q_T^* = [16 - 40]$

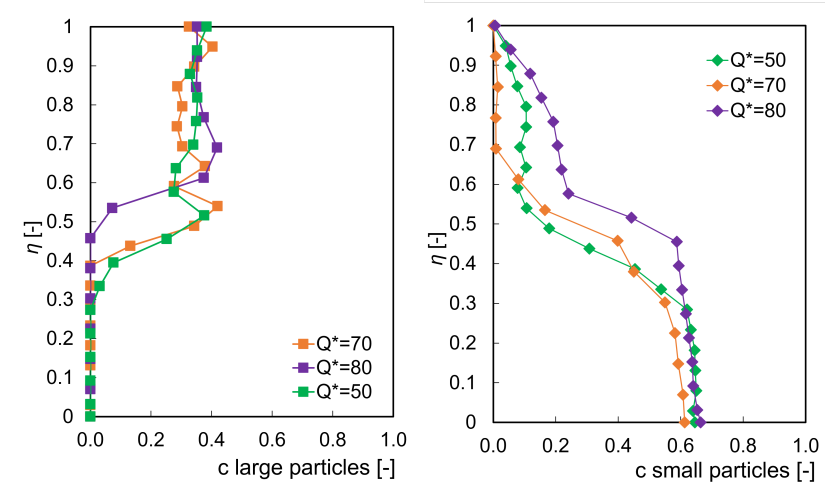

Figure 5.19: Concentration profiles for the group of intermediate discharges $Q_T^* = [50 - 80]$

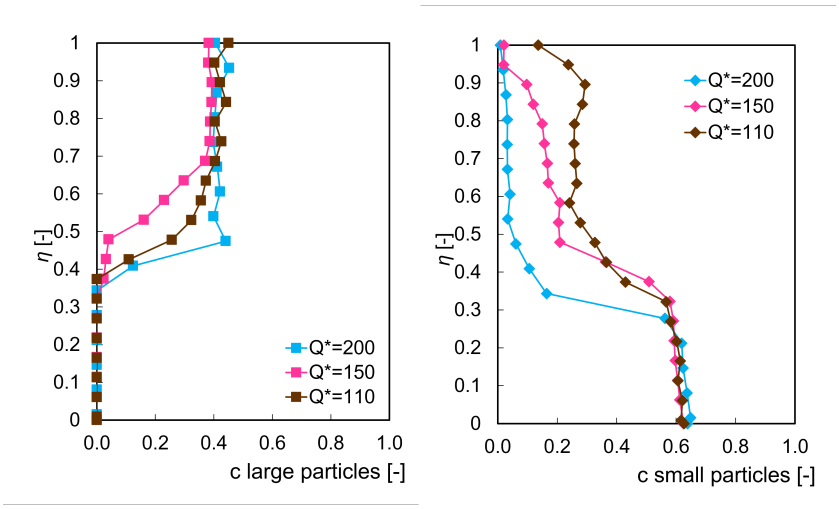

Figure 5.20: Concentration profiles for the group of high discharges for $Q_T^* = [110 - 200]$

5.2.4.3 Granular temperature profiles

Figures 5.21, 5.22 and 5.23 show the granular temperature profiles of the two grain size classes. Let us remember that the granular temperature represents the kinetic energy per unit mass of the fluctuating component of the particles velocity.

We can observe that, generally, the granular temperature of both the two grain-size classes increases going to the free surface and has a similar trend to that of the longitudinal velocity. If we observe the low discharge tests (Figure 5.21), as we could have expected, the granular temperature monotonically increases moving upwards at increasing the discharge.

For the high discharge test (Figure 5.23), we can see that for the small particles we have high gradients from $\eta = 0.75$, but at the same time the particle concentration is really low. For the large particles the gradients are smaller, on the other hand the particle concentration results high.

The granular temperature of the small grain-size class always results grater than that of the large particles for the reason already mentioned (larger relative mean path of the small grain size class).

We also computed (not reported here) the kinetic energy respect the fluctuation of the velocity. In this case, as the granular temperature is multiplied for the mass of the single phase (small and large respectively), the kinetic energy of the large particle result always greater than that of the small particles, leading to hypothesize the non equipartition of the fluctuating of the kinetic energy [19, 25].

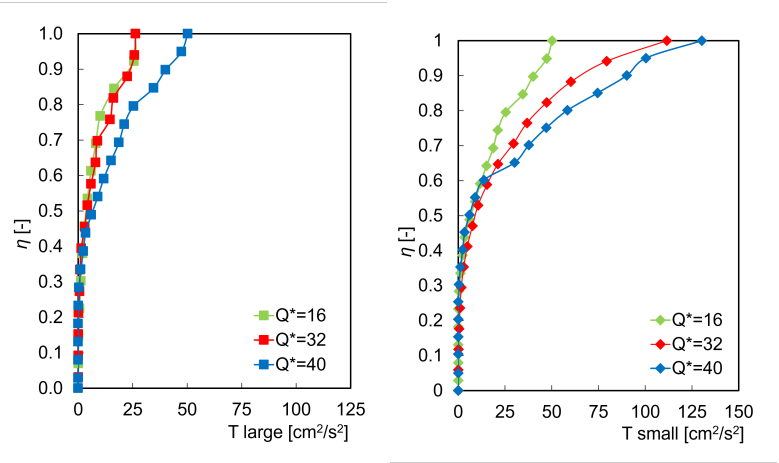

Figure 5.21: Granular temperature for the group of low discharges $Q_T^* = [16 - 40]$.

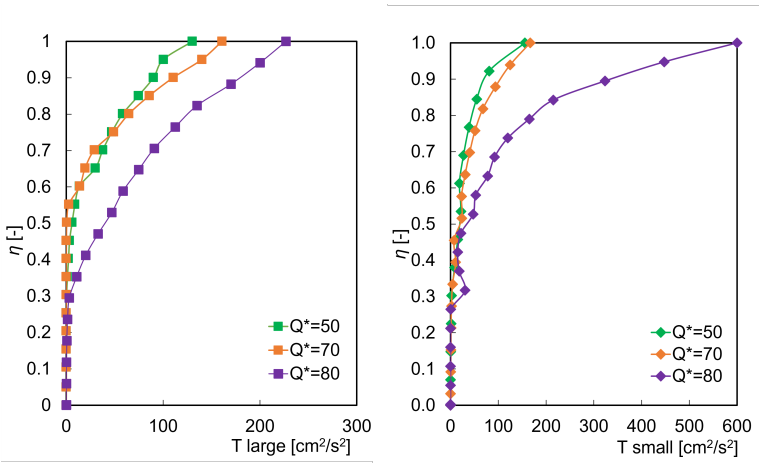

Figure 5.22: Granular temperature for the group of intermediate discharges $Q_T^* = [50 - 80]$

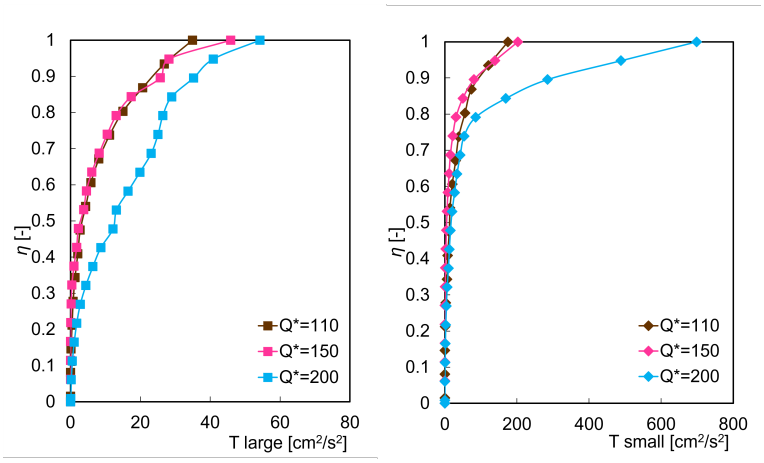

Figure 5.23: Granular temperature for the group of high discharges $Q_T^* = [110 - 200]$

5.2.5 Conclusions

As regards the effect of the different volumetric partition in the uniform channel flow, we can affirm that independently from this quantity, the binary mixture segregate in two layers, in which the large particles are at the top layer and the small one at the bottom. The different volumetric partition influences the dimension of the mixed layer, but the granular discharge results having the key role in the process. The longitudinal velocity and the granular temperature profiles show that the regime is dominated by friction up to high discharge values, independently from the volumetric partition.

5.3 Free surface and bed slopes

The experiments in Mennino et al. [55] underlined that the slope of the free surfaces is steeper or equal to that of the friction angle of the packed material. If we analyse the experiments with equal percentage of the two grain-size classes and an average value for the discharge and the friction angle of the particles, the same results is obtained (Fig. 5.24). Moreover, with respect to the ratio W/h between the width of the channel and flow depth, the slope of the free surface tends to assume a constant value, close to the average friction angle of the two grain-size classes (Fig. 5.25). This result was already observed in Mennino [55] and Taberlet [71], for the case of homogeneous material. According to the flow rates, the uniform flow depths increases for higher values of discharge, as the Fig. 5.25 shows.

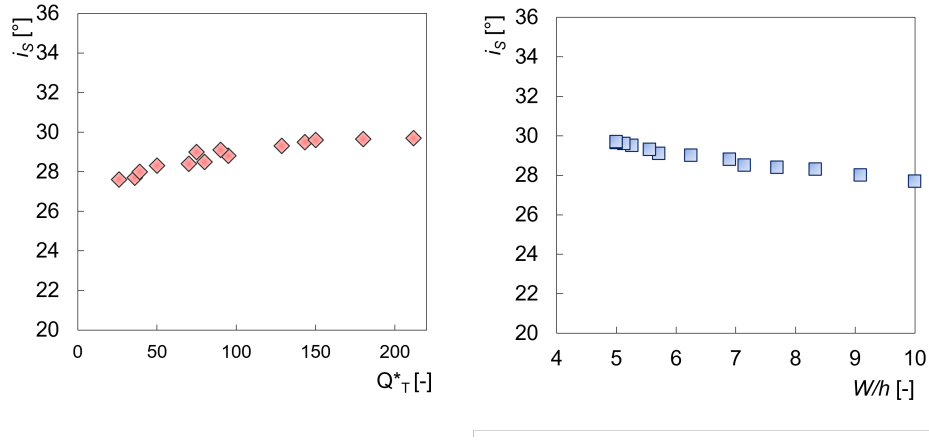

Figure 5.24: Free surface slope as function of the dimensionless discharge and relation between the slope of the free surface and the ratio w/h in experiments with equal percentage of the two grain-size classes.

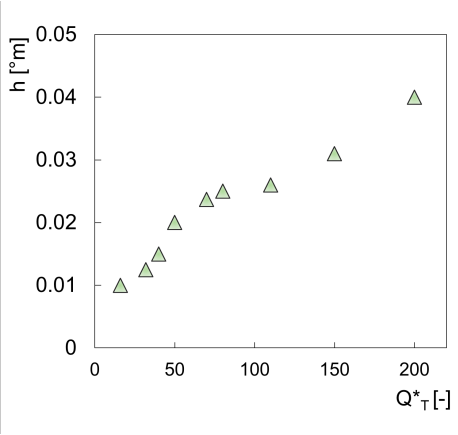

Figure 5.25: Uniform flow depth as a function of the non-dimensional granular discharge.

Chapter 6

Analysis and discussion

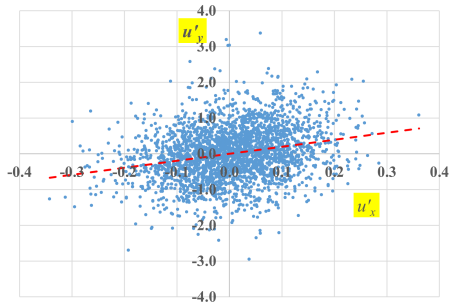

In this chapter we present some further processing of the experimental data, useful to better understand the dynamics of mixtures of different grains size classes. In particular, we wanted to perform some analyses of the mass and momentum balances also in the light of some rheological models existing in the literature.

6.1 Two-dimensional mass and momentum balances of bimodal granular material

In chapter 2 we presented a general approach to non-uniform grain-size granular flow (chapter 2, eq. (2.1)). By introducing the Reynolds decomposition [34] of the variables of the system of Eqs. (2.1), which govern the flow in a 2D uniform channel (x_1, x_2), with the same algebra the system is changed as follows:

- mass balances of the two classes:

$$\frac{\partial}{\partial x_2}(c^\beta u_2^\beta) + \frac{\partial}{\partial x_2}(\overline{c'^\beta\, u'^\beta_2}) = 0 \tag{6.1}$$

- momentum balances for each grain size class β:

$$c^\beta g\rho_s \sin\theta + \frac{1}{\rho_s}\frac{\partial \tau_{12}^\beta}{\partial x_2} - \frac{\partial}{\partial x_2}\left(c^\beta u_1^\beta u_2^\beta\right) - \frac{\partial}{\partial x_2}\left(c^\beta \overline{u'^\beta_1\, u'^\beta_2}\right) + \frac{1}{\rho_s}\frac{\partial}{\partial x_2}\left(\xi_{12}^\beta\right) = 0 \tag{6.2}$$

$$c^\beta g\rho_s \cos\theta + \frac{1}{\rho_s}\frac{\partial \sigma_{22}^\beta}{\partial x_2} - \frac{\partial}{\partial x_2}\left(c^\beta u_2^\beta u_2^\beta\right) - \frac{\partial}{\partial x_2}\left(c^\beta \overline{u'^\beta_2\, u'^\beta_2}\right) + \frac{1}{\rho_s}\frac{\partial}{\partial x_2}\left(\xi_{12}^\beta\right) = 0 \tag{6.3}$$

with $\beta = s, l$. θ is the slope of the loose bed and of the free surface, τ_{12}^β are the tangential stresses (frictional and collisional, chapter 2), the terms $\overline{u'^\beta_1\, u'^\beta_2}$ and $\overline{u'^\beta_2\, u'^\beta_2}$ are Reynolds-like stresses and ξ_{12}^β represents the stresses exerted on the size class β by the other class.

In the momentum balances (Eqs. (6.2) and (6.3)) we neglected the second and third order correlation terms containing the fluctuating components of concentration, since, as we will see, these terms are negligible in particular with respect to the weight forces.

To better analyse the physical processes that occur in the flow of the

bimodal mixture, we have deviated from the experimental data some terms of the above equations.

Since the experimental data, especially those relating to the concentration measurements, are affected by random errors, often not negligible, consisting of a white noise, they have been filtered with a digital signal process in order to reduce the error.

We analysed the variables as discreet signals over time, by using the Fourier transform in order to have the variables in the frequency domain. We calculated the power spectral density (PSD) of the signal, that describes the power present in the signal as a function of frequency, per unit frequency. The spectrum of the signal is typical of a physical process affected by white noise: at lower frequencies the energy in the system is high (granular temperature in our case), then it progressively decreases as the frequency increases until it becomes constant. This trend allows us to understand at what frequency the presence of noise tends to dominate the spectrum and use this value in a filtering process to extract less noisy measurements.

6.2 Considerations on the mass balance

To close the terms of Eqs. (6.1) relevant to the correlations between the floating components, we can adopt a diffusive model similar to that already described in the section section 2.4.1, by introducing suitable *diffusion coefficients* ξ_2^β:

$$\overline{c'^\beta u_2'^\beta} = -\xi_2^\beta \frac{\partial c^\beta}{\partial x_2} = \begin{cases} \overline{c'^s u_2'^s} = -\xi_2^s \dfrac{\partial c^s}{\partial x_2} \\ \\ \overline{c'^l u_2'^l} = -\xi_2^l \dfrac{\partial c^l}{\partial x_2} \end{cases} \tag{6.4}$$

From the physical and dimensional point of view, the diffusion coefficient, as already observed in chapter 2. is proportional to a length scale (for which it seems reasonable to assume the diameter of the particles of the size class in question) and a velocity scale, for which it seems reasonable to assume the square root of the granular temperature (T), which well represents the diffusion process due to the particle velocity fluctuations:

$$\xi_2^\beta \propto d^\beta \sqrt{T^\beta} \tag{6.5}$$

Substituting Eqs. (6.4) into the balance equations (6.1), we obtain:

$$\frac{\partial}{\partial x_2}(c^s u_2^s) - \frac{\partial}{\partial x_2}\left(\xi_2^s \frac{\partial c^s}{\partial x_2}\right) = 0 \tag{6.6}$$

$$\frac{\partial}{\partial x_2}(c^l u_2^l) - \frac{\partial}{\partial x_2}\left(\xi_2^l \frac{\partial c^l}{\partial x_2}\right) = 0 \tag{6.7}$$

These two equations can be integrated, obtaining:

$$c^s u_2^s - \xi_2^s \frac{\partial c^s}{\partial x_2} = \text{const}_1 \tag{6.8}$$

$$c^l u_2^l - \xi_2^l \frac{\partial c^l}{\partial x_2} = \text{const}_2 \tag{6.9}$$

Since the flow is stationary, the vertical mass flux at the bed is zero, and consequently both constants are zero. The above equations become:

$$c^s u_2^s = \xi_2^s \frac{\partial c^s}{\partial x_2} = -\overline{c'^\beta u_2'^\beta} \tag{6.10}$$

$$c^l u_2^l = \xi_2^l \frac{\partial c^l}{\partial x_2} = -\overline{c'^\beta u_1'^\beta} \tag{6.11}$$

In the next Figures the terms of the equation are calculated according to two representative tests R0 and R1. Table 6.1 reports the data of the test used to develop the data analysis. The granular discharge is always

calculated as the sum of Q_S^* and Q_L^* (chapter 4).

Figures 6.1 and 6.2 show average values of the longitudinal velocity, normal velocity, concentration and granular temperature of the two tests. As regards the distribution of longitudinal velocity and concentration for both tests, analogues considerations as in chapter 5 are valid. As in the other tests, the longitudinal component of the two grain size classes can be assumed coincident. Form the concentration profiles, we can observe that the large class is significantly concentrated in the upper part of the flow depth, while the small one populates the lower part of the depth.

The granular temperature results greater for the small particles, due to their owned greater inertia. Besides, we underline that the presence of the small fraction is rather lower than that of the large fraction in the upper layer.

Please note that the dimensionless flow depth η is in these tests refereed to the average value of the layer. The value of the variables (velocity, concentration, granular temperature) are computed respect to y_m, average height of each single layer.

Table 6.1: Data of the representative test for the data analysis.

Test	Q_T^*	P_S [%]	P_L [%]	h_0 [cm]
R0	160	25	75	5.50
R1	170	50	50	5.20

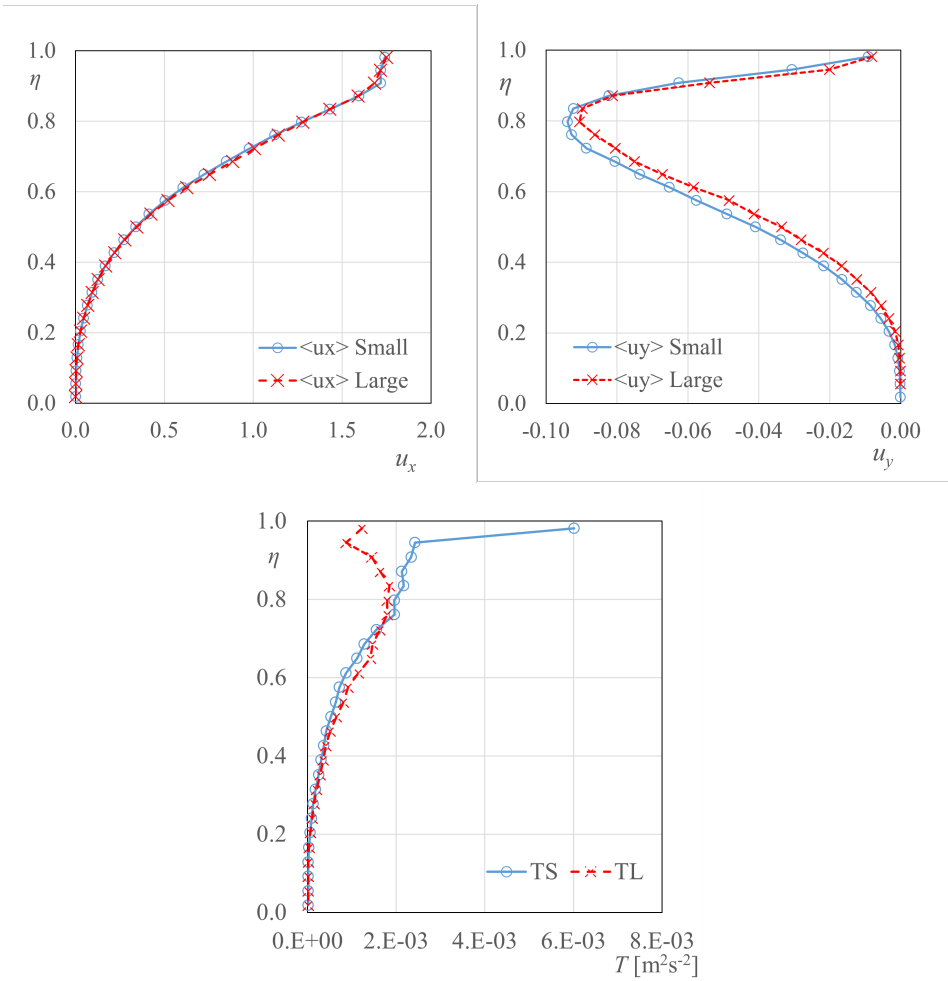

Figure 6.1: Test R0. Distributions of average values.

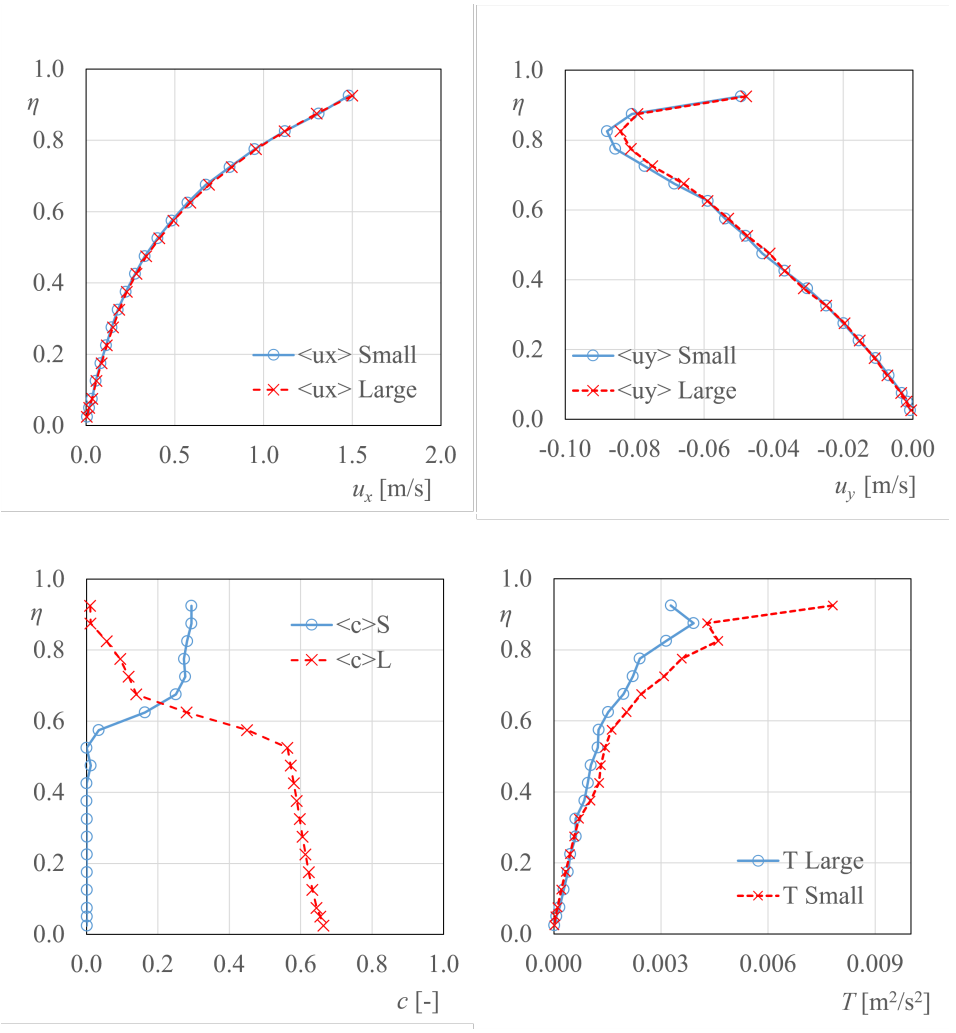

Figure 6.2: Test R1. Distributions of average values.

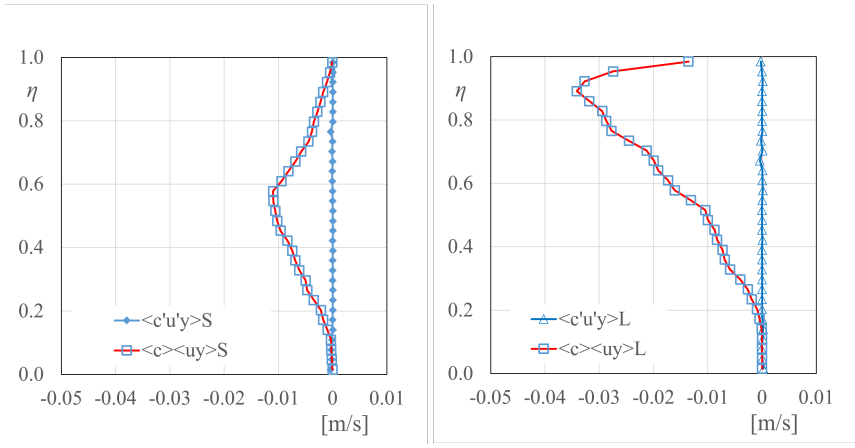

Figure 6.3: Test R0. Mass flux in x_2.

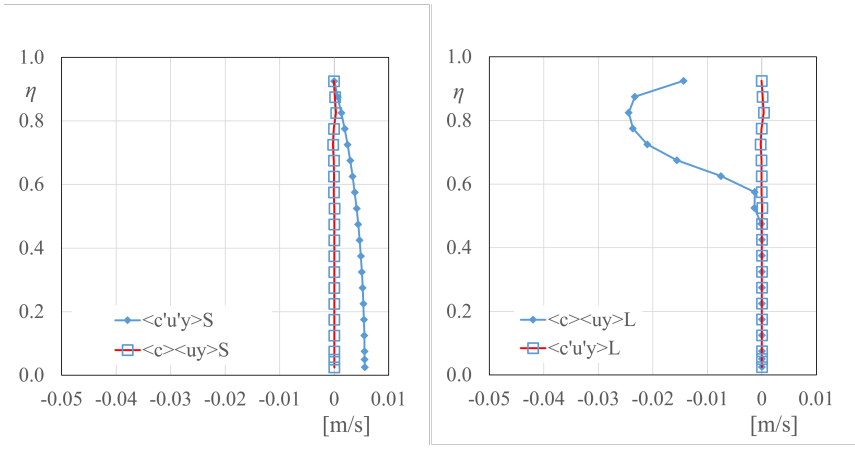

Figure 6.4: Test R1. Mass flux in x_2.

The Figures 6.3 and 6.4 show the distribution of the two terms of Eqs.(6.8) and (6.9) for thee tests R0 and R1 respectively.

The figures shows that the diffusive terms $\overline{c'^{\beta}u_2'^{\beta}}$ are negligible in both cases with respect to the convective ones, both for the small and large classes. In other words, the convective terms are not balanced by the diffusive ones.

This result suggests the presence of a secondary circulation that near the wall induces a flow (descending in this case) much more intense than that which would balance the diffusive component alone. We notice that this flux is greater for the large grain-size class and lower for the small.

The convective flow of coarse grains is generally greater than that of fine grains because near the free surface, where the vertical velocities of the particles are greater, the concentration of coarse grains is greater.

The existence of secondary circulations was found in case of homogeneous granular flows [55, 33, 65]. In particular Heyman et al. [33] found that the combination of side wall velocity profiles provides a secondary flow structure. They found that for a low flow rate a longitudinal vortex induces an upward movement of the particles on the wall and a reverse rotation at higher flow rates. Figure 6.5 shows a general sketch of the flow regimes at the wall.

The presence of secondary circulation also testifies to the probable presence of transversal gradients of both concentrations and velocities. This hypothesis is also evidenced by the differences found in the longitudinal mass fluxes (per unit of width) measured near the transparent wall, which are systematically lower than the areal averaged fluxes obtained from the global discharges measurements.

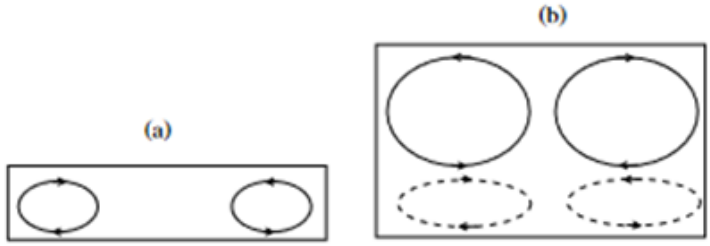

Figure 6.5: Sketch of the structure of the flow regime obtained by [33]. Upward motion of the particle (a) for low flow rate and reverse direction of the motion for high flow rate (b) [33].

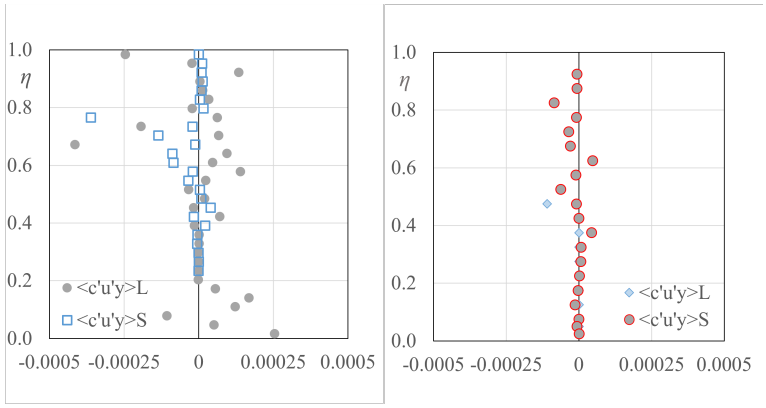

Figure 6.6: Comparison of the diffusive flux in x_2 of the two fractions: test R0 on the left and R1 on the right.

Figure 6.6 shows the comparison between the flux direction in x_2 of the two fractions. We can notice that there are not remarkable differences in the normal direction of the two grain size classes. We underline that these flux are rather small compared to the measurement error is high.

Figure 6.7 and 6.8 instead show the distribution of longitudinal mass fluxes for the two classes. It is possible to argue that the mass diffusive fluxes in the longitudinal direction $\overline{c'^{\beta}u_1'^{\beta}}$ are negligible for both classes with respect to the convective fluxes $c^{\beta}u_1^{\beta}$. This result confirms that in these tests the frictional regime prevails throughout the flow depth.

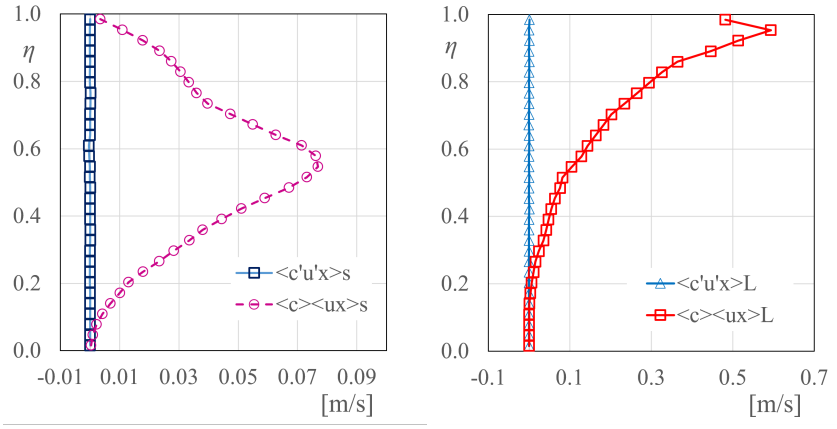

Figure 6.7: Test R0. Mass flux in x_1.

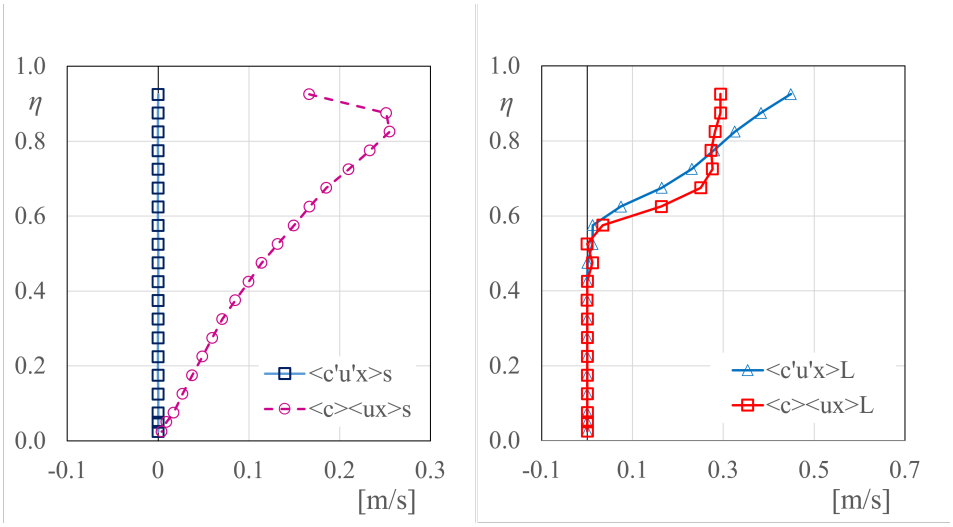

Figure 6.8: Test R1. Mass flux in x_1.

It is then possible to calculate the granular discharge for unit width from the side-walls distribution of velocity and concentration of the two classes:

$$q_x^\beta = \int_0^{h_0} u_1^\beta c^\beta \tag{6.12}$$

The discharge calculated with Eq. 6.12 is always smaller that total discharge measured at with the volumetric method (chapter 3) at the end of the channel. The side-wall flow rate results lower for both grain sizes. This result confirms the presence of transverse gradients of velocity and concentrations. In other words, the flow is three-dimensional and corresponds to the results found for the homogeneous material by Meninno et al. [55], but also by other authors ([72, 45]).

While it is practically impossible to obtain velocity measurements within the flow far from the wall, it is instead possible to measure everywhere the

relative concentration of the two classes.

To do this, we inserted a small pipe (visible in Figure 6.12) from the bottom of the channel through which we suck up a certain volume of material at different distances along the normal direction x_2. By analyzing these samples of collected material it is possible to obtain the distribution of relative concentration of the two classes along the flow depth.

Please note that in this way it is not possible to obtain the absolute concentration, since the distribution of the voids is not known. We therefore introduced the concept of *relative concentration* defined as:

$$c_r^\beta = \frac{c^\beta}{c^s + c^l} \tag{6.13}$$

Figures 6.9, 6.10, and 6.11 present the comparison between the distribution of relative concentration measured in the center of the channel and the same distribution measured at the lateral wall with the optical method and rescaled according to Eq.6.13 in 3 different tests. The figures show that the smaller particles occupy in the center of the channel a portion of the flow depth thicker than near the wall in all tests. Vice versa for large particles. This result leads to the conclusion that the stratification is also present inside the flow field, but with different intensity from the side walls.

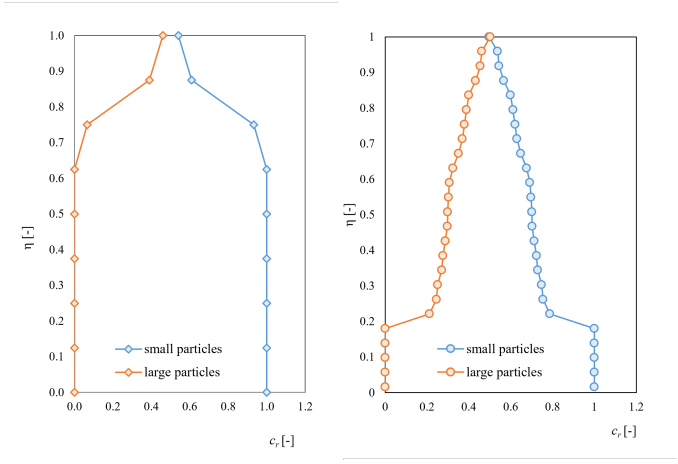

Figure 6.9: Test with $P_L = 75\%$: c_r in the middle of the flow (left) and from the side-walls (right).

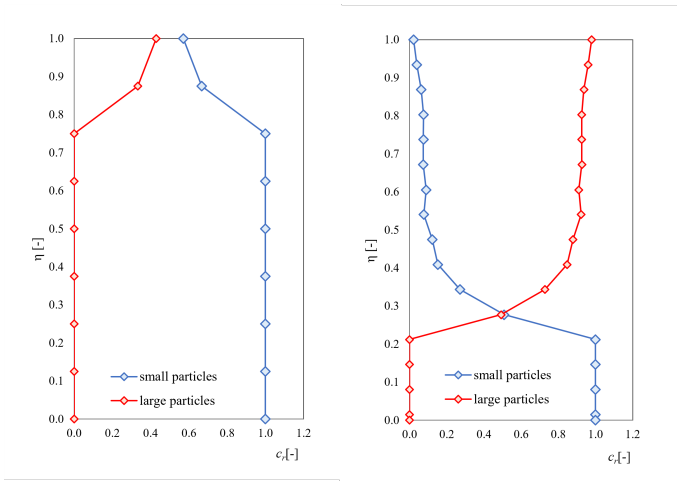

Figure 6.10: Test with $P_S = P_L = 50\%$: c_r in the middle of the flow (left) and from the side-walls (right).

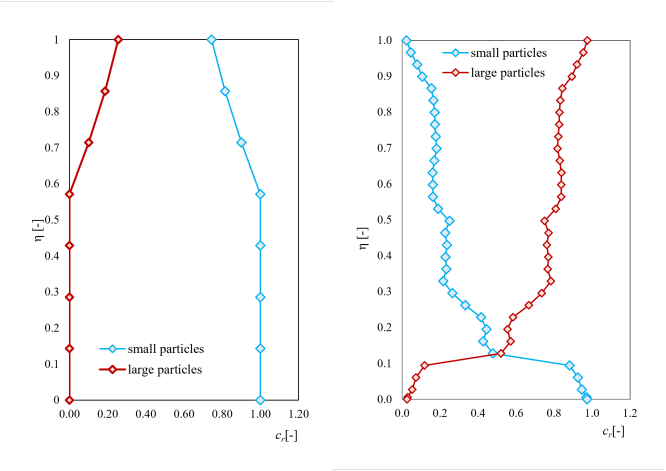

Figure 6.11: Test with $P_S = 75\%$: c_r in the middle of the flow (left) and from the side-walls (right).

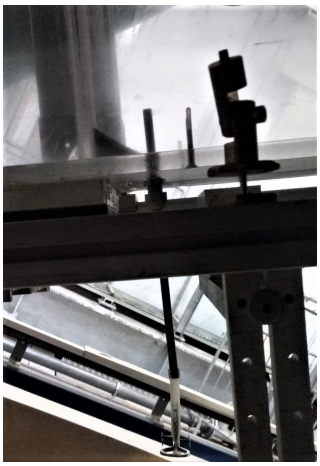

Figure 6.12: Small pipe used to measure the particle concentration in the middle of the flow.

6.3 Considerations on the momentum balances

Also for the momentum balances (Eqs. 6.2 and 6.3) it is possible to make similar considerations to those made for mass balances. We can first integrate the equations along the normal direction between the free surface h and the generic distance x_2 from the bed:

$$\rho_s g \sin\theta \int_{x_2}^{h} c^\beta dx_2 = \frac{1}{\rho_s}\tau_{12}^\beta - c^\beta u_1^\beta u_2^\beta - c^\beta \overline{u'^\beta_1 \, u'^\beta_2} \tag{6.14}$$

$$\rho_s g \cos\theta \int_{x_2}^{h} c^\beta dx_2 = \frac{1}{\rho_s}\sigma_{22}^\beta - c^\beta u_2^\beta u_2^\beta - c^\beta \overline{u'^\beta_2 \, u'^\beta_2} \tag{6.15}$$

with $\beta = s, l$. We neglected the inter-class stresses ξ^β, which depend on the difference in velocity between the classes, since the measurements shows that the velocity distribution is sensibly equal for the two classes.

In order to integrate the above equations it is necessary to preliminary define the rheological and closure relations of all the stresses appearing in the equations.

As already mentioned, this is a still open problem on which there are different approaches and different models.

In a preliminary approach, a rheological model of frictional type could be applied at the terms τ_{12} and σ_{11} and σ_{22} (Armanini et al. [3]) and apply the dense gas analogy to the terms related to the correlations between the fluctuating components (Reynolds-like stresses), although this approach is unorthodox in the theories and applications reported in the literature on kinetic theories. In fact, these theories do not contemplate the presence of Reynolds-like terms, while they include in the constitutive relationship and in the rheological relationship the effect of the collisional fluctuations of the particles [27].

While aware that this problem goes beyond the scope of the thesis, we tried to compare with each other some terms of the above equations. For this purpose we also calculated the collisional stresses applying the dense gas analogy, both for shear and normal stresses. The Reynold-like terms can be integrated according to the kinetic theory.

Figure 6.13 and 6.15 show the trend of these terms that appear in the momentum balance equations in the two directions x_1 and x_2. In particular the figures shows the Reynolds-like stress (red bullets), the collisional shear stress, calculated according to the dense gas analogy and the longitudinal component of the gravity force (first term of Eqs. 6.14).

The Reynolds-like stresses result much lower than that calculated according to the kinetic theories, that balances relatively well the longitudinal component of the weight force, for the large particle.

Accordingly, also the trend of the granular temperature previously shown (Figure 6.1, 6.2) show the presence of a layer close to the free surface dominated by the instantaneous collisions. By proceeding towards the static bed, this collisional stress tends rapidly to become null.

On the right of Figure 6.13 and 6.15 we can observe the behaviour of the same variables for the small fractions. Obviously, at the free surface, due to the low concentration of smaller fraction, all terms (Reynolds-like, average stresses and longitudinal wight component) tend to vanish. As regards the distributions of the force for the small fractions, as we already mentioned, this results zero in the upper part ($\eta = x_2/h > 0.8$), while it tends to increase with a evolution slightly parabolic while approaching the static bed.

In the lower part of figure 6.13 and 6.15 the total shear stresses are plotted. We can observe a triangle-like evolution of the longitudinal weight force of the sum of the large and small fraction.

The figures 6.14 and 6.16 show the same balances for the normal stresses. Both the trends have a linear evolution, but with different slopes in the upper layers ($\eta > 0.65$) and in the lower value ($\eta < 0.6$) respectively. Obviously the difference between these two gradients is due to the voids trend in particular for $\eta > 0.6$. This result suggests that assuming the total concentrations constant in the blanc is a rough approximation.

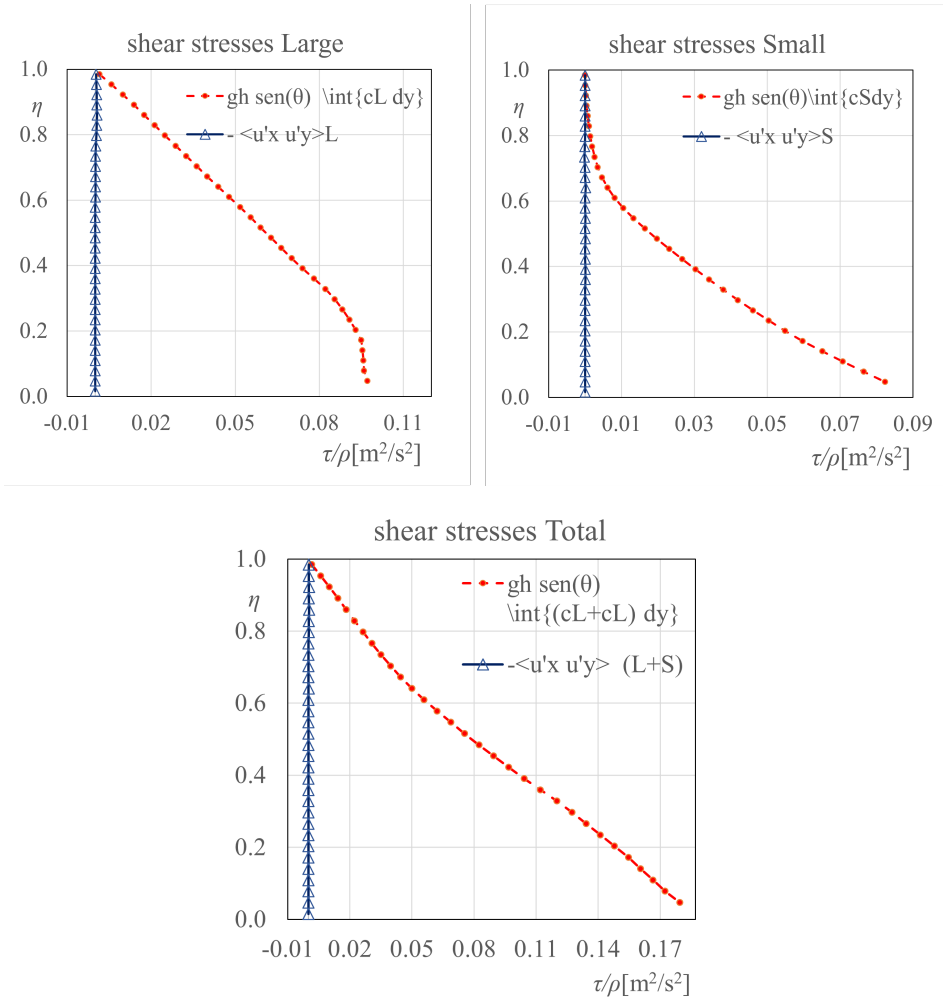

Figure 6.13: Shear stresses - test R0.

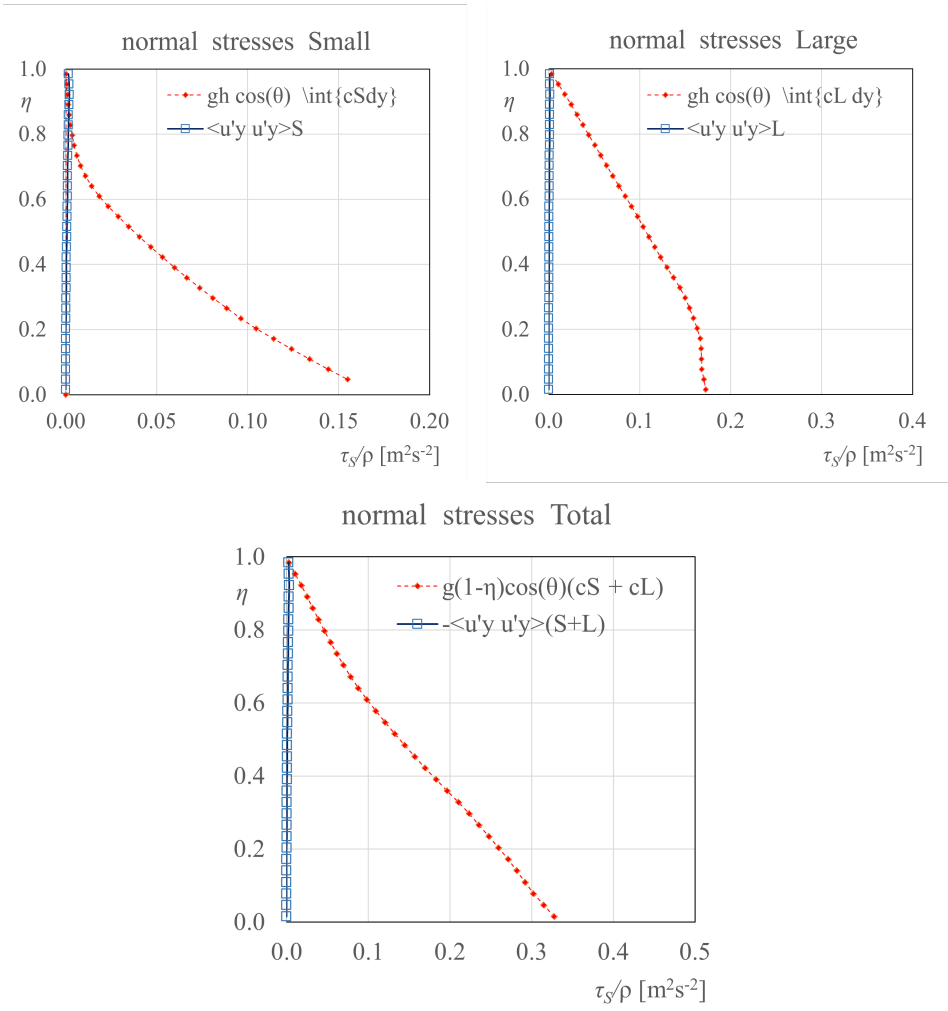

Figure 6.14: Normal stresses - test R0.

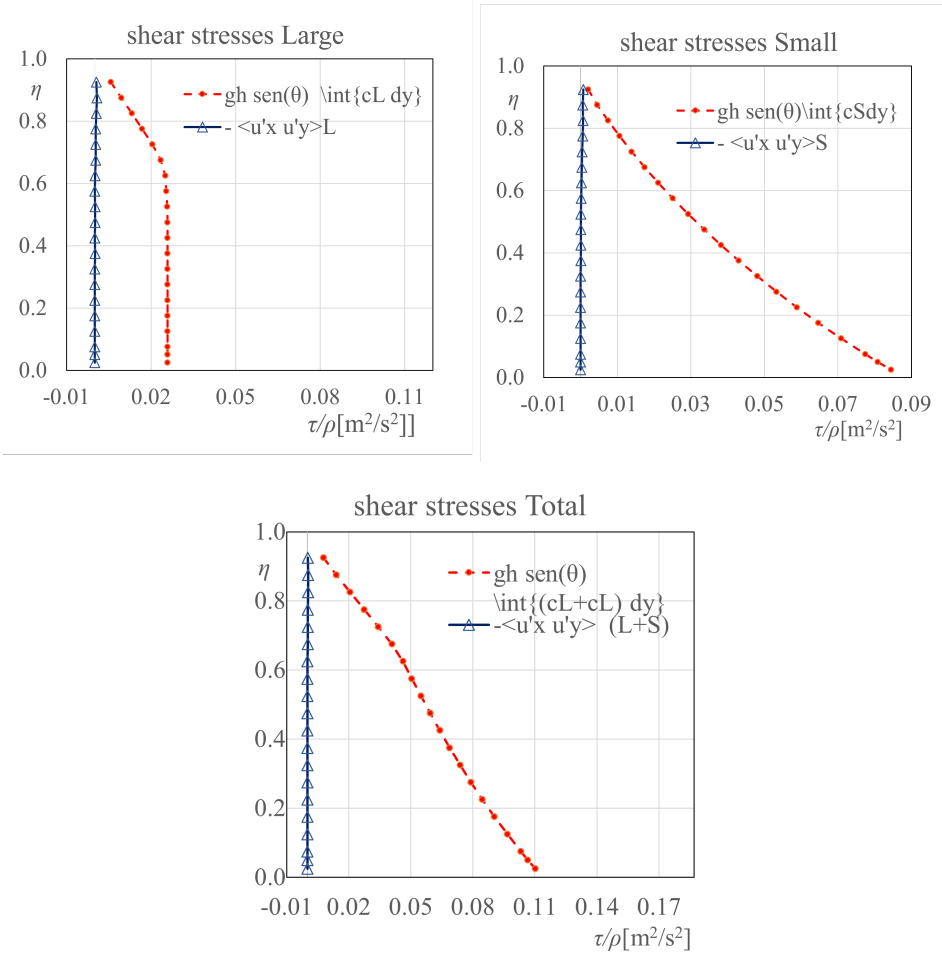

Figure 6.15: Shear stresses - test R1.

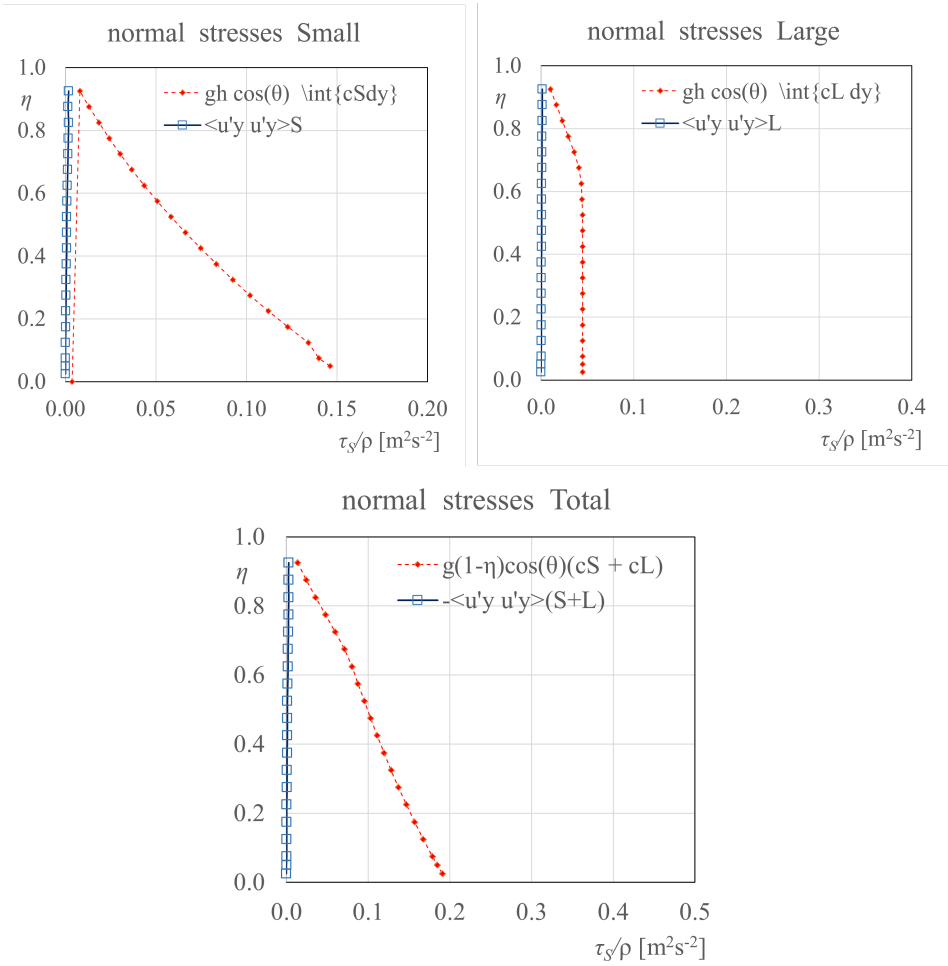

Figure 6.16: Normal stresses - test R1.

Chapter 7

Conclusion and future developments

This work addresses the problem of particle segregation in the flow of a binary mixture of dry granular material. The phenomenon is studied through a series of experimental investigations on a channel flow in statistically stationary and homogeneous conditions, fed with a constant flow rate of different combinations of the concentration of the two classes.

Firstly, the existence of a uniform channel flow condition was demonstrated also in the case of binary mixtures. In particular, the homogeneous and stationary conditions were found for different values of flow rates and volumetric partition of the particles.

It is also known that the uniform flow solution is generally used as a reference state in mathematical modelling, and in particular to derive the closure relations for the depth (or areal) integrated equations when applied to real cases.

Moreover, the experimental data shows that the two grain-size classes,

almost double in size in this experimental work, have always nearly the same longitudinal velocity. This result becomes important in analysing binary mixtures and relative phenomena: the *isokinetic hypothesis* (same velocity for the two grain size classes) is fundamental in many mathematical and numerical models.

The experiments also show how segregation works in the binary mixture. In the section of channel upstream of the section in uniform conditions a process of mixing of the particles develops that leads to their stratification in the uniform flow stretch: we have found that large particles accumulate in the part of the flow depth close to the free surface, while the finer particles tend to occupy the part of the flow depth close to the erodible bed. Between these two layers there is often a layer in which the two size fractions are well mixed together. This result confirms the experiments and studies present in the literature, which describe segregation as a combination of the processes of *kinetic sieving* and *percolation* and also by secondary circulation, as observed in our experiments.

The experiments show that segregation of the particles does not change much according to the feeding discharge. From low up to high flow rates, after an initial adaptation time, the particles segregate and at the end of the process the small ones are found at the bottom and the large fraction close to the surface, with a difference only in the dimension of *mixing* layer.

Furthermore, experiments show that in the flow of binary mixtures two types of regimes are present: in case of low flow rate, the frictional regime is predominant all along the flow depth. For higher flow rates there is a coexistence along the flow depth of the frictional and collision regimes, but the collision regime is dominant in a layer close to the free surface with thickness of about 0.2 times the flow depth. This effect is gradually more evident as the concentration of the larger particles feeding the mixture

is greater. This aspect is fundamental for choosing the correct closure relations to use in the models.

Furthermore, we have also observed that the granular temperature of small particles is always higher than that of large particles. This is also an important consideration useful for applying the dense gas analogy (kinetic theories) to segregation theories.

Finally, all the experiments show the existence of a transversal velocity component, which most likely derives from the presence of secondary circulation on the flow.

The results of this experimental work, data and related observations and considerations, could be interpreted with the few existing models or, more reasonably, could be used to refine and improve these models, perhaps trying to extend the different models of uniformly sized materials referred to in the first part of the thesis, to the case of bi- or poly-dispersed mixtures.

Bibliography

[1] Agrawal, K., Loezos, P., M., S., and Sundaresan, S. The role of meso-scale structures in rapid gas–solid flows. *Journal of Fluid Mechanics 445* (2001), 151–185.

[2] Aranson, I. S., and Tsimring, L. S. Continuum theory of partially fluidized granular flows. *Physical Review E 65* (2002), 061303.

[3] Armanini, A. Closure relations for mobile bed debris flows in a wide range of slopes and concentrations. *Advances in Water Resources 81* (2015), 75–83.

[4] Armanini, A. *Bedload Transport*. Springer International Publishing, 2018, pp. 87–114.

[5] Armanini, A., Capart, H., Fraccarollo, L., and Larcher, M. Rheological stratification in experimental free-surface flows of granular–liquid mixtures. *Journal of Fluid Mechanics 532* (2003), 269–319.

[6] Armanini, A., Fraccarollo, L., and Larcher, M. Liquid-granular channel flow dynamics. *Powder Technology 182* (2008), 218–227.

[7] ARMANINI, A., LARCHER, M., AND FRACCAROLLO, L. Intermittency of rheological regimes in uniform liquid-granular flows. *Physical Review E 79* (2009), 051306.

[8] ARMANINI, A., LARCHER, M., NUCCI, E., AND DUMBSER, M. Submerged granular channel flows driven by gravity. *Advances in Water Resources 63* (2014), 1–10.

[9] ARMANINI, A., AND ROSSI, G. Shallow water approach to dry granular flows driven by gravity: the problem of closure relations. *Submitted* (2020).

[10] ARNARSON, B. ., AND JENKINS, J. T. Binary mixtures of inelastic spheres: Simplified constitutive theory. *Physics of Fluids 16*, 12 (2004), 4543–4550.

[11] BAGNOLD, R. A. Experiments on a gravity-free dispersion of large solid spheres in a Newtonian fluid under shear. *Proceedings of the Royal Society of London. Series A. Mathematical and Physical Sciences 225*, 1160 (1954), 49–63.

[12] BARTELT, P., AND MCARDELL, B. W. Granulometric investigations of snow avalanches. *Journal of Glaciology 55*, 193 (2009), 829–833.

[13] BENYAHIA, S., SYAMLAL, M., AND O'BRIEN, T. J. *Summary of MFIX Equations 2012-1*, 2012.

[14] BOUCHAUD, J.-P., CATES, M. E., PRAKASH, J. R., AND EDWARDS, S. F. A model for the dynamics of sandpile surfaces. *Journal de Physique I 4*, 10 (1994), 1383–1410.

[15] BRIAN, U., AND BEHRINGER, R. P. Self-diffusion in dense granular shear flows. *Physical Review E 69* (2004), 031308.

[16] Bridgwater, J. Segregation Mechanisms in Condensed Granular Flow. In *Solid Mechanics and Its Applications*, A. D. Rosato and D. L. Blackmore, Eds., vol. 81. Springer Netherlands, Dordrecht, 2000.

[17] Buades, A., Coll, B., and Morel, J.-M. Non-Local Means Denoising. *Image Processing On Line 1* (2011), 208–212.

[18] Campbell, C. S. Rapid Granular Flows. *Annual Review of Fluid Mechanics 22*, 1 (1990), 57–90.

[19] Ceresiat, L., Kolehmainen, J., and Ozel, A. Charge transport equation for bidisperse collisional granular flows with non-equipartitioned fluctuating kinetic energy. *Journal of Fluid Mechanics 926* (2021), A35.

[20] Chapman, S., and Cowling, T. G. *The Mathematical Theory of Non-Uniform Gases. An Account of the Kinetic Theory of Viscosity, Thermal Conduction and Diffusion in Gases.* Cambridge University Press, 1970.

[21] Dolgunin, V., and Ukolov, A. Segregating modeling of particle rapid gravity flow. *Powder Tachnology 83*, 2 (1995), 95–103.

[22] Drahun, J., and Bridgwater, J. The mechanisms of free surface segregation. *Powder Technology 36*, 1 (1983), 39–53.

[23] Fan, Y., Schlick, C. P., Umbanhowar, P. B., Ottino, J. M., and Lueptow, R. M. Modelling size segregation of granular materials: the roles of segregation, advection and diffusion. *Journal of Fluid Mechanics 741* (2014), 252–279.

[24] Frey, P., and Church, M. Bedload: a granular phenomenon. *Earth Surface Processes and Landforms 36*, 1 (2011), 58–69.

[25] GALVIN, J. E., DAHL, S. R., AND HRENYA, C. M. On the role of non-equipartition in the dynamics of rapidly flowing granular mixtures. *Journal of Fluid Mechanics 528* (2005), 207–232.

[26] GDR-MIDI. On dense granular flows. *The European Physical Journal E 14* (2004), 341–365.

[27] GOLDHIRSCH, I. Scales and kinetics of granular flows. *Chaos: An Interdisciplinary Journal of Nonlinear Science 9*, 3 (1999), 659–673.

[28] GOLDSHTEIN, A., AND SHAPIRO, M. Mechanics of collisional motion of granular materials. Part 1. General hydrodynamic equations. *Journal of Fluid Mechanics 282* (1995), 75–114.

[29] GOUJON, C., DALLOZ-DUBRUJEAUD, B., AND THOMAS, N. Bidisperse granular avalanches on inclined planes: A rich variety of behaviors. *The European Physical Journal E 23*, 2 (2007), 199–215.

[30] GRAY, J. M. N. T. Particle Segregation in Dense Granular Flows. *Annual Review of Fluid Mechanics 50*, 1 (2018), 407–433.

[31] GRAY, J. M. N. T., AND ANCEY, C. Multi-component particle-size segregation in shallow granular avalanches. *Journal of Fluid Mechanics 678* (2011), 535–588.

[32] GRAY, J. M. N. T., AND CHUGUNOV, V. A. Particle-size segregation and diffusive remixing in shallow granular avalanches. *Journal of Fluid Mechanics 569* (2006), 365–398.

[33] HEYMAN, J., BOLTENHAGEN, P., DELANNAY, R., AND VALANCE, A. Experimental investigation of high speed granular flows down inclines. In *European Physical Journal Web of Conferences* (2017), F. Radjai,

S. Nezamabadi, S. Luding, and J. Y. Delenne, Eds., vol. 140, EDP Sciences, p. 03057.

[34] Hill, K., and Tan, D. S. Segregation in dense sheared flows:gravity, temperature gradients, and stress partiotioning. *Journal of Fluids Mechanics 756* (2014), 54–88.

[35] Iverson, R. M. The physics of debris flows. *Reviews of Geophysics 35*, 3 (1997), 245–296.

[36] Jaeger, H. M., Nagel, S. R., and Behringer, R. P. Granular solids, liquids, and gases. *Reviews of Modern Physics 68* (1996), 1259–1273.

[37] Jenkins, J. T. Dense inclined flows of inelastic spheres. *Granular matter 10* (2007), 47–52.

[38] Jenkins, J. T., and Hanes, D. M. Collisional sheet flows of sediment driven by a turbolent fluid. *Journal of Fluid Mechanics 370* (1998), 29–52.

[39] Jenkins, J. T., and Larcher, M. Dense, layered, inclined flows of spheres. *Phys. Rev. Fluids 2* (2017), 124301.

[40] Jenkins, J. T., and Richman, M. W. Kinetic theory for plane flows of a dense gas of identical, rough, inelastic, circular disks. *The Physics of Fluids 28*, 12 (1985), 3485–3494.

[41] Jenkins, J. T., and Savage, S. B. A theory for the rapid flow of identical, smooth, nearly elastic, spherical particles. *Journal of Fluid Mechanics 130* (1983), 187–202.

[42] JOHNSON, P. C., AND JACKSON, R. Frictional–collisional constitutive relations for granular materials, with application to plane shearing. *Journal of fluid Mechanics 176* (1987), 67–93.

[43] JOHNSON, P. C., NOTT, P., AND JACKSON, R. Frictional–collisional equations of motion for participate flows and their application to chutes. *Journal of Fluid Mechanics 210* (1990), 501–535.

[44] JOP, P., FORTERRE, Y., AND POULIQUEN, O. A constitutive law for dense granular flows. *Nature 441* (2006), 727–730.

[45] JOP, P., FORTERRE, Y., AND POULIQUEN, O. Initiation of granular surface flows in a narrow channel. *Physics of Fluids 19*, 8 (2007), 088102.

[46] LARCHER, M., AND JENKINS, J. T. Segregation and mixture profiles in dense, inclined flows of two types of spheres. *Physics of Fluids 25*, 11 (2013), 113301.

[47] LARCHER, M., AND JENKINS, J. T. The evolution of segregation in dense inclined flows of binary mixtures of spheres. *Journal of Fluid Mechanics 782* (2015), 405–429.

[48] LOIS, G., LEMAÎTRE, A., AND CARLSON, J. M. Emergence of multi-contact interactions in contact dynamics simulations of granular shear flows. *Europhysics Letters (EPL) 76*, 2 (2006), 318–324.

[49] LORENZINI, G., AND MAZZA, N. *Debris Flows. Phenomenology and Rheological Modelling.* WIT Press, 2004.

[50] LOUGE, M. Y. Model for dense granular flows down bumpy inclines. *Physical Review E 67* (2003), 061303.

[51] Louge, M. Y., and Keast, S. C. On dense granular flows down flat frictional inclines. *Physics of Fluids 13*, 5 (2001), 1213–1233.

[52] Mandal, S., and Khakhar, D. V. Dense granular flow of mixtures of spheres and dumbbells down a rough inclined plane: Segregation and rheology. *Physics of Fluids 31*, 2 (2019), 023304.

[53] McElwaine, J., and Nishimura, K. Size Segregations in Snow Avalanches. In *IUTAM Symposium on Segregation in Granular Flows* (2000), D. L. Rosato, Anthony D.and Blackmore, Ed., Springer, Springer Netherlands, pp. 81–88.

[54] McElwaine, J., and Nishimura, K. Size Segregations in Snow Avalanches. In *IUTAM Symposium on Segregation in Granular Flows* (2000), D. L. Rosato, Anthony D.and Blackmore, Ed., Springer, Springer Netherlands, pp. 81–88.

[55] Meninno, S., Armanini, A., and Larcher, M. Gravity-driven, dry granular flows over a loose bed in stationary and homogeneous conditions. *Physical Review Fluids 3* (2018), 024301.

[56] Middleton, G. V. *Experimental Studies Related to Problems of Flysch Sedimentation.* No. 7 in Geological Association of Canada special paper. Toronto, Business and Economic Service Ltd., 1970, pp. 253–272.

[57] Nucci, E. *The mechanics of submerged granular flows.* PhD thesis, 2015.

[58] Otsu, N. A Threshold Selection Method from Gray-Level Histograms. *IEEE Transactions on Systems, Man, and Cybernetics 9* (1979), 62–66.

[59] OTTINO, J. M., AND KHAKHAR, D. V. Mixing and segregation of granular materials. *Annual Review of Fluid Mechanics 32*, 1 (2000), 55–91.

[60] PITMAN, E. B., AND LE, L. A two-fluid model for avalanche and debris flows. *Philosophical Transactions of the Royal Society A: Mathematical, Physical and Engineering Sciences 363*, 1832 (2005), 1573–1601.

[61] PIZER, S. M., AMBURN, E. P., AUSTIN, J. D., CROMARTIE, R., GESELOWITZ, A., GREER, T., TER HAAR ROMENY, B., AND ZIMMERMAN, J. B. Adaptive histogram equalization and its variations. *Computer Vision, Graphics, and Image Processing 39*, 3 (1987), 355–368.

[62] POULIQUEN, O., CASSAR, C., JOP, P., FORTERRE, Y., AND NICOLAS, M. Flow of dense granular material: towards simple constitutive laws. *Journal of Statistical Mechanics: Theory and Experiment 2006*, 07 (2006), P07020.

[63] PUDASAINI, S. P. A general two-phase debris flow model. *Journal of Geophysical Research: Earth Surface 117*, F3 (2012).

[64] ROSATO, A. D., AND BLACKMORE, D. L. *IUTAM Symposium on Segregation in Granular Flows: Proceedings of the Iutam Symposium Held in Cape May, Nj, U.S.A. June 5-10, 1999*. Springer Netherlands, 2000.

[65] ROSSI, G. *Mechanics and numerical simulations of Dry Granular Flows driven by gravity*. PhD thesis, 2018.

[66] Savage, S. B. The Mechanics of Rapid Granular Flows. In *Advances in Applied Mechanics*, vol. 24. Elsevier, 1984, pp. 289–366.

[67] Savage, S. B., and Hutter, K. The motion of a finite mass of granular material down a rough incline. *Journal of Fluid Mechanics 199* (1989), 177–215.

[68] Savage, S. B., and Hutter, K. The motion of a finite mass of granular material down a rough incline. *Journal of Fluid Mechanics 199* (1989), 177–215.

[69] Savage, S. B., and Lun, C. K. K. Particle size segregation in inclined chute flow of dry cohesionless granular solids. *Journal of Fluid Mechanics 189* (1988), 311–335.

[70] Schlick, C. P., Isner, A. B., Freireich, B. J., Fan, Y., Umbanhowar, P. B., Ottino, J. M., and Lueptow, R. M. A continuum approach for predicting segregation in flowing polydisperse granular materials. *Journal of Fluid Mechanics 797* (2016), 95–109.

[71] Taberlet, N., Richard, P., Jenkins, J. T., and Delannay, R. Density inversion in rapid granular flows: the supported regime. *The European Physical Journal E 22* (2007), 17–24.

[72] Taberlet, N., Richard, P., Valance, A., Losert, W., Pasini, J. M., and Delannay, R. Superstable granular heap in a thin hannel. *Phys. Rev. Lett. 91,264301* (2003).

[73] Thornton, A. R., Gray, J. M. N. T., and Hogg, A. J. A three-phase mixture theory for particle size segregation in shallow granular free-surface flows. *Journal of Fluid Mechanics 550* (2006), 1–25.

[74] TOMASI, C., AND MANDUCHI, R. Bilateral filtering for gray and color images. In *Sixth International Conference on Computer Vision (IEEE Cat. No.98CH36271)* (1998), Narosa Publishing House, pp. 839–846.

[75] TRIPATHI, A., AND KHAKHAR, D. V. Density difference-driven segregation in a dense granular flow. *Journal of Fluid Mechanics 717* (2013), 643–669.

[76] VALLANCE, J. W., AND SAVAGE, S. B. Particle Segregation in Granular Flows Down Chutes. In *IUTAM Symposium on Segregation in Granular Flows* (Dordrecht, 2000), A. D. Rosato and D. L. Blackmore, Eds., Springer Netherlands, pp. 31–51.

[77] VAN DER VAART, K., GAJJAR, P., EPELY-CHAUVIN, G., ANDREINI, N., GRAY, J. M. N. T., AND ANCEY, C. Underlying asymmetry within particle size segregation. *Physical Review Letters 114* (2015), 238001.

[78] VAN DER VAART, K., THORNTON, A. R., JOHNSON, C. G., WEINHART, T., JING, L., GAJJAR, P., GRAY, J. M. N. T., AND ANCEY, C. Breaking size-segregation waves and mobility feedback in dense granular avalanches. *Granular Matter 20*, 3 (2018), 20–46.

[79] WIEDERSEINER, S., ANDREINI, N., ÉPELY CHAUVIN, G., MOSER, G., MONNEREAU, M., GRAY, J. M. N. T., AND ANCEY, C. Experimental investigation into segregating granular flows down chutes. *Physics of Fluids 23*, 1 (2011), 013301.

[80] XIAO, H., UMBANHOWAR, P. B., OTTINO, J. M., AND LUEPTOW, R. M. Modelling density segregation in flowing bidisperse granular

materials. *Proceedings of the Royal Society A: Mathematical, Physical and Engineering Sciences 472*, 2191 (2016), 20150856.